UNIVERSITY OF CAPE TOWN

SUBMITTED IN PARTIAL FULFILLMENT OF THE REQUIREMENTS FOR MASTERS DEGREE

MASTERS DISSERTATION

THESIS TITLE

The effect of the surface condition of Aluminium ingot (AA3003) during roll bonding with clad Aluminium alloy (AA4045) to form an Aluminium brazing material

MUTSAKATIRA INNOCENT T

MTSINN004

SUPERVISOR

DR SARAH GEORGE

Plagiarism Declaration

I, Innocent Tapiwa Mutsakatira, know the meaning of plagiarism and declare that all the work in this document save for that which is properly acknowledged, is my own.

Signature:…….Signed by candidate……..

Date:……..27/01/2020……
……

ACKNOWLEDGEMENTS

This project could have not been successful without the Lord's Grace. If the Lord takes you there, surely he will take you through.

I would like to thank the following people and institutions for their invaluable help during the course of this research:

Dr. S. George, my supervisor, for her continuous and invaluable guidance, encouragement, commitment and constructive criticism during this work. Secondly for the generous scholarship she awarded me from the University of Cape Town.

The UCT CME staff: Prof Robert Knutsen, Richard Curry, Penny Louw, Soraya Von Willingh. Thank-you for always being ready to help with the use of the testing equipment.

The UCT Mechanical Engineering Workshop staff, for the fabrication of specimens and testing equipment.

Helen George for her tireless and sleepless nights editing and proof reading this document.

Hulamin staff for providing the materials and also allowing me to visit their plant to enhance my understanding of the project.

Mike Shirran for acting as the co-supervisor providing his industrial knowledge.

My family (the Mutsakatira Clan) and my friends who helped me preserve my mental sanity during this journey.

ABSTRACT

Hulamin is the leading producer of aluminium products in South Africa. One of the products made at Hulamin is the aluminium brazing sheet. The aluminium brazing sheet is made from two aluminium alloys, AA3003 and AA4045. The main alloying element in the 3XXX series alloy is manganese and the main alloying element in the 4XXX series alloy is silicon. An aluminium brazing sheet is manufactured during an industrial process called "accumulative roll bonding", where AA4045 is termed "the clad" and AA3003 "the core". The two materials are stacked together with the core sandwiched between two clad layers. Before the materials are stacked together, they undergo surface preparation. At Hulamin, the surface roughness of the core is kept at 10 µm and the surface roughness of the clad at 1 µm. After surface preparation, the stacked material is put into a hot rolling mill, where it undergoes reduction through several passes until it reaches the desired gauge.

The aim of this project is to determine the effect of the surface roughness of both the clad and the core on the quality of the bond after roll bonding. While the relevant literature specifies that an increase in surface roughness increases bond strength, the current set surface finishes being implemented at Hulamin have been obtained through trial and error, with no validated experimental work to support them. This research aims to find the optimum surface finish in order to streamline the process of surface preparation.

A design matrix was constructed based on the surface finish being used at Hulamin, where the core was at 10 µm and the clad at 1 µm. Fourteen surface conditions were formulated and three tests were performed on each surface condition. The samples were manually ground on different grit papers to an average surface roughness of 0.5 µm, 1 µm and 3 µm for the clad and 7 µm, 10 µm, 15 µm and 25 µm for the core. Simulation of the hot rolling at the University of Cape Town's (UCT's) Centre for Materials Engineering (CME) laboratory was achieved using plane strain compression testing (PSC) on the Gleeble 3800. The PSC sample geometry of 30 mm x 50 mm x 10 mm was achieved by stacking a 5 mm sample from the clad liner plate and a 5 mm thick sample from the as-cast core material. To simulate the hot roll bonding the tests were run at 450 ^{o}C at a strain rate of 1.5 s^{-1}. The test parameters were obtained from the Hulamin mill log *data*.

In order to assess the strength of the bond, *post* PSC test, tensile shear testing was performed on specimens wire-cut from the gauge of the deformed PSC sample. The tensile shear

specimens were designed according to ASTM D3165. The tensile shear tests were performed on a Zwick Universal Testing machine, in conjuction with single-camera Digital Image Correllation (DIC). The purpose of the DIC was to monitor the strain localisation at the interface. The tensile test was run at 0.0012 mm/min at room temperature. The shear test results confirmed that surface roughness played a major role in the bond strength formed between these two dissimilar materials. It was found that the Hulamin benchmark surface preparation, set at 10 µm and 1µm, could be improved by increasing the surface roughness of the core to 15µm while keeping the clad surface finish constant.

The rolling direction (RD) of the specimen was cut, mounted and polished for microstructural feature characterisation, using light microscopy and scanning electron microscopy (SEM) with backscattered electron (BE) imaging. In order to characterise the bond further, energy-dispersive X-ray spectroscopy (EDS) was performed across the interface of the samples to show the diffusion of Si. Microstructural analysis revealed that a poor bond resulted in the presence of large voids, while a high integrity metalurgical bond contained very small voids. Also, a good metallurgical bond allowed for the diffusion of Si across the bond, although these results were qualitative because diffusion of Si across the interface is largely time- and temperature-dependent.

Combined strain and microstructural results showed that finer surface roughnesses yielded poorer bonds because of minimal frictional force and that rougher surface finishes also yielded poorer bonds, owing to larger troughs on the surface of the material that led to void formation at the interfaces, which in turn caused sites of delamination.

There had to be an optimum surface finish that existed between the two alloys where the finish would obtain a metallurgical bond that was of optimum strength. Should this optimum finish be exceeded, the strain level would inevitably increase during tensile shear testing, with the induced voids increasing in size and Si diffusion across the interface decreasing, thereby indicating a compromise in the quality of the bond.

It was found that the Hulamin benchmark surface preparation, set at 10 µm and 1µm, could be improved by increasing the surface roughness of the core to 15µm while keeping the clad surface finish constant. The findings of this research could be of significant value to Hulamin in the improvement of the quality and cost of the end product under consideration.

Table of Contents

LIST OF FIGURES

LIST OF TABLES

ABBREVIATION LIST

ARB	Accumulative Roll bonding
Al	Aluminium
AFM	Atomic Force Microscope
BSE	Backscattered Electrons
B	Breadth of sample
Δ F	Change in UTS relative to the Hulamin UTS
Cu	Copper
Ø	Diameter
DIC	Digital Image Correlation
EDS	Energy-Dispersive X-ray spectroscopy
FEM	Finite Element Modelling
HV	Hardness Value
HT	Heat Treatable
Fe	Iron
L	Length of anvil
LMS	Light Microscopy
Mg	Magnesium
Mn	Manganese
µm	Micrometre
ND	Normal Direction
σ	Normal Stress
NHT	Non-heat Treatable
RD	Rolling Direction

SEM	Scanning Electronic Microscope
Si	Silicon
K	Shear flow stress
τ	Shear stress
ε	Strain
HBF_4	Tetra-flouroboric acid
TD	Transverse Direction
TC1	Thermocouple 1
TC2	Thermocouple 2
UTS	Ultimate Tensile Strength
W	Width of anvil

1 INTRODUCTION

1.1 Background and motivation for research

Hulamin is the leading producer of aluminium products in South Africa. One of the products made at Hulamin is the aluminium brazing sheet. This brazing material is made using a roll bonding technique by cladding the core alloy to an alloy that has a low melting point. Either both sides of the core are clad with a non-braze alloy or one side is clad. The core and clad layers are chosen based upon the required properties of the final material. The brazing material is made by hot rolling two aluminium alloys together, *viz.* AA3003 and AA4045. Brazing is a metal-joining process in which the filler is heated above melting point and distributed between close-fitting parts by capillary action [1]. Before the rolling process, the clad and the core undergo surface preparation. There is little literature to validate the standard surface finish of both the core and the clad. However, the literature does specify that Surface Roughness (Ra) does play a significant role in the formation of the metallurgical bond when two materials are compressed together [2]. During the roll bonding process at Hulamin, the aim is to keep the surface roughness of the core below 10 µm and the clad at 1µm. These smooth finishes are historical values that have been used by Hulamin for many years, with no theoretical basis on record. Hulamin wants to establish if these set values do, in fact, optimise the strength of the bond. An understanding of the set values will also determine whether surface preparation is, in fact, necessary since it is a costly and time-consuming process.

This research investigates the effects of various average surface roughness values on bond strength. The roll bonding simulation was performed using the Gleeble 3800, followed by the mechanical tensile shear testing of the bond and the microstructural characterisation of said metallurgical bond.

1.2 Aim of study

The main aim of this study was to determine the effect of variations in surface roughness on the achieved roll bond strength of the two aluminium alloys, AA3003 and AA4045.

1.3 Objectives of study

In order to achieve the main aim of this study, the following objectives should be achieved:

- To perform a series of plane strain compression (PSC) tests to simulate the roll bonding conditions on samples with a variety of imposed surface roughnesses on both the core and the clad material layers.

- To assess the integrity of the metallurgical bond achieved for a variety of surface roughness combinations.
    - Test the integrity/strength of the bond using tensile shear testing in conjunction with the digital image correlation (DIC).
    - Evaluate the bond interface using light and scanning electron microscopy, as well as energy dispersive x-ray spectroscopy.
- Compare the most favourable surface roughness combinations with the industry standard values used at Hulamin.

1.4 Scope of work

A literature review was undertaken to understand the behaviour of the materials of interest. The physical properties, chemical composition, the microstructure and the homogenisation of both the clad (AA4045) and the aluminium ingot (AA3003) were investigated.

A detailed study of the rolling process currently being utilised at Hulamin in Pietermaritzburg was undertaken. Qualitative and quantitative experiments were conducted to determine the strength of the bond between the core and the clad. To evaluate the quality of the bond strength several tests were conducted in the CME lab and a microstructural analysis was performed, using appropriate microscopes. Deductions and recommendations were based on the results.

2 LITERATURE REVIEW

2.1 Material of concern

2.1.1 Pure Aluminium

The metal Aluminium (Al) has been found to have several properties valuable in modern manufacturing. Aluminium is a conductive metal and also it tends to have a higher affinity for oxygen than other elements [3]. Al does not exist as a pure metal in the earth's crust but exists as a mixture of Al oxides. Therefore, a series of processes is required for the extraction of the pure metal. Bauxite is the principal rock where Al can be obtained [4]. The bauxite rock undergoes crushing and then purification using the Bayer process. Sodium hydroxide is used in this process to produce a precipitate, (Al_2O_3). The aluminum ore undergoes electrolysis to obtain pure Al where cryolite (Na_3AlF_6) is the electrolyte [5]. The whole process from extraction to the manufacture of the end products is summarised in Figure 2-1.

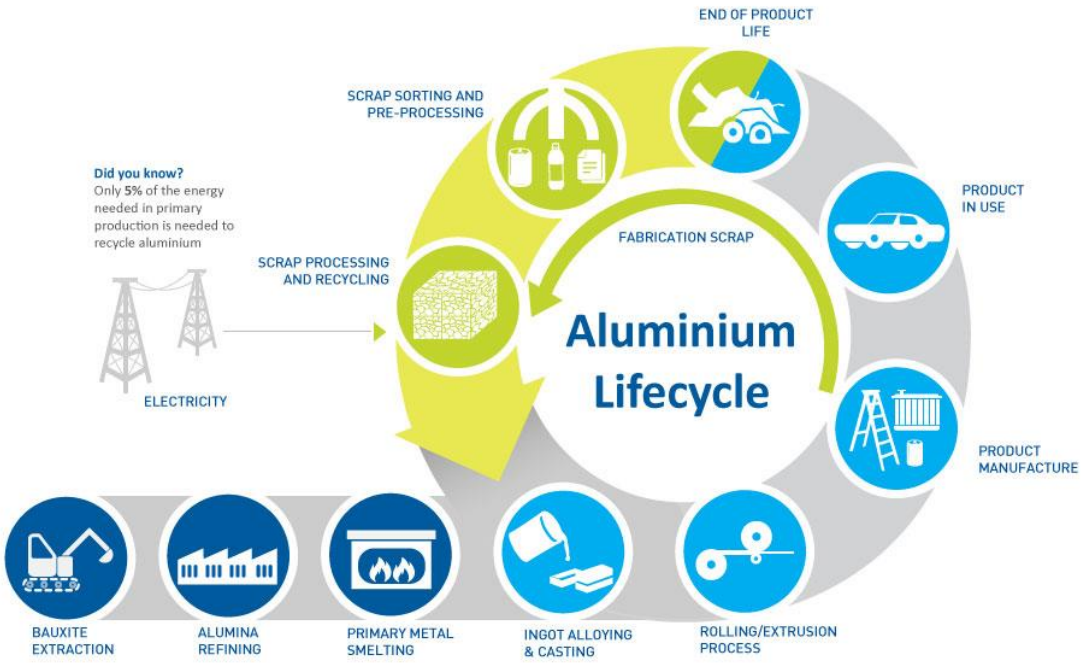

Figure 2-1 Life cycle of pure Aluminium [6]

2.1.2 Properties of pure Aluminium

Aluminium alloys have been found to possess several mechanical properties that have increased its demand in modern industry. Its four most important properties are a high resistance to corrosion, an ability to conduct electricity, a comparatively low mass density and the fact that its mechanical strength can be increased by alloying [7]. Additional desirable properties include ductility, formability, reflectivity and the fact that it is non-magnetic.

Table 2-1 Properties of 99.95% pure Aluminium [6]

Properties	Numeric Value
Density	2.70 kg/cm^3
Young's Modulus of elasticity	69 ×10 ^{3} MPa
Ultimate Tensile Strength	140-330 MPa
Modulus of rigidity(shear)	26.14×10 ^{3} MPa
Poisson's ratio	0.33
Thermal conductivity at 250ºC	2.1-2.3W/cm K
Melting point	645-660º C
Electrical conductivity at 200ºC	3.6×10^7 s/M

In contrast to its alloyed counterparts, aluminium in its pure state has few uses. Alloying is the addition of other metals to enhance physical and chemical properties. The pure metal Al is a face-centred cubic crystalline structure that alloys readily with other metals [8]. Aluminium alloys are classified as heat treatable or non-heat treatable after being alloyed. This classification dictates their use in industry.

2.1.3 Heat treatable alloys

The tensile strength of heat treatable Al alloys is enhanced through precipitation hardening [5]. The precipitates impede the movement of dislocations from one grain to another. Most heat treatable alloys contain amounts of Cu, Mg and Si. These elements become more soluble in Al as the temperature is elevated. The alloying process takes place at specific temperatures and for specific time periods for each Al alloy until the required properties have been achieved [9]. A list of the heat treatable alloys can found in Table 2-2.

2.1.4 Non heat treatable alloys

The tensile strength of non-heat treatable Al alloys is enhanced only by work hardening. (The tensile strength of these alloys cannot be increased by precipitation hardening.) [5] These Al alloys contain amounts of Mn, Mg and Si. Work hardening involves cold rolling and other mechanical processes that reduce the surface area of the alloy.

Table 2-2 Classification of wrought Al alloys [8]

Series	Metals Present	Attributes	Tensile Strength (MPa)	HT	N-HT
1xxx	99% Pure Al	• Electrical conductivity • Corrosion resistance • Formability	69-180		
2xxx	Al-Cu	• Higher mechanical strength • Corrosion resistance	186-428	✓	
3xxx	Al-Mn	• Corrosion resistance • High formability	110-283		✓
4xxx	Al-Si	• Good flow characteristics	172-379	✓	
5xxx	Al-Mg	• High corrosion resistance • Moderate strength and toughness	124-352		✓
6xxx	Al-Mg-Si	• High corrosion resistance • Excellent extrudability • Moderate strength	124-400	✓	
7xxx	Al-Zn	• High toughness version	221-607	✓	

2.1.5 Major attributes of the alloys

Table 2-3 Tempers in brief[10]

Temper	Description		Application
F	As fabricated	This type of designation is used for cast products that have been made from certain shaping processes, like extrusion, forging, drawing and rolling [11]. These processes are used when there is no special control over the thermal conditions during hardening or working.	Forging stock, formability
O	Annealed	Annealing has been described as heating a cast metal and then allowing it to cool off slowly in order to eliminate internal stresses and improve the physical properties of the cast. It is also a designation that is used for cast products that have been manufactured using certain of the shaping processes, like extrusion and forging [11]. Annealing is the reverse of hardening, as heat is applied to soften the alloy in order to lower its mechanical strength. In other words, annealing can be described as a method to achieve the lowest strength condition for a particular alloy, while maximising the subsequent workability of the alloy by using heat.	Forging stock, formability
T	Solution heat treated	Non-heat treatable alloys are given this designation because their physical properties, e.g. toughness and hardness, have been improved by strain hardening [10]. A product can be strain hardened only or a combination of strain hardening and partial annealing can be used.	Where highest mechanical properties are required

H	Work hardened	The designation W applies to alloys that are very unstable at room temperature, with their strength diminishing with the passage of time [11]. An alloy with this designation is rarely a finished product because of its instability and will require various treatments to make it stable.	Formability
W	Unstable / Spontaneous	These are the heat treatable alloys. They are the most stable under room temperature of those listed in Table 2-2, as their physical properties are sustained after heat treatment	Temporary state prior to rolling or treatment

2.2 Aluminium alloy AA 3003

AA 3003 falls under the 3xxx series designation. The major element in this alloy is Mn. AA 3003 is a non-heat treatable aluminium alloy that is used for quite a number of applications in modern industry because of its high formability qualities. It is AA3003 that is used as the core material during roll bonding when brazing materials are made because it neither melts nor undergoes dissolution during brazing [1].

2.2.1 AA 3003 Composition

The composition of alloy AA3003 is shown in Table 2-4 and the typical physical properties are shown in Table 2-5.

Table 2-4 AA3003 composition [11]

3003	**Weight %**					
	Mn	Fe	Cu	Si	Zn	Al
	1.10-1.5	0.00-0.70	0.05-0.20	0.00-0.05	0.00-0.10	Balance

Table 2-5 Physical properties of AA3003 [11]

Property	Numerical Value
Proof stress	50MPa (min)
Ultimate Tensile stress	140 MPa-180 MPa
Modulus of elasticity	69.5 GPa
Hardness Brinell	28 HB
Density	2.73 gcm^{-3}
Melting point	640-655 ºC

2.2.2 Effects of adding the major elements in AA 3003

Table 2-6 Effects of the minor elements in brief

Mn	The addition of Mn promotes the formation of the cubic alpha phase, $AlFeMnSi$ [1]. Mn has been found to increase the yield strength and also the ultimate tensile strength of the alloy [12]. Studies have established that ductility is not compromised by the adding of Mn, hence the alloy AA3003 has high formability qualities. Mn also enhances the corrosion resistance of the alloy.
Cu	The addition of Cu has been found to improve the strength of the alloy, although this is dependent on the concentration of the added element. In addition, the corrosion potential is reduced in the alloy matrix. Thus, the addition of this element also increases the corrosion resistance of the alloy.
Fe	The concentration of Fe is critical because in large amounts it forms β $AlFeSi$, which is needle shaped [1]. The β phase causes porosity in the alloy, which is not beneficial.
Mg	The addition of Mg to AA3003 serves to increase the strength of the alloy without compromising ductility [5].
Minor elements	Si is a minor element in the alloy AA3003. The composition of Si in the alloy has to be regulated since it can affect the mechanical properties of the alloy. The presence of Si results in a reduction of the thermal coefficient of expansion, in low shrinkages in the alloy and also in high fluidity [13].

2.2.3 Micro-structure of AA3003

As described above, AA3003 has Mn as the major alloying element and Si, Fe and Cu as alloying minor elements. The content of Fe and Si determine how AA3003 precipitates. Every

particle has a part that is homogenous both structurally and chemically, this part being called a phase. The presence of the minor alloys Fe and Si reduces the solubility of Mn in molten AA3003. The dominant phases of the AA3003 alloy are $(Mn, Fe)Al_6$ and $Al_{15}(Fe, Mn)_3\ Si_2$. It has been established that $(Mn, Fe)Al_6$ has an orthorhombic crystal structure [14].

2.2.4 Homogenised structure of AA3003

As described above, AA3003 contains the elements Si, Fe and Mn. (The presence of Cu is of minimal significance.) These three elements precipitate in different ways that contribute to the overall microstructure of the alloy. During solidification, AA3003 forms $(Mn, Fe)Al_6$ and $\alpha - Al(Mn, Fe)Si$ as inter-dendritic eutectic particles [15]. To achieve particle dispersion and reduce the concentration of Mn in the solid solution before the rolling of the ingot cast, AA3003 must be homogenised, because homogenisation aids in obtaining the correct volume fraction and distribution of the constituent particles, these two factors influencing the recrystallisation and the ultimate mechanical properties of the alloy [16]. The homogenisation process occurs at a controlled temperature and pressure while the change in the microstructure of the ingot is monitored. When cast ingot AA3003 is heated at 600 ºC at a heating rate of $50Kh^{-1}$ and then quenched in water, some of the $(Mn, Fe)Al_6$ particles will transform into $\alpha - Al(Mn, Fe)Si$ [15]. The change in the microstructure can be identified using back-scattered electron imaging.

2.2.4.1 Evolution of the AA3003 phase particles during homogenisation

The evolution of the phase particles was described using the micrographs taken in BEM mode. The network interconnected eutectic particles were distributed in the inter-dendritic regions and grain particles. In this structure it was the $(Mn, Fe)Al_6$ particles that dominated, as opposed to the $\alpha - Al(Mn, Fe)Si$ particles, and this is shown in Figure 2-2 (a). All of the particles appeared to be clustered together in this phase. The morphology of the alloy AA3003 gradually changed as heat was increased at specific time periods. The inter-dendritic network began to break away and move apart and there was also a small change in the average thickness of the particles. This is illustrated in Figure 2-2 (b). More $\alpha - Al(Mn, Fe)Si$ was now dominating the micro-structure. As the temperature further increased, the presence of very fine dispersoids was noted in the micro-structure, especially at the dislocations. The dislocations acted as the nucleation sites of the dispersoids [16]. During the above process, the particles became increasingly coarse and the dispersoids increased in molecular size. This is shown in Figure 2-2(c).

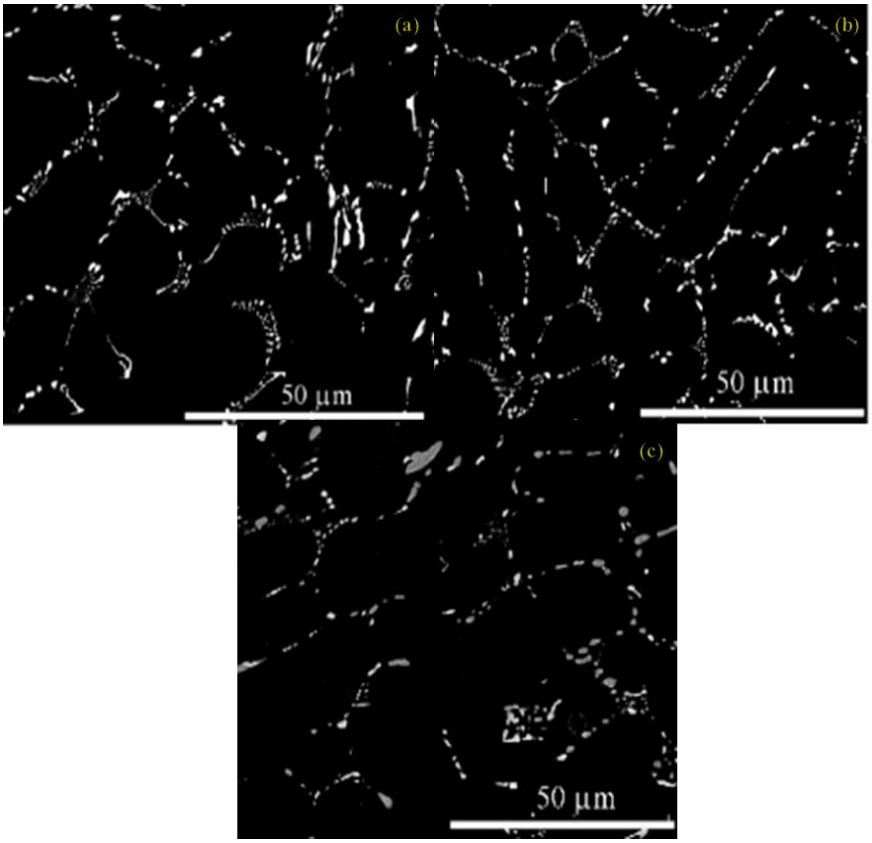

Figure 2-2 Evolution of microstructure of AA3003 during homogenisation [15]

2.3 Aluminium alloy AA4045

This type of alloy falls within the 4xxx series. It is heat treatable and has very good flow characteristics. This wrought aluminium alloy has Si as the main alloying element in the AA4045 and Mn as a minor alloying element. AA4045 is mainly used as a filler material since it has a wide range of melting points [17].

2.3.1 AA4045 Composition

The composition of the alloy AA4045 is shown in Table 2-7, and the physical properties are shown in Table 2-8.

Table 2-7 The chemical composition of 4xxx series alloy [17]

4045	**Weight %**				
	Al	Si	Cu	Fe	Mn
	Balance	7.5% ± 0.7	0.25% Max	0.8% Max	0.1% Max

Table 2-8 Physical properties of a 4xxx series alloy [18]

Property	Numerical Value
Melting point	582.5ºC
Brazing process temperature	605ºC
Thermal conductivity	180 W/(m*K)
Electrical conductivity	158

2.3.2 Microstructure of AA4045

As stated above, Si is the major element in AA4045. The AA4045 alloy forms a eutectic system, which is the main reason why it is used as a clad brazing material. Referring to the phase diagram in Figure 2-3, at 12 wt % Si is the eutectic point of the alloy. The eutectic point is a composition of the alloy that has the lowest melting point. In the eutectic mixture of AA4045 two solids are formed where one is richer in Al and the other is richer in Si. In Figure 2-3 the mixture on the left of the 12 wt % Si is called the hypoeutectic mixture [19]. Si melts at 1414 °C and solidifies with no hot cracking complications. Si has a density of 2.34 g cm $^{-3}$. Thus, when the alloys melting point is exceeding, the pure Si will precipitate when the alloy is cooled.

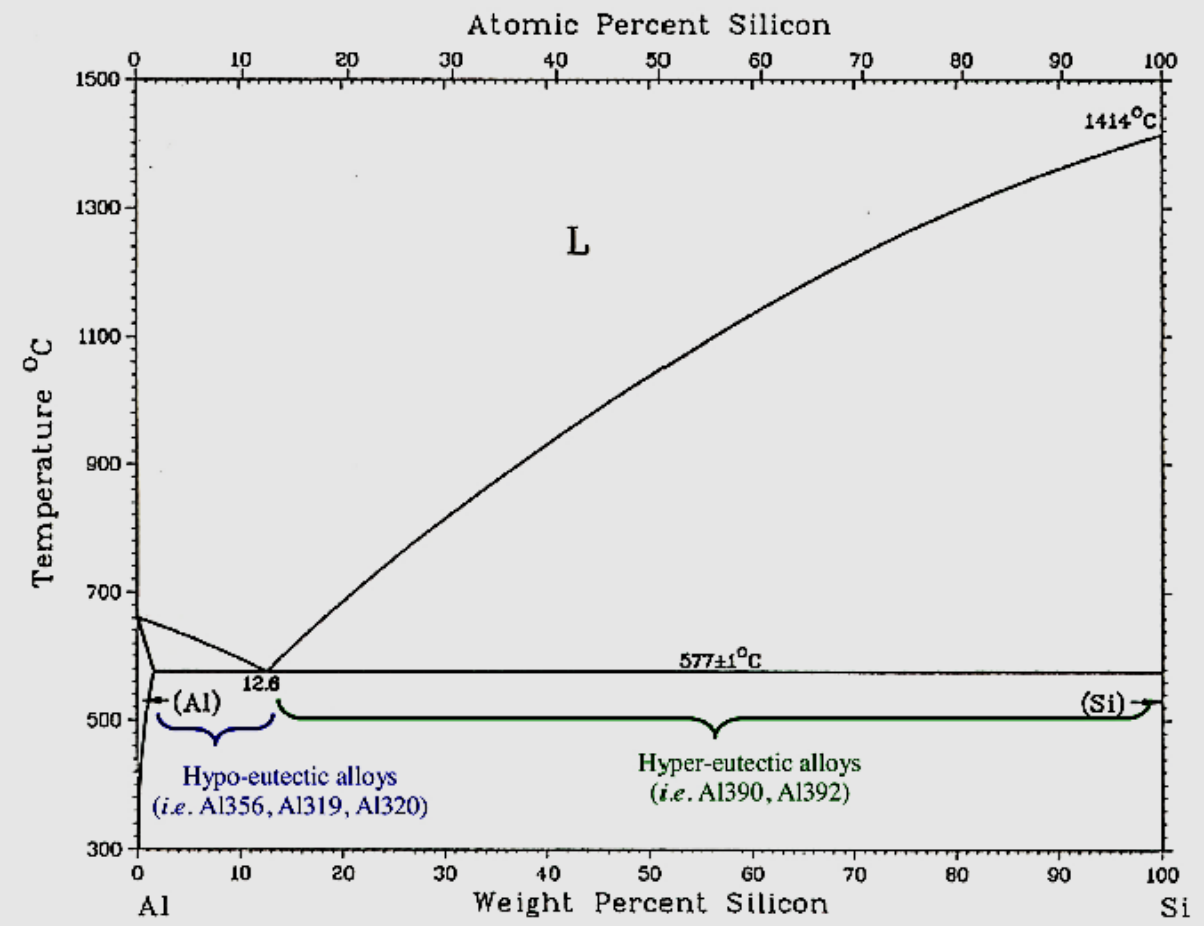

Figure 2-3 Al-Si phase diagram [20]

2.4 Brazing

Brazing is a method used to join dissimilar metals by use of a filler metal that has a lower melting point. The filler metal melts first and is evenly spread, filling the required joint, and, upon cooling, a metallurgical bond will have been formed [21]. The brazing process is straightforward but the actual manufacturing of the brazing sheet, involving both the core (AA3003) and the clad (AA4045), requires careful consideration of several factors. The clad AA4045 is a hypoeutectic material with several compositions that result in the formation of a eutectic mixture. In this eutectic state the clad reaches the lowest melting point that can be manipulated during brazing. In fact, AA 4045 can melt between 577 and 605 ºC depending on the chemical position [22]. The brazing process is usually performed by heating the joint in a vacuum at a temperature around 600 ºC. Because the clad has a lower melting point than 600 ºC, at this stage it would have already started melting and filling up the joint. As the joint is filled, the Si starts to diffuse from the clad into the core. The rate of diffusion depends on the concentration of Si in the clad and also on the temperature at which the brazing process is

taking place [23]. After the diffusion of the Si articles into the core, the filler and the flux will be allowed to cool and solidify and a metallurgical bond will be formed.

Table 2-9 Composition of cladding alloy for brazing (element in wt %) [1]

Brazing Sheet composition	**Elements in wt.%**								
	Cu	Fe	Mg	Mn	Ni	Si	Ti	Zn	Sr
Lower limit	0.05	0.05	***	***	***	3	0.01	***	0.005
Upper Limit	1.0	0.5	1.5	1	2.5	15	0.15	7	0.05

2.4.1 Characteristics and uses of brazing sheets

The ability of the filler material to form fillets is one of the major properties that is expected of a brazing material. The brazing material is expected not to buckle at elevated temperatures and should have good heat transfer characteristics, *e.g.* being able to dissipate heat quickly. The brazing material is used to form heat exchangers and radiators, thus the sheets need also to be corrosion resistant [23].

2.5 Surface Topography

The surface preparation technique of the core and the clad before roll bonding plays a major role in bond formation. The surface topography is the deflection of the surface from the local plane. The material surface topography affects the quality of the metallurgical bond that is formed. They are several ways to alter the surface of materials in order to achieve the required surface topography. Lapping, etching, grinding, polishing and penning are some of the methods applied in modern industry [24]. Surface roughness and surface waviness are the principal causes of concern when dealing with surface characterisation or surface topography. Irregularities along the predominant surface pattern in terms of height can be described as surface roughness, while surface waviness implies surface irregularities at a wider spacing than surface roughness [24].

2.5.1 Surface Characterisation Techniques

Table 2-10 shows the techniques used to determine the surface topography of various materials. The technique used on a particular material is dependent on its surface condition. Either contact

or non-contact techniques can be implemented but the aim is always to achieve highly accurate results without in any way deforming the surface of the material.

Table 2-10 Overview of surface characterisation technique [24]

Technique	Description	Vertical Resolution
Atomic Force Microscopy	The AFM is able to perform friction force imaging, topography imaging and also surface profilometry [24]. The AFM can function in different modes, *viz.* contact mode, tapping mode and non-contact mode. The softness of the sample and the required resolution determine the mode to be used. Soft materials usually require the non-contact mode as this does not deform the material or achieve distorted results. Harder materials would require either the contact or the tapping mode.	<0.03 – 0.05nm
Confocal Microscopy	This technique focuses a laser beam on the surface of the sample to obtain 2D and 3D morphology images, as well as topography images [24].	> 0.1nm
Optical Interferometry	This technique involves the focusing of a beam of light on the surface of a given sample, using lenses. The surface topography imaging comes from the ability of the material to reflect the beam of light that has been focused on it. This technique produces 2D and 3D images of the surfaces, as well as topography images [25].	>0.1nm

2.6 Cladding

The application of a material over another material to improve surface dependent properties and to enhance bulk dependant properties can be termed “cladding” [26]. There are various methods used for cladding in the aluminium industry, *e.g.* strip cladding, roll bonding or welding [26].

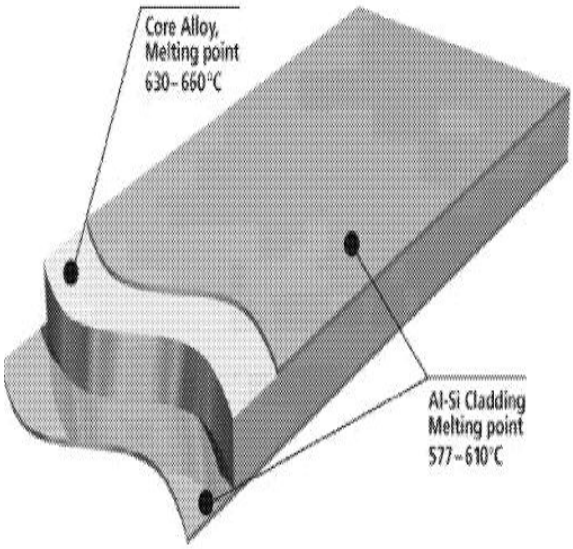

Figure 2-4 An illustration of cladding [1]

2.6.1 Strip cladding

This is a fusion welding technique where the strip welding material is deposited at a high rate on to the component in order to achieve a corrosion resistant surface [27]. It is highly appropriate in the case of large and thick components. Nuclear power plants make use of this type of cladding in their operations since it protects specific components from corrosion more effectively than do other cladding methods.

2.6.2 Roll bonding

Roll bonding is a solid-state joining method. It makes use of plastic deformation of the core and the clad to produce a single material of ultra-fine mechanical structure [2]. There are several key controlling variables that need to be considered during roll bonding. These include the grain size of the core material, thickness reduction, surface roughness, applied pressure, rolling temperature, preheat temperature, annealing temperature and the coefficient friction between the material and the roller [28]. To investigate the effect of one variable, all the other factors must be kept constant. Before rolling occurs, the materials must undergo several surface preparation processes in order to achieve appropriate final surface conditions. The materials are preheated to a certain temperature, hot rolled and cold rolled to the final gauge.

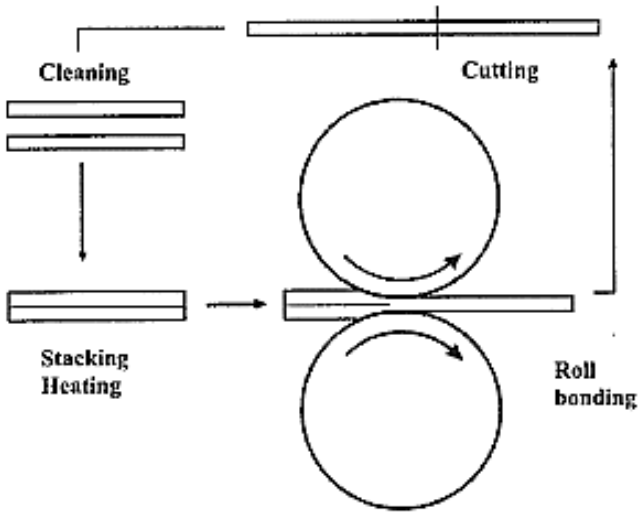

Figure 2-5 Schematic process of Roll Bonding [2]

In roll bonding three pieces of material (one for the core and two for the clad) are first cleaned to remove any impurities on their surfaces before roll bonding is commenced. Care is taken not to alter the quality of the product. The materials to be bonded are stacked and heated and then roll bonding is commenced [2]. The process is repeated until the required thickness of the product is achieved. In ARB, after every cycle there is a 50% reduction in the thickness of the materials that are roll bonded. In order to achieve the required thickness, ARB is based upon Equations 2-1 and 2-2 below, where t_0 is the initial thickness and t_n is the thickness of a layer after *n* cycles, where there is a 50% reduction in thickness after every cycle.

$$t_n = \frac{t_0}{2} \qquad \text{2-1 [1]}$$

Thus, total reduction will be

$$= t_0 - \frac{t_0}{2} \qquad \text{2-2 [2]}$$

Cold roll bonding is performed at room temperature, while hot roll bonding occurs at higher temperatures. The optimum conditions for roll bonding are determined by the materials involved, since materials have different chemical and physical properties and respond differently to heat and stress. The scope of this thesis focuses on controlling the variables during the roll bonding process, with particular reference to surface condition, *i.e.* surface roughness and surface contamination. There have been several attempts to explain the solid state joining of two materials, the most prevalent being the Thin Film Theory and the Diffusion Bonding Theory. It is now generally accepted that solid state bonding is dependent on a

combination of the above two processes, because they have been found to occur simultaneously and, furthermore, are dependent on the same variables. Diffusion bonding is caused by a concentration gradient that emerges when the two materials to be bonded are brought together at high pressure and temperature [28]. Diffusion of atoms from one material to another across the bond interface occurs because of cohesion and adhesion of atoms. The atoms of the bonding elements are brought together in a way that alters the equilibrium distance between them, this resulting in the atoms attracting and hence forming a bond [29]. The Thin Film Theory involves the exposure of virgin material when the two materials to be bonded are compressed at high temperature and pressure [30]. The extruded virgin material will merge and form a weld. Surface condition is a major concern prior to ARB since it determines the bond strength between the clad and the core. This research focuses on the surface condition of the materials before roll bonding to determine the optimum conditions in the achievement of good bond strength.

There are quantitative and qualitative experiments that can be conducted to determine bond strength. Quantitative experimentation involves the collecting of *data* that can be used to evaluate bond strength. Qualitative experimentation focuses on the analysis of the microstructure of the brazing material, using Light Microscopy (LMS), Scanning Electron Microscopy (SEM) and Energy-Dispersive X-ray spectroscopy (EDS). Important considerations pertaining to surface condition prior to ARB are explained below:

2.6.2.1 Surface roughness R_a

The surface roughness of both the core and the clad is of great significance before roll bonding can commence. This is because a higher frictional coefficient tends to produce a metallurgical bond between the core and the clad with a much greater bond strength. This is due to the fact that a rough surface has many surface asperities [30]. According to the Thin Film Theory, when the two surfaces of a clad and a core are brought together at a certain pressure and temperature, the micro particles at the surfaces of the materials tend to expand and break up, leaving a nascent underlying surface. Further rolling (according to the ARB Theory) will then cause the nascent region to extrude through the cracks formed in the surface layers. As the extruding continues through the cracks, the extrusions will merge and form the metallurgical bond [30]. Thus, ARB is a repeated process that continues until the required thickness has been achieved.

According to the Thin Film Theory, there are many mechanical methods that can be used to improve the surface roughness of the core and the clad [2]. These have not been adequately

explored at Hulamin, where, currently, only the time-consuming scalping method is used to improve surface condition. This results in very smooth finishes but there is, in fact, no hard evidence that such finishes are desirable. The practice was started on the advice of another rolling manufacturer and was never interrogated. This mechanical method does successfully remove the surface oxides formulated during casting, making the surface uniform. At the same time, some surface asperities are created, which are required for bonding [31]. The question here is what range of surface roughnesses would create significantly more surface asperities to optimise bond strength, while also ascertaining the point at which the bond strength could be compromised. When two metals are rolled together there is a certain threshold surface roughness that yields high shear stress and once this threshold is exceeded the shear bond strength tends to decrease [32]. Little work has been done to determine the reason why the bond strength decreases when the surface roughness is increased beyond the optimal range, but some researchers attribute this to the voids that are introduced at the interface of the bond. This causes the formation of delamination areas and the presence of these delamination areas in turn causes strain localisation, leading to bond weakness [33].

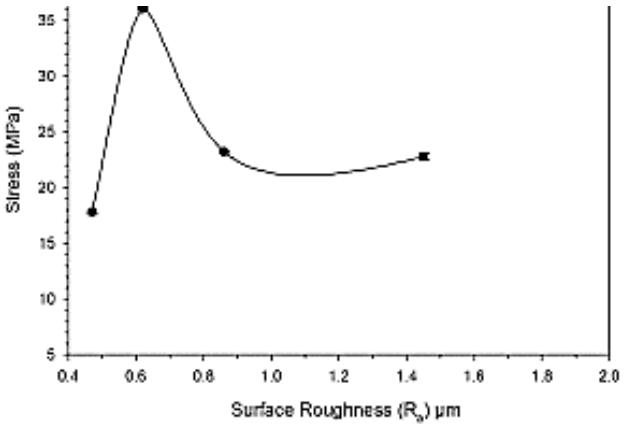

Figure 2-6 The variation of the stress with the surface roughness after cladding AA7075 with AISI 1080 steel [32]

2.6.2.2 Surface contamination

The use of degreasers is always implemented as a way to remove foreign contamination found on the surface of both the core and the clad [34]. The main aim is to mitigate interference with the surface aspirities when they merge during roll bonding [2].

2.6.2.3 Oxide films

Aluminium alloys tend to have a thick oxide layer on the surface of the metal. Studies have shown that the presence of a thicker oxide film on the surface tends to interfere with the

formation of the nascent region [2]. This interference leads to weaker bond strength between the core and the clad. It is suggested that roughening the surface breaks down the continuous layer of surface oxide, hence promoting bond formation. In addition, the presence of these surface oxides results in voids and cracks at the interface, which lead to areas of delamination [29]. Most companies utilise mechanical scalping of the surface of both the core and the clad as the way to reduce the oxide layer thickness and also improve the surface roughness of the core.

Table 2-11 Effects of improving surface conditions [34]

Task	Bond Strength	Reason
Degreasing	Enhanced	No foreign interference will interfere with the surface asperities
Electro polishing	No bonding	Absence of surface asperities
Machining	Enhanced	Promotes formation of surface asperities

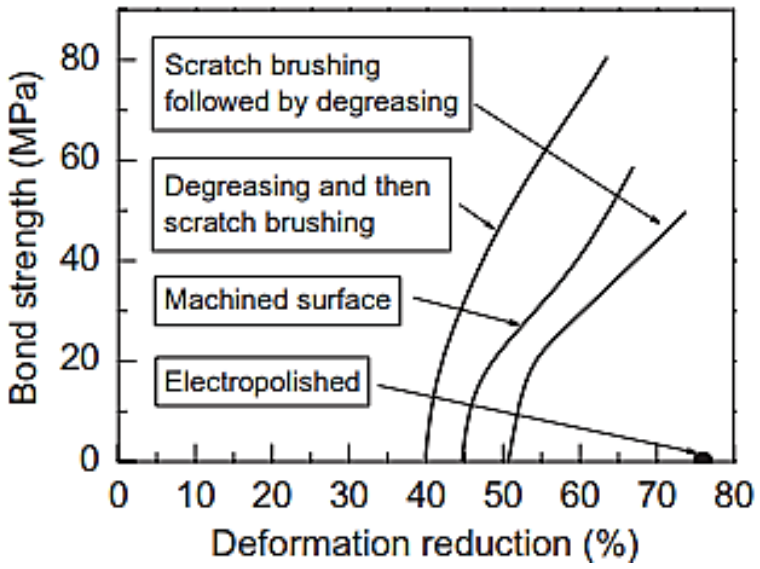

Figure 2-7 Deformation against bond strength for Aluminium alloys [34]

2.7 Plane Strain Compression (PSC)

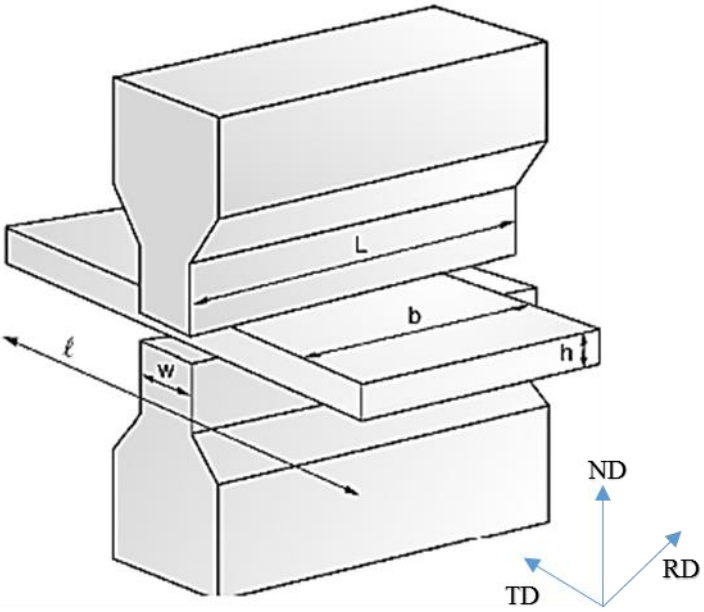

Figure 2-8 PSC gleeble 3800 setup [35]

A laboratory setup has been developed to simulate the industrial hot roll bonding method using the Gleeble 3800. The flow of stress in roll bonding can be determined using PSC [36]. The principle of the Gleeble 3800 uses electrical resistive heating to reach the target deformation temperature and the use of hydraulics to exert pressure/deformation load on the samples. During roll bonding, deformation occurs on two planes, the rolling plane and the normal plane. The same concept is used during the PSC tests on the Gleeble 3800. The samples of the PSC need to be designed according to [37] to have reliable and repeatable experimental results. The rolling direction (RD) is measured along the length direction of the anvil, the normal direction (ND) is measured along the thickness direction of the sample and the transverse direction (TD) is measured along the breadth of the sample. The most important conditions that need to be followed are governed by Equation 2-3 and Equation 2-4 [2]. Note that L is the length of the anvils, b is the breadth of the sample, h is the thickness of the sample and l is the length of the sample.

$$\frac{L}{b} > (6 - 10) \qquad \text{2-3 [35]}$$

Great caution is required if the deformation is to be homogenous between the anvils. It is necessary to conform strictly to the ratio shown in Equation 2-4.

$$\frac{b}{h} = (2 - 4) \qquad \text{2-4 [35]}$$

Table 2-12 PSC ratios [35]

Ratio	Range	Interpretation
$\frac{b}{h}$	Less than 2	The sample is too thin
$\frac{b}{h}$	Greater than 4	The sample is too thick

The standard specimen dimensions for PSC testing are 30 mm × 20 mm × 10 mm. The temperature gradient is controlled by the thermocouples attached to the samples. During deformation, the true strain is defined by Equation 2-5.

$$\varepsilon = In\frac{h}{h_o} \qquad 2\text{-}5\ [35]$$

where h is the initial height and h_o is the final height of the specimen after PSC. The resulting stress σ will be governed by Equation 2-6, where F is the applied force and $l \times b$ is the surface area.

$$\sigma = \frac{F}{l \times b} \qquad 2\text{-}6\ [35]$$

2.7.1 Friction correction

During PSC, the anvils come into contact with the sample to cause deformation. The friction that exists between the points of contact can be determined from three conditions. The friction can be sliding friction, sticky friction or a combination of the two. These conditions arise because of different situations during the test. The force exerted by the anvils on a sample results in a shear stress induced in the sample. When the coulomb friction is constant, that condition is known as sliding friction, while sticky friction occurs when the shear pure stress in the sample is equal to the stress at the point of contact [37]. Equation 2-7 analyses the average pressure exerted by the anvils on the samples under the sliding friction condition.

$$\frac{\sigma}{2k} = \frac{h}{\mu w}\left[e^{\frac{\mu b}{h}} - 1\right] \qquad 2\text{-}7\ [35]$$

where k is the shear flow stress, w is the width of the anvils and μ is the coefficient of friction.

The average pressure exerted on the anvils under sticky friction can be described and is shown by Equation 2-8.

$$\frac{\sigma}{2k} = 1 + \frac{b}{4h} \qquad \text{2-8 [37]}$$

A situation can also occur where sticky friction and sliding friction coexist at the point of contact of the anvil and the sample, with a resultant change in friction, but this does not occur throughout the surface of the anvil. The position where friction changes is termed as z_0. When sliding friction and sticky friction coexist, z_0 is determined by Equation 2-9.

$$z_0 = \left(\frac{h}{2\mu}\right) ln\left(\frac{1}{2\mu}\right) \qquad \text{2-9 [37]}$$

According to [37], if $2z_0 > w$, the deformation will occur under sliding friction conditions, and if $w > 2z_0 > 0$, the deformation will occur under partial sticky friction and then under sticky friction, $0 > 2z_0$. These conditions result in different strain rates during deformation.

$$\varepsilon_{sticky} = V\left[\frac{2}{D(h-h_0)}\right]^{0.5} ln\frac{h}{h_0} \qquad \text{2-10 [38]}$$

$$\varepsilon_{slide} = \frac{V}{b_0}\left[\frac{2(h-h_0}{D}\right]^{0.5} \qquad \text{2-11 [38]}$$

2.8 Comparison of techniques to determine bond strength

After roll bonding, there are several techniques that can be implemented to evaluate the quality of the bond strength between two bonded metals. Destructive and non-destructive techniques are used for this purpose. However, most studies have proved that destructive tests are the more efficacious in determining bond strength. A comparison of the techniques that can be implemented is presented below.

2.8.1 Tensile Shear Test

To be able to determine the strength of a metallurgical bond formed between two materials, either dissimilar or similar, the bond should be subjected to a tensile shear test. Rectangular specimens are obtained from the bonded specimen and prepared according to ASTM D3165. Notches are engraved on to the surface of the specimen to prevent deformation of the bond owing to bending [39]. The specimen geometry is according to Figure 2-9. The spaces between the notches determine the shear zone.

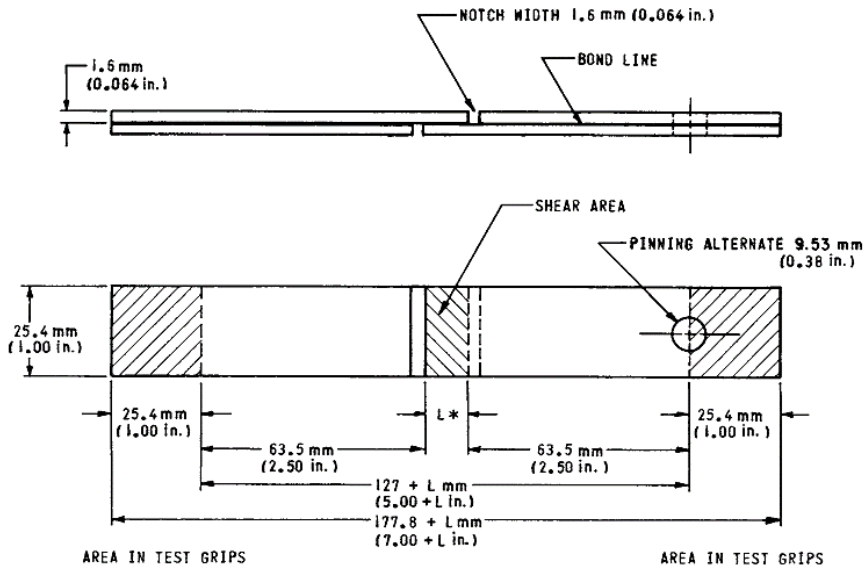

Figure 2-9 Tensile shear test specimen [39]

2.8.2 Lap shear test

This technique is widely used in determining the shear strength, creep and thermal fatigue of a bond when two materials have been soldered together at an offset [40]. The lap shear test evaluates the strength of the bond when the two materials are being pulled in opposite directions. The bond strength is usually denoted by dividing the axial load by the area of contact (solder joint).

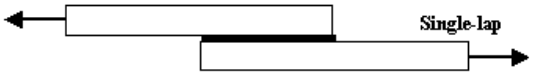

Figure 2-10 Shear tests specimens [40]

2.8.3 Peel test

The peel test is another technique of determining the shear strength of a bond between two dissimilar or similar materials. The specimens are designed according to Figure 2-11, where the unbonded section is the one that is clamped in the grips and pulled apart [41]. An autograph recording is done as the test is carried out so that the average peel strength is determined.

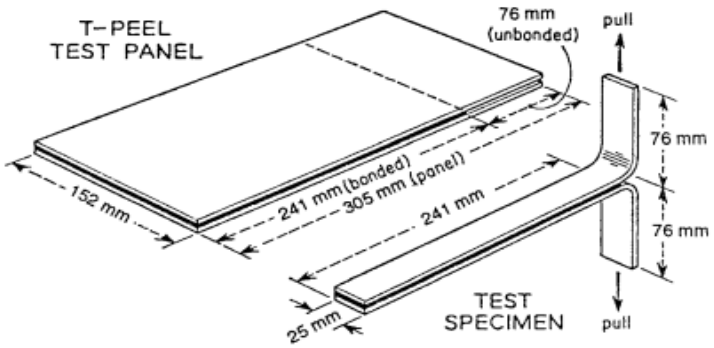

Figure 2-11 A more detailed Peel test experimental setup [41]

2.8.4 Digital Image Correlation (DIC)

This technique uses the analysis of high-resolution images taken prior to and after a tensile shear test is performed. It uses the concept of finite element analysis to analyse the distribution of the strain across a bond interface. It must be noted that while extensometers give point wise *data*, DIC gives a whole range of point wise inspection across the entire bonded interface [42]. It is therefore preferable. To obtain satisfactory results a speckle pattern is applied before the test is run on the sample. A beam of light will be focused on the sample during the test to determine the movement of the speckles. An analysis of the before-and-after images provides a satisfactory strain map of the bonded region [43].

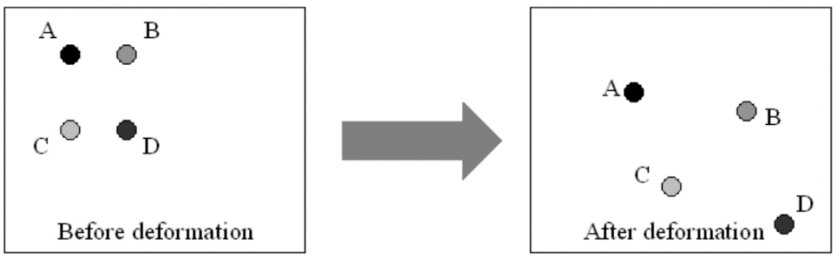

Figure 2-12 DIC concept [43]

The DIC software analyses the distance between the final and initial positions and correlates to the material properties, *e.g.* stress and strain. With the specimen shown in Figure 2-13, the indicated area is the main area of interest, from which the points on the strain map will be obtained.

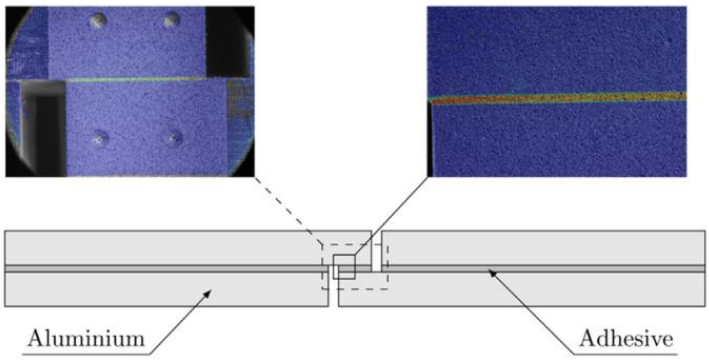

Figure 2-13 The two measuring areas of a tensile shear test specimen [42]

2.8.4.1.1 FEM Techniques in conjunction with the DIC

The DIC produced strain map distributions at the interfaces between clad and core, thereby providing results that were more meaningful. The tensile shear tests on the Zwick when run in conjunction with Dante Dynamic, with a 2D setup. The results analysed using ISTRA 4D software. During the tensile testing, the load is applied axially along the length of each specimen, this resulting in axial stresses and strains being induced in each specimen. When a small element in a material is subjected to uniaxial loading, the stress and strain distribution can be described using the Von Mises Theory. This theory states that when maximum shear energy in a system is equal to the yield point during the tensile test, failure will occur [52]. The samples for this research were designed according to ASTM D3165 and in all these samples the induced notches resulted in the strain localising in the shear region. The DIC could identify the x, y displacement, the Lagrange Shear strain and the Engineering Principal Strain across the bond interfaces of all tested samples.

The Von Mises Theory is illustrated in Figures 2.14 and Figures 2.15

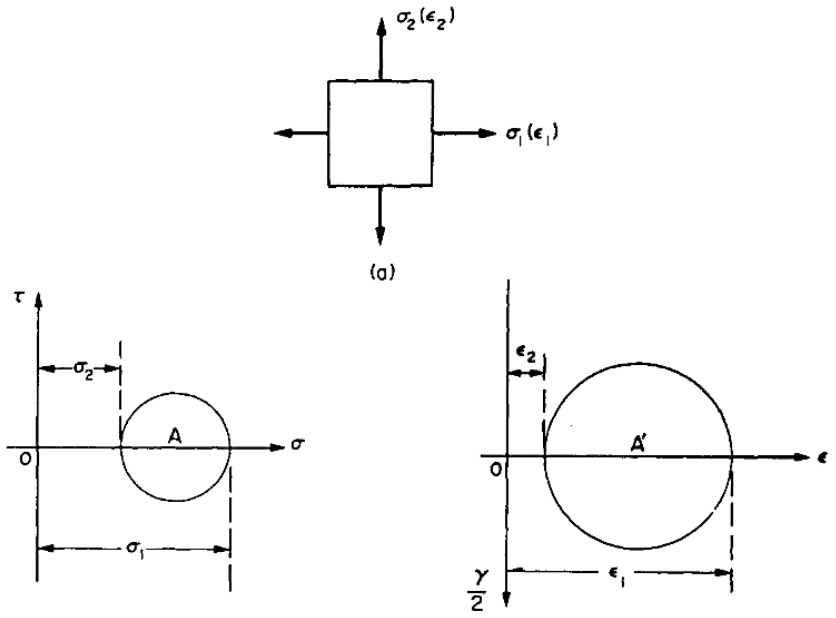

Figure 2-14 Stress, strain relationship [52]

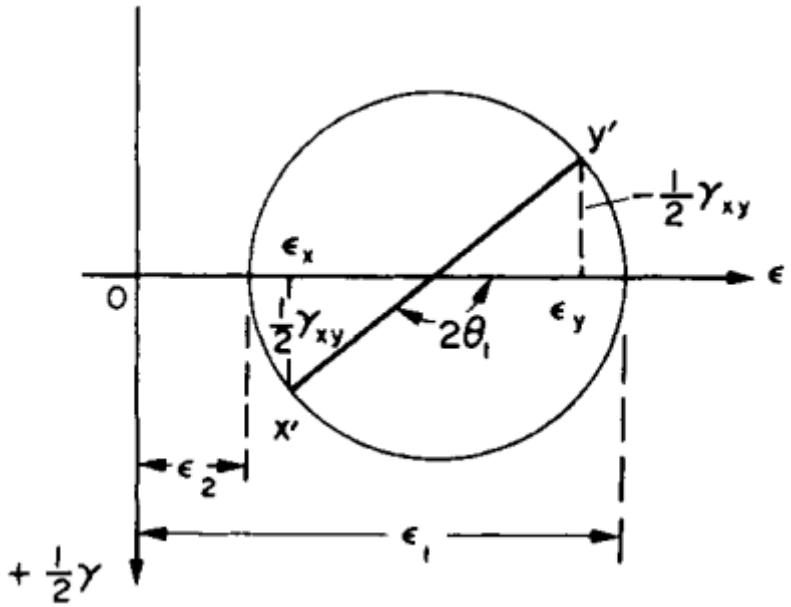

Figure 2-15 Strain Mohr circle in detail [1]

The Von Mises theory can be expressed by means of an equation where the maximum shear stress is denoted by Equation 2-12 below:

$$\frac{1}{2}\gamma_{max} = \pm\frac{1}{2}\left\{\left[\varepsilon_x - \varepsilon_y{}^2\right] + \gamma_{xy}{}^2\right\}^{\frac{1}{2}} \qquad \text{2-12 [52]}$$

where γ_{max} is the maximum shear strain that the material can withstand before failure, ε_x is the principal shear strain in the x, direction, ε_y is the principal shear strain in the y-y direction and γ_{xy} is the shear strain in the xy-xy direction.

2.9 Microstructural Features

2.9.1 Bond quality

After the formation of the metallurgical bond through roll bonding, the quality of the bond can also be analysed through microscopic examination. The interface between the two materials is the main area of interest. As mentioned previously, surface preparation plays a major role in the bond strength and rougher surfaces tend to produce stronger bonds. A good bond is supposed to have a fine interface that shows no signs of porosity or delamination [44]. Delamination at the interface leads to strain localisation at that point [33]. A good quality bond is represented by Figure 2-16 (a) and a poor bond is seen in Figure 2-16 (b) [33].

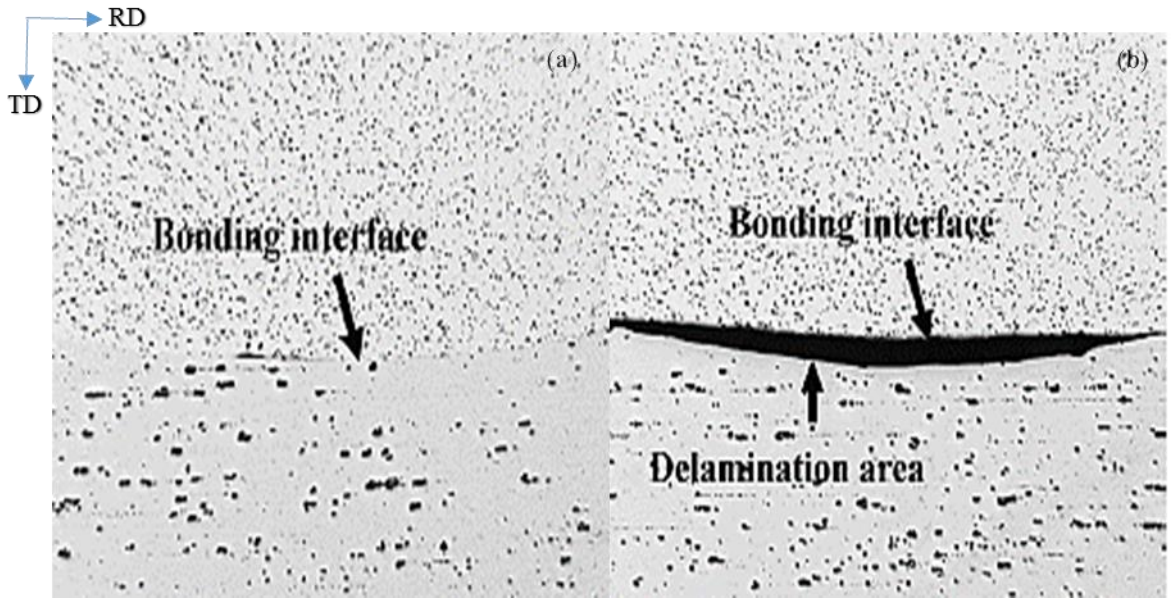

Figure 2-16 Cross section view of the bonding interface of two different bonds [33]

3 EXPERIMENTAL METHOD

3.1 Experimental methodology

This section describes the experimental methodology used to investigate the effect of surface roughness on bond strength during the roll bonding of AA3003 H-14 (core) and AA4045 (clad). As stated previously, the surface finish of the core at Hulamin is kept at 10 µm, while the surface finish of the clad is kept at 1 µm. During the course of the experimentation, the surface finishes of both the core and the clad were altered to provide a range of finishes, in order to determine the best surface finish for each material that would result in the strongest bond. All mechanical testing of the strength of the various combinations was based on the tensile shear test, according to the ASTM D3165, this in conjunction with Digital Image Correlation (DIC). In each case, the DIC was used to determine the map of strain across the interface of the two bonded materials. SEM micrographs of the bond interface were taken to analyse the bond quality, *i.e*. porosity and the presence of voids. A correlation was performed to validate the results obtained from the DIC with the SEM micrographs and a surface condition that yielded better bond strength was proposed.

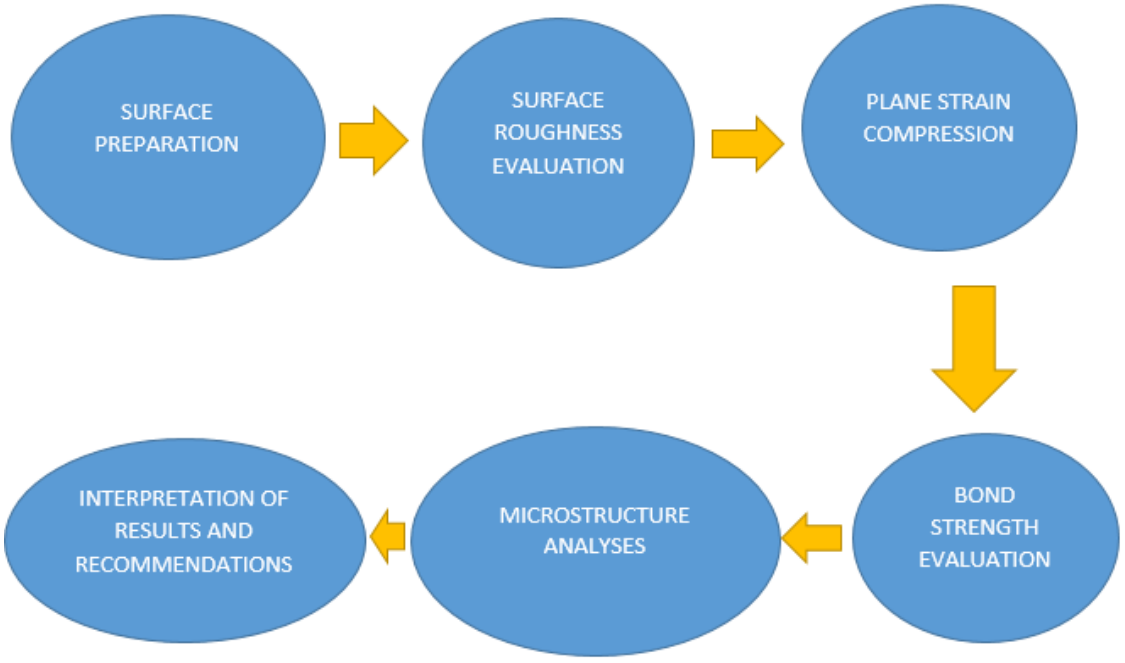

Figure 3-1 Experimental layout

3.2 Materials to be investigated

3.2.1 AA3003/ 9031 H-14

The A4-sized, as cast block of AA3003 H-14 was supplied by the manufacturer, Hulamin. Smaller rectangular blocks were cut from this block that conformed to the PSC dimensions. The properties of the material are listed below in Table 3-1.

Table 3-1 Chemical composition of the investigated AA3003 H-14 obtained from Hulamin data sheets [10]

W %	Si	Fe	Cu	Mn	Mg	Cr	Zn	Ti
Min	-	-	0.05	1.0				
Max	0.6	0.7	0.2	1.5	-	-	0.1	-

Table 3-2 Mechanical properties of the investigated AA3003 - H14 obtained from Hulamin data sheets [10]

Temper	Thickness (mm)	Yield Strength (MPa)	Ultimate Tensile Strength (MPa)
H14	0.63-1.2	115	140-180
	>1.2-6.3	115	140-180
	>6.3-25.0	115	140-180

Table 3-3 Physical properties of the investigated AA3003-H14 obtained from Hulamin data sheets [10]

Property	Value	Unit
Density	2.73	gcm^{-3}
Melting Point	640-655	ºC
Thermal Conductivity	159	W/mK
Thermal Expansion	23×10^{-6}	/ºC
Resistivity	42	nΩ.m
Modulus of Elasticity	69	GPa
Modulus of Rigidity	26.1	GPa

3.2.2 AA4045

The A4 block of AA4045 was received from Hulamin in liner condition prior to rolling. The liner plate had been homogenised and had undergone several rolling passes and was thus ready for roll bonding with the core, AA3003.

Table 3-4 Chemical composition of the investigated AA4045 obtained from Hulamin data sheets [45]

W %	Si	Fe	Cu	Mn	Mg	Cr	Zn	Ti
Min	9	-	-	-	-	-		
Max	11	0.8	0.3	0.05	0.05	-	0.1	0.02

Table 3-5 Physical properties of the investigated AA4045 obtained from the Hulamin data sheets [45]

Property	Value	Unit
Density	2.67	gcm^{-3}
Melting Point	573.9-599	ºC
Thermal Conductivity	171	W/mK
Thermal Expansion	23×10^{-6}	/ºC
Resistivity	38.2	nΩ.m

Figure 3-2 A4 block of AA 4045 as received in liner condition

3.3 Equipment used

3.3.1 Surface preparation

- Manual polisher
- Grits (-Grinding paper-)
- Hot mounter
- Automatic polisher

3.3.2 Materials used

- A4 block of AA3003 H-14 core
- A4 block of AA4045 clad

3.3.3 PSC

The Gleeble 3800 is able to perform multiple hits on a test sample at a set strain rate and temperature. The set temperature is achieved only through direct resistive heating. Monitoring of the temperature gradient during the whole process is done by thermocouples attached to the samples before running the test to maintain the temperature gradient in the experiment.

3.3.4 Tensile shear tests

- Zwick Tensile testing machine
- Digital Image Correlation (by Dante Dynamics)

3.3.5 Microstructure Analysis

- Struers Labopress Hot mounter
- Struers Manual polisher
- Struers automatic polishing machine with diamond lubricants and OP-S
- Barkers anodising solution (- $2\% HBF_4$ in distilled water -)
- ZEIS Light microscope
- FEI Nova Nano SEM

3.4 Design Matrix

The stipulated design matrix is shown below in Tables 3-6 and 3-7 and was based on the set surface finishes, as obtained from Hulamin (core at 10 µm/clad at 1 µm). The micron sizes had to be converted into the American grit sizes.

Table 3-6 American Standard Grit sizes [46]

Grit Size	Micron	Appropriate Grit Size
800	25	800
1200	15	1200
1800	10	2000
2800	7	2400

Table 3-7 Design Matrix

Plate Clad Roughness (AA4045)		$R_{ave\ 0.5}$	$R_{ave\ 1.0}$	$R_{ave\ 3.0}$	$R_{ave\ 7.0}$
Core Roughness (AA3003 H-14)	$R_{ave\ 7}$	✓	✓	✓	
	$R_{ave\ 10.0}$	✓	✓	✓	✓
	$R_{ave\ 15.0}$	✓	✓	✓	
	$R_{ave\ 25.0}$	✓	✓	✓	

3.5 Surface Preparation of the samples

Surfaces of the samples were prepared according to the design matrix shown in Table 3-7.

3.5.1 Surface roughness R_a preparation of AA3003 H-14 (Core)

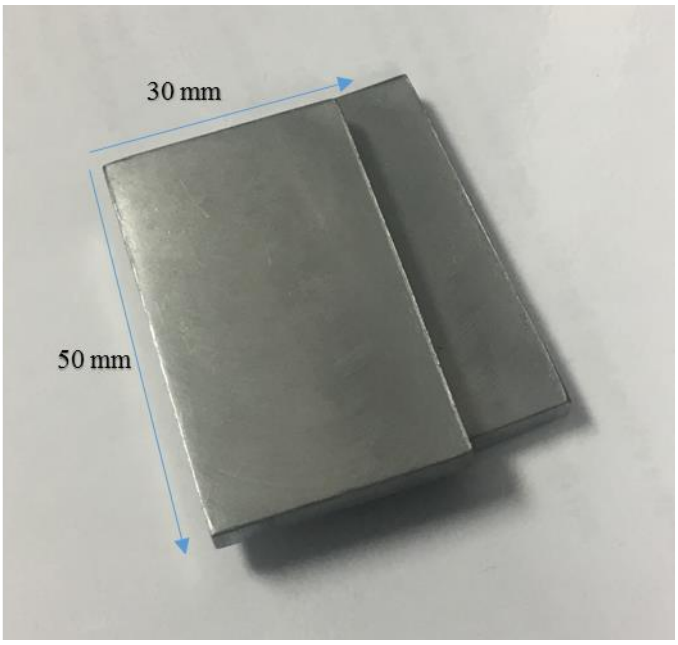

Figure 3-3 50 mm by 30 mm by 5 mm block of AA3003-H14 awaiting surface preparation

i. Thirty-nine samples, each with dimensions of 50 mm × 30 mm × 5 mm, were cut from the A4 as cast block of AA3003 (See Figure 3-3 above).
ii. For nine of these 39 samples, the RD sides that would be in contact with the anvils were ground in one direction on 1200 grit paper and the RD sides that would not be in contact with the anvils were ground in one direction on 800 grit paper.
iii. The nine samples were then degreased using acetone and dried to remove any contamination.
iv. The process was repeated with a further 12 samples, but instead of 800 grit, 2000 grit paper was used.
v. Then the process was repeated with a further nine samples, but instead off 2000 grit, 1200 grit paper was used.
vi. The process was then repeated with a further nine samples, but instead off 1200 grit, 2400 grit paper was used.
vii. After cleaning, each set of samples was stored in a labelled desiccant to await the PSC tests.

3.5.2 Surface roughness R_a preparation of AA4045 (Clad)

i. In the same way as above, 39 samples, each with dimensions of 50 mm × 30 mm × 5 mm, were cut from the A4 liner plate of AA4045.
ii. For nine of these 39 samples, the RD sides that would be in contact with the anvils were ground in one direction on 1200 grit paper and the RD sides that would not be in contact with the anvils were polished in one direction with 3 µm Diamond paste.
iii. The samples were put in an alcohol bath for a few minutes and then dried.
iv. The process was repeated with a further nine samples, but instead of 3 µm Diamond paste, 1 µm Diamond paste was used.
v. The process was repeated with a further nine samples, but instead of 1 µm Diamond paste, .5 µm Diamond paste was used.
vi. Then the process was repeated with a further 12 samples, but instead of .5 µm Diamond paste, they were ground on the non-anvil side in one direction on 2400 grit paper.
vii. After cleaning, each set of samples was stored in a labelled desiccant to await the PSC tests.

3.6 Preparation for Hot Plan Strain Compression

3.6.1 PSC Geometry

Roll bonding simulation is performed to combine two materials to simulate the industrial roll bonding of the brazing sheet. As mentioned in the literature, the rolling process in the manufacture of brazing sheet has a lot of variables that influence the quality of the bond formed between clad and core [2]. In industry, the clad and the core material undergo surface preparation before roll bonding. The clad liner is stacked on top of the core, since it is lighter, and then it goes through a hot furnace. The stacked material then goes through a rolling mill where it is reduced in thickness until it reaches the desired gauge. The same rolling process can be simulated on a Gleeble 3800 in the laboratory at the University of Cape Town, Centre for Materials. As mentioned in the literature, the rolling process variables play a critical role in the bond formed between the clad and the core layers. The only variable in these simulated tests is the surface condition. Therefore, the reduction ratio, deformation force, strain rate and deformation temperature were kept constant in every test performed on the Gleeble 3800. (See Figure 3-4 for attachment of thermoucples for temperature control.)

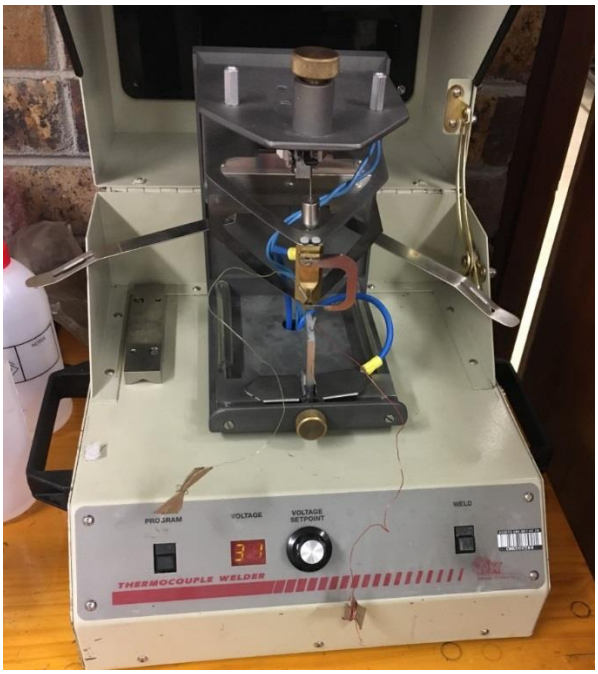

Figure 3-4 Spot welding of the thermocouples done at 31V

Table 3-8 Recommendation geometry as stated by the good practice guide [37]

Title	Symbol	Relationship	Permissible Value	Preferred Value
Length ratio	l_r	$\frac{l}{p}$	≥ 3	3
Breadth ratio	b_r	$\frac{b}{p}$	≥ 2	5
Height ratio	h_r	$\frac{p}{t}$	≥ 1.5	1.5

Modifications to the samples were done so that they satisfied the conditions stated in Table 3-9. The modified anvils were made at the UCT Mechanical Engineering workshop from steel M300. (See Figure 3-5 below.) The anvils went through heat treatment in a furnace at 1000ºC for 30 minutes. The anvils were quenched in oil and then tempered at 600ºC. This brought the hardness of the anvils to 47HV. The samples and the anvils had the dimensions specified in Table 3-10.

Table 3-9 Geometry of the anvils and the samples modified according to the [37]

Title	Symbols	Value
Anvil length	A_l	70 mm
Anvil width	p	13 mm
Width of sample	b	50 mm
Length of sample	l	30 mm
Thickness of sample	t	10 mm
Breadth ratio	b_r	3.85
Length ratio	l_r	2.3
Height ratio	h_r	1.3

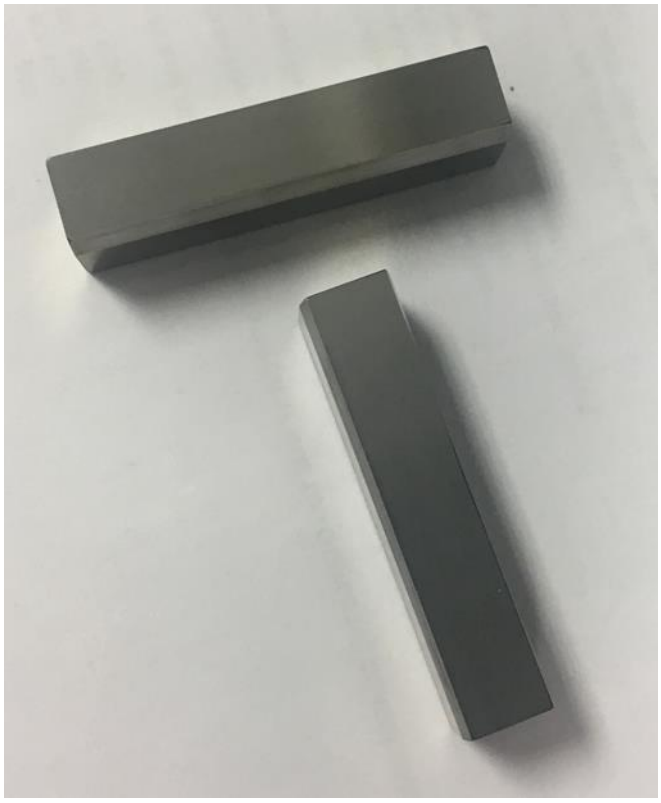

Figure 3-5 PSC anvils designed according to [37]

3.6.2 Hulamin Log mill parameters

The log mill parameters from Hulamin were used to determine the parameters to be used for FEM and also for the hot PSC.

Table 3-10 Hulamin Mill Log *data*

Pass	**Initial Gauge**	**Final Gauge**	**Change in Gauge**	**Gauge Reduction**	**True Strain**	**Mill Speed**	**Roll Diameter**
	T_i (mm)	T_f (mm)	Δt (mm)	% redu	ε	V (ms^{-1})	m
1	0.569	0.568	0.002	0.292	-0.003	30	0.89
2	0.568	0.565	0.003	0.493	-0.005	30	0.89
3	0.565	0.561	0.004	0.673	-0.007	30	0.89
4	0.561	0.556	0.005	0.820	-0.008	30	0.89
5	0.556	0.550	0.006	1.061	-0.011	147	0.89
6	0.550	0.542	0.008	1.453	-0.016	147	0.89
7	0.542	0.530	0.012	2.212	-0.022	147	0.89
8	0.530	0.515	0.015	2.827	-0.029	147	0.89
9	0.515	0.496	0.019	3.717	-0.038	147	0.89

True strain is calculated according to Equation 3-1.

$$\varepsilon = ln\frac{t_f}{t} \qquad 3\text{-}1\ [35]$$

It is also shown in the literature that PSC occurs either under sticky friction or under sliding friction. This results in different strain rates for each condition. The strain rates are calculated using Equation 3-2 (sticky friction) and Equation 3-3 (sliding friction), using the information given in Table 3-11 below.

$$\varepsilon_{stick} = V[\frac{2}{D(t-t_f)}]^{0.5} ln\frac{t}{t_f} \qquad 3\text{-}2\ [38]$$

$$\varepsilon_{slide} = \frac{V}{b_0}[\frac{2(t-t_f}{D}]^{0.5} \qquad 3\text{-}3\ [38]$$

Table 3-11 Strain rate calculations for sticky friction and at sliding friction conditions at Hulamin for a deformation temperature of 504 °C

Pass	$\boldsymbol{\varepsilon_{stick}}$	$\boldsymbol{\varepsilon_{slide}}$	**Def Force**
	s^{-1}	s^{-1}	MN
1	4.565	3.223	3.476
2	5.495	4.193	2.752
3	6.966	4.909	6.174
4	7.722	5.438	7.537
5	8.829	6.209	7.903
6	51.012	35.808	9.938
7	63.643	44.504	10.168
8	72.993	50.881	11.140
9	85.280	59.174	11.443

3.6.2.1 PSC testing parameters

The Hulamin mill log *data* sheet aided in providing information in order for the processing parameters to be closely related to the industrial conditions for the simulations using PSC on the Gleeble 3800. The deformation temperature was set at 450 ºC. The average true strain per pass was set at 0.9. The heating rate was set at 3 ºC per second, thus a time of 150 seconds was taken to reach the deformation temperature. The control thermocouple was attached to the core, since the clad had a lower melting point than the core, owing to the alloying elements

variations. The clad material had a lower melting point of ≈ 574 ºC and a lower resistivity coefficient than the core sample, having a melting point of ≈ 640 ºC [45]. Thermocouples were welded to the samples to monitor the temperature gradient during the test and labelled $TC_{1,}$ and $TC_{2.}$ TC_1 was attached to the core sample while TC_2 was attached to the clad. It was noticed that for every test there was an average temperature gradient of 50 degrees across the sample junction. The interpass time was set at 150 seconds to enable enough time at deformation. The specimens were cooled using air to avoid microstructural changes in the deformed sample. The temperature gradient during the test was guided by the information in [37]. The anvils were insulated with tantalum to avoid localised heating during the testing. After every test the anvils were cleaned to remove any foreign matter that might hinder even direct heating.

Table 3-12 PSC parameters

Condition	**Value**	**Units**
Deformation strain rate	1.5	Sec^{-1}
True Strain	0.9	
Deformation temperature	450	ºC
Deformation Force	3,432	KN
Heating rate	3	ºC Sec^{-1}
Thermocouples	Braided K Type	
Cooling method	Compressed air	
Lubrication	Tantalum	
Materials	Aluminium alloys AA3003 and AA4045	
Geometry	50 ×30×10	mm
Anvil width	13	mm

3.6.3 Finite Element Modelling (FEM)

FEM was used to simulate the flow of stress before the PSC test was performed, using SOLIDWORKS 2018. The parameters were the same as the log mill parameters at Hulamin. (See Table 3-11.) The FEM setup is illustrated in Figure 3-6.

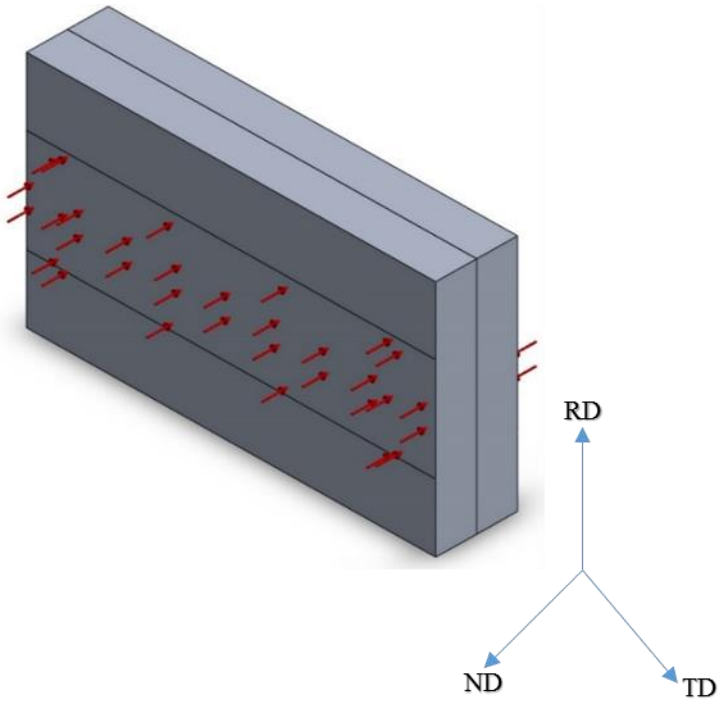

Figure 3-6 Schematic illustration of the FEM setup

The material properties of both the clad and the core used in the FEM analysis are shown in Table 3-13 and Table 3-14.

Table 3-13 3003 Material properties used for FEM obtained from Solidworks Package 2020

	Properties
Mode type of test	Linear Elastic Isotropic
Failure criterion	Max Von Mises Stress
Yield strength	4.13613e+007 N/m^2
Tensile Strength	1.10297e+008 N/m^2
Elastic Modulus	6.9e+010 N/m^2
Poison's ratio	0.33
Mass density	2700 kg/m^3
Shear Modulus	2.7e+010 N/m^2

Table 3-14 4045 Material properties used for FEM obtained from Solidworks Package 2020

	Properties
Mode type	Linear Elastic Isotropic
Failure criterion	Max Von Mises Stress
Yield strength	3.15e+008 N/m^2
Tensile Strength	7.9e+010 N/m^2
Elastic Modulus	7.9e+010 N/m^2

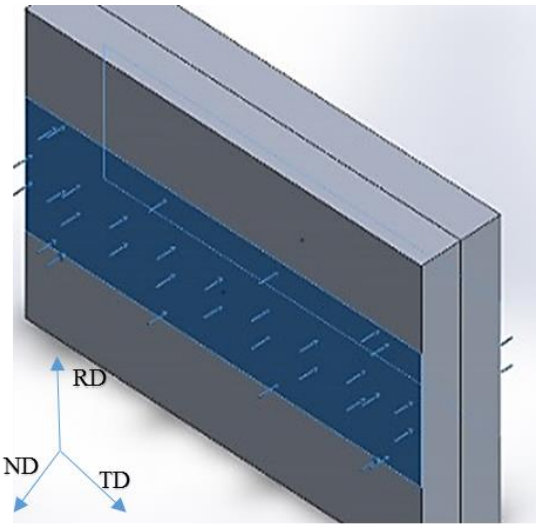

Figure 3-7 Load distribution during the FEM

3.7 Mechanical Characterisation

3.7.1 Shear Bond Strength Evaluation in conjuction with the DIC

In order to quantify the shear bond strength, the PSC samples were wire cut along the TD plane and designed according to ASTM D3165. (See Figures 3-8 and Figure 3-9.)

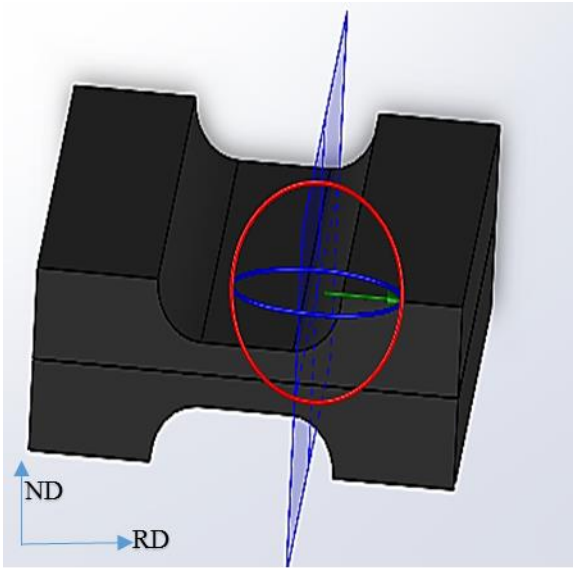

Figure 3-8 Sectioning along the TD of the PSC sample after the PSC test

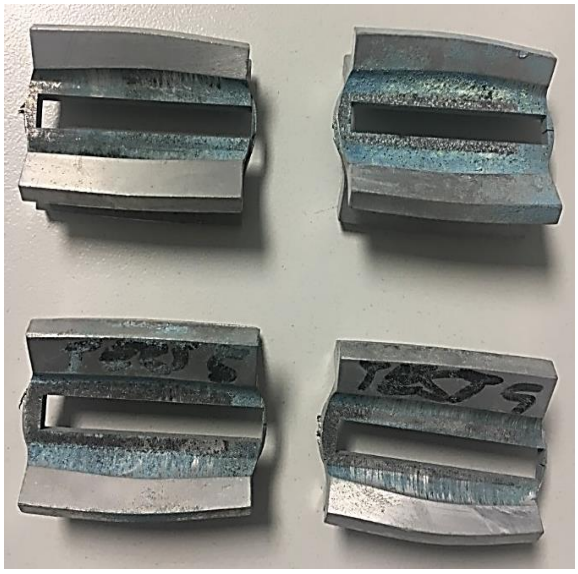

Figure 3-9 PSC samples sectioned along the TD plane

Tensile tests were performed on the Zwick Roel Tensile testing machine, using the 1kN load cell and tensile grips rated at 10kN, with a DIC camera and digital extensometers set up to monitor strain and extension during the test. DIC uses a high-speed camera that takes images during the tests and a correlation is done at the end of the test to relate the initial and final positions of a speckle pattern across the surface of the sample. The samples had to undergo surface preparation before the test was carried out. The samples were degreased using acetone and sprayed with a speckle pattern and left to dry. The speckle pattern is displayed in Figure 3-10.

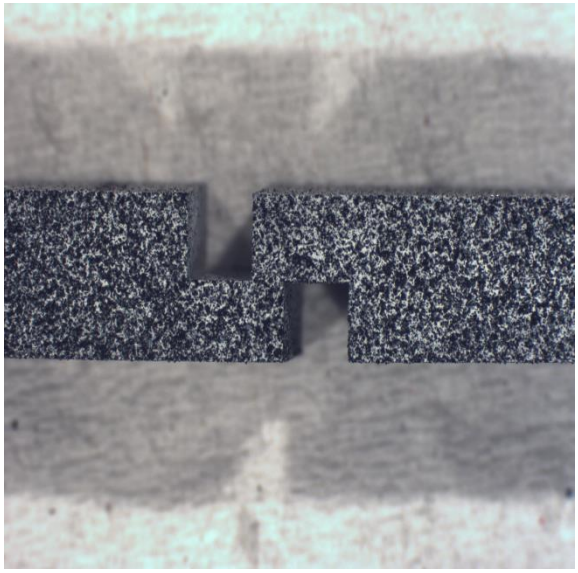

Figure 3-10 One sample after the spraying of the speckle pattern awaiting test

During the loading of samples into the tensile grips, great caution was exercised to avoid misalignment of the upper grip and the lower grip, in order to avoid bending stresses in the specimen, which would compromise the accuracy of the results. (See Figure 3-11)

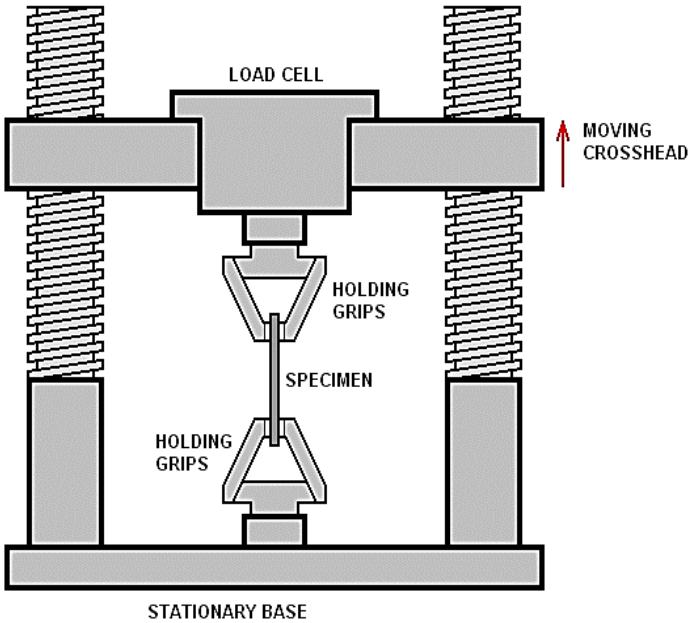

Figure 3-11 Schematic diagram of the tensile testing machine [47]

3.7.1.1 Specimen configuration according to ASTM D3165

Refer to Fig. 2.9

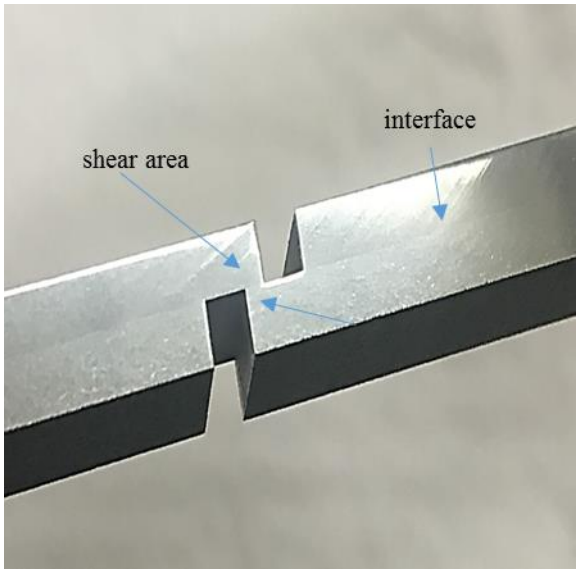

Figure 3-12 Tensile shear test specimen showing the shear area

The shear area was the most critical area in this test. The maximum permissible length between the notches was governed by this relationship, as shown in Equation 3-4:

$$L = \frac{F_{ty} \times t}{150\% \times \tau} \qquad 3\text{-}4 \ [39]$$

where L is the overall permissible length of the overlap, t is the thickness of the sample from the bond line, F_{ty} is the yield stress of the sample and τ is the average shear strength in the bond. L' was the length of the overlap used in this test. This value had to be less than the maximum permissible length of overlap L, to avoid exceeding the yield point of the materials in tension during the experiment [39]. The value of F_{ty} was obtained from the Hulamin Materials *Data* Sheet and the assumed value of τ was obtained from the results of the FEA simulation. The test was run at an approximate strain rate of 0.0012mm min^{-1}, as recommended by the ASTM D3165.

Table 3-15 Maximum permissible overlap length relation

Yield stress	**Thickness**	**Shear strength of bond**	**Overlap**	**Max Overlap**
F_{ty}	t	τ	L'	L
$180MPa$	2 mm	$4.22MPa$	1 mm	8.5 mm

3.8 Microstructure Characterisation

Microstructure characterisation was used to validate and interpret the results obtained from the tensile shear tests. The microscopic techniques employed were Optical Microscopy (OM) and Scanning Electron Microscopy (SEM). In addition, an Energy-dispersive X-ray spectroscopy (EDS) was performed to determine the diffusion of silicon across the interface. The diffusion of silicon into the core from the clad layer is temperature- and time-dependant, but also relies on a good bond across the interface to facilitate the diffusion[28].

3.8.1 Light Microscopy

A good bond formed between two materials after roll bonding should be free of defects and free of voids[33]. The bond interface should be a smooth line without any signs of discontinuity. Light microscopy was used to identify if localised melting had occurred. This could be identified by the presence of dendritic grains in areas where melting and re-solidification had occurred. The Nikon light microscope was used to analyse the bond interface of these samples and micrographs were taken at three sections along the interface.

3.8.1.1 Surface preparation

The fractured tensile shear test specimens were cut down into 5 mm strips, using a micro cutter. In each case, the section that was used for analysis was the central strip of the deformed tensile shear test specimen. The specimen was mounted in the hot mount, using a nonconductive transparent polymer resin (Clarofast). Each section was analysed in the RD and the TD plane. The samples had to undergo grinding, using the automatic grinding machine set at 150 rpm. Great caution had to be taken not to deform the samples by introducing bevelling. The samples were ground on 1200 grit paper and then were bathed in ethanol to remove any foreign impurities. After being ground, the samples had to undergo polishing. The polishing steps are summarised in Table 3-16.

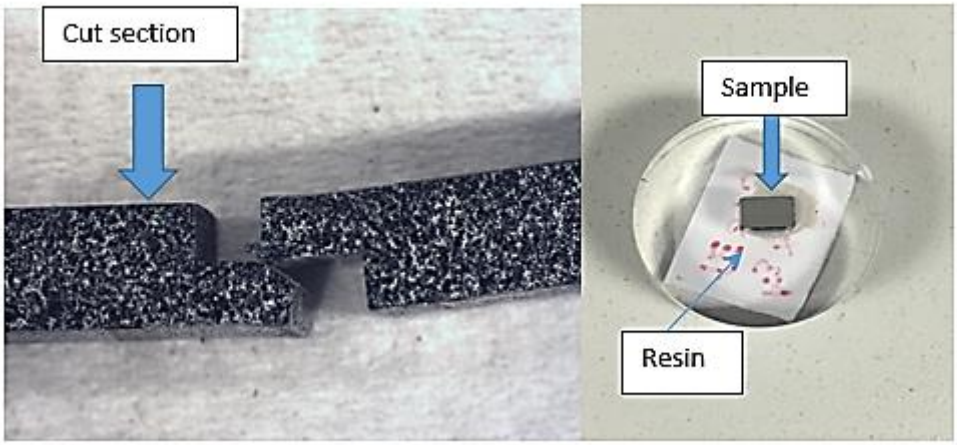

Figure 3-13 Sample cut. mounted and ready for surface preparation

Table 3-16 Grinding and polishing in summary

Pad	Lubricant	Speed (Rpm)	Force (N)	Time (mins)
1200 grit SiC	Water	150	20	3
Mol	Diamond Paste 3 µm	150	20	12
Nap	Water	150	10	6
Nap	Diamond Paste 1 µm	150	10	6
Nap	OP Suspension	150	10	10
Nap	Water	150	10	1

After the surface preparation, the samples were anodised. Anodic oxidation is an electrolytic process for the deposition of aluminium oxide on the surfaces of samples. The thickness of the anodic oxide layer would result in the interference of film colours when viewed under polarised light [33]. The aluminium plate, which acted as the cathode, was immersed in Barkers solution, which had been created by mixing 97 ml of distilled water with 3 ml of tetra floroboric acid (HBF_4), using a magnetic stirrer; The samples were fully immersed, using tweezers, for 25 seconds (Great caution was taken to avoid over-anodising the samples.); After anodisation, the samples were bathed in ethanol and dried before being viewed under the SEM.

Table 3-17 Anodising parameters

Conditions	
Voltage	20V
Current	0.4-0.6A
Electrolyte	3% Barkers Reagent (97ml of water plus 3ml of HBF_4)
Time	20-25s

3.8.2 SEM Micrographs

After light microscopy, the samples were taken to UCT's Electron Microscope Unit, where SEM and EDS were performed. The SEM micrographs were taken using the Nova Nano SEM microscope. The microscope was operated at 20 kV, at a working distance of 11 mm with a SEM Magnification of 6.00kx. Backscattered electrons were bombarded on to the specimen to obtain the SEM micrographs in backscatter mode. EDS line scans were then performed to observe the possible diffusion of silicon across the interface. (This method enables the identification of silicon across the interface.) [48] The purpose of the test was to determine the surface condition that most favoured the diffusion of silicon into the core. In order to determine the amount of silicon that had diffused into the core, an electronic line scan with 20 points was drawn across the bond interfaces of the samples. The EDS concentration profiles were then used to give the quantitative results of the diffusion bonding. This test was performed in the Nova Nano SEM, in Backscatter Detector mode, at a Voltage of 20 KV, a dwell time of 60 seconds, a spot size of 4.5 and at a working distance of 6 mm from the detector.

4 FINITE ELEMENT MODELLING

4.1 Results from the FEM analysis using Solid works 2018

The results of the Finite Element Modelling are presented below. They were based on the industrial mill log parameters used at Hulamin. The intention was to establish if it were possible to bond the two materials when stacked together, prior to the actual roll bonding on the Gleeble.

4.1.1 Von Mises Stress

Von Mises stress represents the magnitude of a stress that will cause any material to fracture when subjected to a load during deformation [49]. The FEA modelling results indicated how the stress varied on a bonded sample. The areas shown in blue indicated low stress, while the area shown in red indicate high stress. The section represented by the green-yellow colour indicated moderate stress, thus an even flow of stress on the bonded section. The minimum stress (blue) was 0.000519 N/m^2 and the maximum stress (red) was 0.000618 N/m^2.

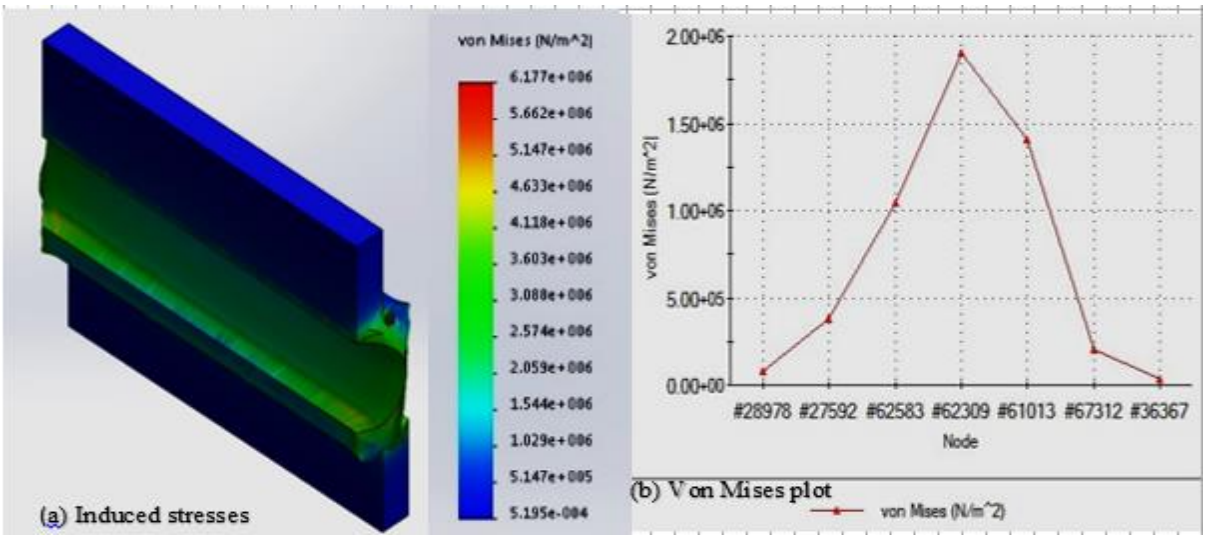

Figure 4-1 FEA results (a) Induced stresses (b) Von Mises Plot across the bonded region

The Von Mises plot taken across the interface along the TD plane (bonded region) indicated that the Von Mises stress was maximum at the central region of the specimen. From this it could be deduced that the bond was much stronger at the central region than at the edges. Thus, after the PSC tests, the ASTM D3165 samples had to be cut from the central region of the bond.

5 RESULTS AND DISCUSSION OF THE PLANE STRAIN COMPRESSION RESULTS

This section serves to illustrate how the clad and the core were bonded during the PSC tests. To have valid results the following principles had to be maintained. The two methods used to validate the PSC results in the Gleeble 3800 are explained in detail below.

5.1 Validation of the Plane Strain Compression Results

5.1.1 Symmetrical and unsymmetrical deformed plane strain samples

Post-test physical analysis was done to the samples to observe the symmetricity of the deformation. It was noted that in most cases the deformation in the tests was symmetrical, although in two specimen's deformation was unsymmetrical hence had to be repeated.

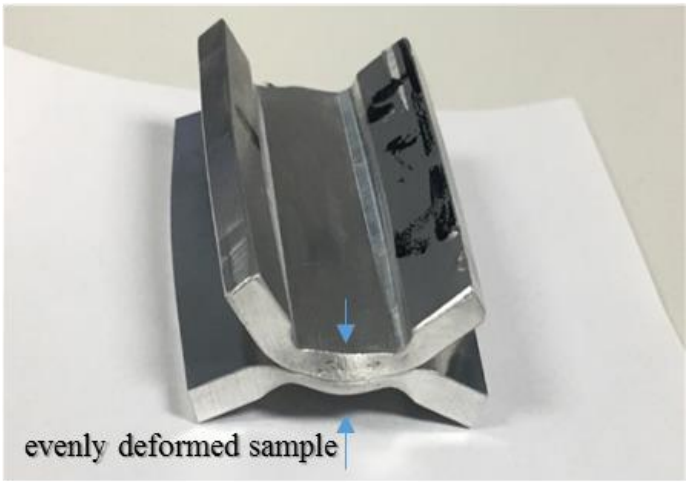

Figure 5-1 Symmetric deformation of Test 1 when a 7 µm core was bonded with a 1 µm clad.

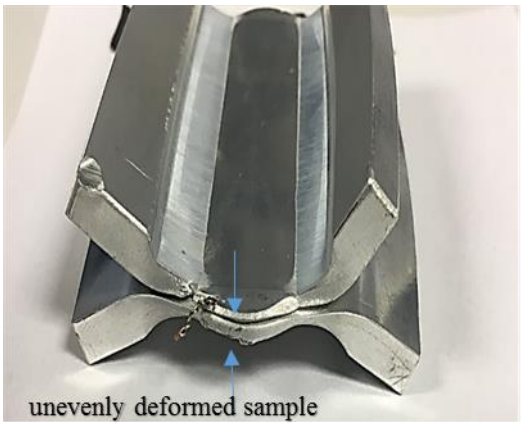

Figure 5-2 Unsymmetric deformation of Test 1 when a 7 µm core was bonded with a 1 µm clad.

The lack of uniformity of the deformation could also be observed when the initial thickness and the final thickness of the deformed zones were measured. A digital Vernier calliper was used to obtain these *data*, which are displayed in Table 5-1.

Table 5-1 Initial and final thickness of the deformed zone after the Hot PSC tests

Condition	**TESTS**	**h_i (mm)**	**h_f (mm)**	**Δh(mm)**
Core 7.0µm x clad 0.5µm	TEST 1	10	4.07	5.93
	TEST 2	10	4.48	5.52
	TEST 3	10	4.01	5.99
Core 7.0µm x clad 1µm	TEST 1	10	4.48	5.52
	TEST 2	10	4.21	5.79
	TEST 3	10	4.01	5.99
Core 7.0µm x clad 3µm	TEST 1	10	4.3	5.70
	TEST 2	10	4.00	6.00
	TEST 3	10	4.01	5.99
Core 10µm x clad 0.5µm	TEST 1	10	4.35	5.65
	TEST 2	10	4.01	5.99
	TEST 3	10	4.48	5.52
Core 10µm x clad 1µm	TEST 1	10	4.01	5.99
	TEST 2	10	4.48	5.52
	TEST 3	10	4.50	5.50
Core 10µm x clad 3µm	TEST 1	10	4.35	5.65
	TEST 2	10	4.48	5.52
	TEST 3	10	4.07	5.93
Core 10µm x clad 7µm	TEST 1	10	4.00	6.00
	TEST 2	10	4.33	5.67
	TEST 3	10	4.35	5.65
Core 15µm x clad 0.5µm	TEST 1	10	4.04	5.96
	TEST 2	10	4.02	5.98
	TEST 3	10	4.6	5.40
Core 15µm x clad 1µm	TEST 1	10	4.5	5.50
	TEST 2	10	4.16	5.84
	TEST 3	10	4.15	5.85
	TEST 4	10	4.23	5.77
Core 15µm x clad 3µm	TEST 1	10	4.00	6.00
	TEST 2	10	4.15	5.85
	TEST 3	10	4.06	5.94

Core 25µm x clad 0.5µm	TEST 1	10	4.13	5.87
	TEST 2	10	4.23	5.77
	TEST 3	10	4.04	5.96
Core 25µm x clad 1µm	TEST 1	10	4.50	5.50
	TEST 2	10	4.02	5.98
	TEST 3	10	4.11	5.89
Core 25µm x clad 3 µm	TEST 1	10	4.04	5.96
	TEST 2	10	4.11	5.89
	TEST 3	10	4.30	5.70
	TEST 4	10	4.02	5.98

The displayed results in Table 5-1 show that the test specimens had an average change of thickness of approximately 5.79 mm, ± 0.19 mm.

5.1.2 Temperature

It was noted that the two alloys, AA3003 and the AA4045, responded to the electrical resistance heating quite differently, owing to the variation in the alloying and, consequently, to the conductivity of each. Localised heating was a problem in some of the tests, resulting in the localised melting of AA4045, which had a lower melting point than the AA3003 alloy. Localised heating could be minimised by improving the contact between the two layers during testing. When there was poor contact, fluctuations of the inputted power was observed. The thermal profile of the tests included a hold-on time of 100 seconds at the test temperature. The average temperature gradient observed in the tests was 50ºC. The temperature gradient across the two samples was measured as the difference between TC_1 and TC_2. (See Figure 5-3 and Table 5-2)

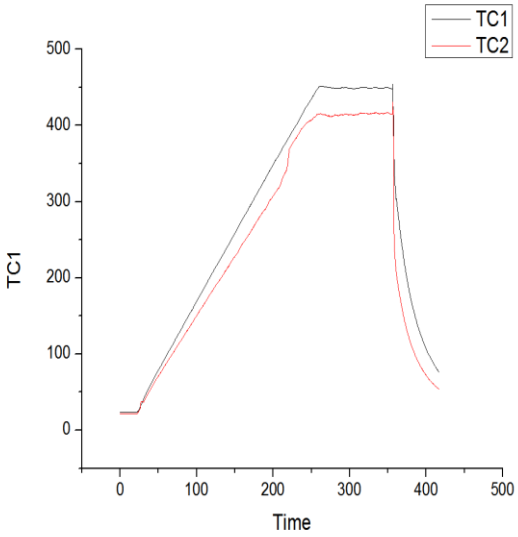

Figure 5-3 Thermocouple temperature against time for Test 1 when the 7 µm core was bonded with a 1 µm clad

Table 5-2 Gleeble Temperature imported from the PSC Tests just before deformation

Condition	TESTS	TC_1 (ºC)	TC_2 (ºC)	ΔT(ºC)
Core 7.0µm x clad 0.5µm Target Temp = 450ºC	TEST 1	450	400	50
	TEST 2	450	400	50
	TEST 3	450	420	30
Core 7.0µm x clad 1µm Target Temp = 450ºC	TEST 1	450	420	30
	TEST 2	450	440	10
	TEST 3	450	420	30
Core 7.0µm x clad 3µm Target Temp = 450ºC	TEST 1	450	420	30
	TEST 2	450	420	30
	TEST 3	450	400	50
Core 10µm x clad 0.5µm Target Temp = 450ºC	TEST 1	450	430	20
	TEST 2	450	430	20
	TEST 3	450	400	50
Core 10µm x clad 1µm Target Temp = 450ºC	TEST 1	450	430	20
	TEST 2	450	430	20
	TEST 3	450	400	50
Core 10µm x clad 3µm Target Temp = 450ºC	TEST 1	450	420	30
	TEST 2	450	420	30
	TEST 3	450	420	30
Core 10µm x clad 7µm Target Temp = 450ºC	TEST 1	450	430	20
	TEST 2	450	420	30
	TEST 3	460	430	30
Core 15µm x clad 0.5µm Target Temp = 450ºC	TEST 1	450	445	5
	TEST 2	450	420	30
	TEST 3	450	410	40
Core 15µm x clad 1µm Target Temp = 450ºC	TEST 1	450	420	30
	TEST 2	450	430	20
	TEST 3	450	440	10
Core 15µm x clad 3µm Target Temp = 450ºC	TEST 1	450	400	50
	TEST 2	450	400	50
	TEST 3	450	430	20
Core 25µm x clad 0.5µm Target Temp = 450ºC	TEST 1	450	420	30
	TEST 2	450	420	30
	TEST 3	10	420	30
Core 25µm x clad 1µm Target Temp = 450ºC	TEST 1	450	400	50
	TEST 2	450	400	50

	TEST 3	450	420	30
Core 25µm x clad 3 µm Target Temp = 450ºC	TEST 1	450	420	30
	TEST 2	450	445	5
	TEST 3	450	420	30
	TEST 4	450	420	30

It can be noted from the results illustrated in Table 5-2 that the average ΔT of the tests was approximately 30 ± 20 ºC. This standard deviation in the results is considered acceptable in the work by [38] for repeatability purposes.

5.1.3 Summary

The Gleeble 3800 uses resistive heating to achieve deformation temperature. The temperature was controlled by thermocouples welded to the samples. There was a control thermocouple that controlled the temperature through a feedback loop. In order to achieve uniform heating in the Gleeble 3800, good contact between the anvils and the samples was required. According to [50], to be able to attain valid and repeatable results using the Gleeble 3800, the temperature gradient should be $\pm$ 30ºC. The two alloys used in this research had different conductivities and melting points. AA4045 had the lower melting point of $\pm$ 573ºC. Thus, poor contact resulted in fluctuating heating, causing the clad to melt and necessitating the aborting of the test. Uniform heating was obtained when tantalum foil was used as a diffusion barrier and lubricant layer between the anvils and the samples. It must be noted that the point of contact between the AA3003 and AA4045 samples was considered to be a high heat zone since there was no lubricant in this junction, owing to the fact that the presence of lubricant here would negatively affect the roll bonding process [34]. Three tests were performed per condition and it was noted that an average of 30 ± 20 ºC temperature gradient was obtained.

6 RESULTS AND ANALYSIS OF THE TENSILE SHEAR TESTS

The main focus of the project was to establish whether surface roughness played a significant role in the mechanical strength of the bond formed between AA3003 and AA4045 during roll bonding. In the literature it was shown that there were several conditions that affected the bond strength between clad and core. A rougher surface had relatively more surface asperities. When these two materials were bonded at intense pressure and a high temperature the surface asperities would merge and form a cold weld, thus forming a metallurgical bond. The increase in surface roughness reduced the force required to break the oxide layer, thus facilitating bonding [51]. The surface asperities were varied according to the design matrix set up in Chapter 3. To determine the strength of a bond, a tensile shear test was performed on bonded samples with various combinations of surface roughness. (See Table 3-7) The tensile shear test specimens were designed according to the ASTM D3165.

Table 6-1 Tensile shear test geometry according to the ASTM D3165

Fundamental	**Magnitude**
Length	50 mm
Width	6.35 mm
Gauge length	10 mm
Grip area	20 mm
Thickness	4 mm
Notch width	2 mm
Notch spacing	1 mm
Shear area	6.35 mm^2
Test speed	0.0012 mm/min

6.1 Force/Extension Graphs for clad and core

At Hulamin, the surface finish of the clad and the core is currently kept at 1µm and 10 µm respectively. The literature specified that there was an optimum surface finish that could be obtained when two materials were bonded together [2]. An increase in surface roughness proportionately increased the bond strength until the optimal degree of surface roughness had been reached. Beyond the optimal degree of surface roughness, the bond strength would, in fact, deteriorate. (In other words, after this optimal degree of surface roughness had been reached, the rougher the surface became, the weaker the resultant bond.) This relationship

between the degree of surface roughness and resultant bond strength is illustrated below, reflecting the 39 tests performed on the different surface conditions.

The engineered surface finishes of the clad from 0.5µm to 7 µm were roll bonded to the engineered surfaces of the core from 7 µm to 25 µm, from which the following graphs (Figure 6-1 to 6-7) were extrapolated.

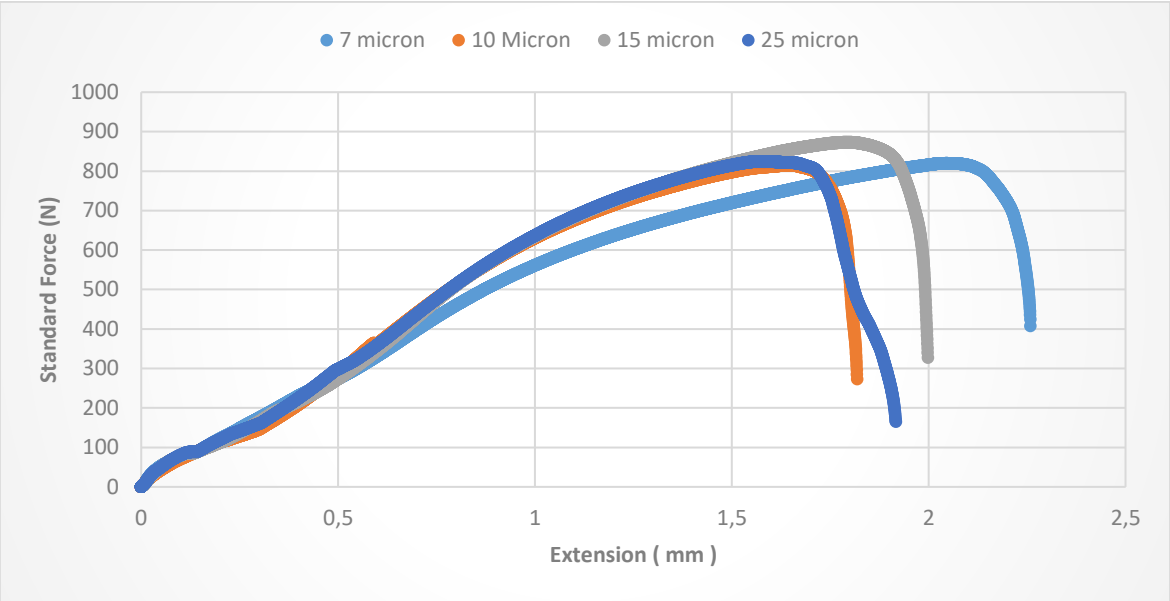

Figure 6-1 Force Extension graph when clad was kept at 0.5 µm

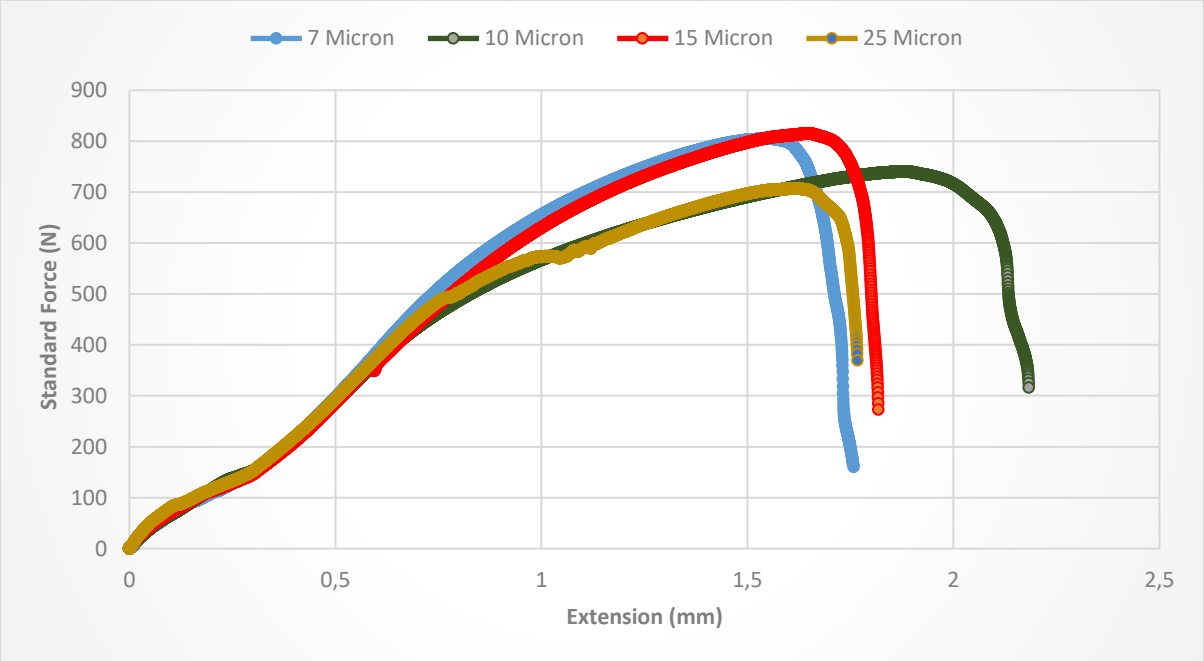

Figure 6-2 Force Extension graph when clad was kept at 1 µm

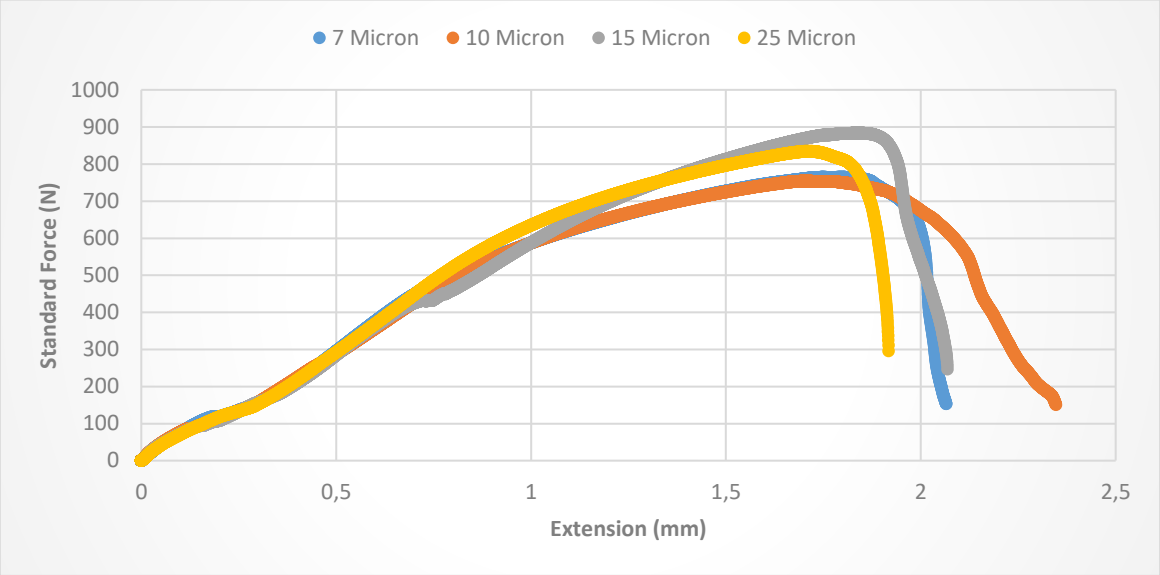

Figure 6-3 Force Extension graph when clad was kept at 3 µm

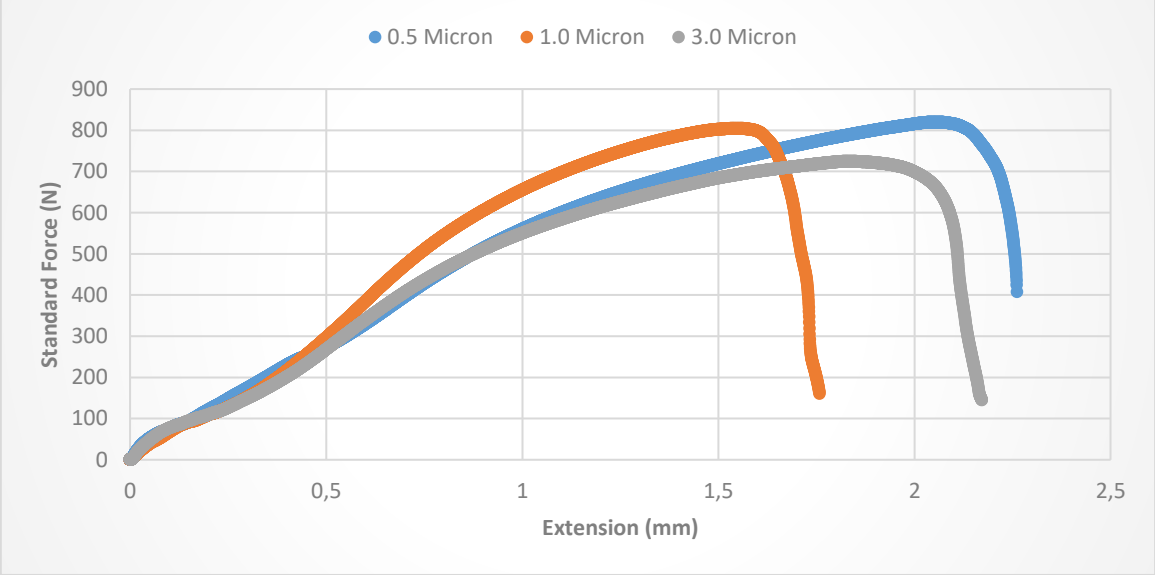

Figure 6-4 Force Extension graph when core was kept at 7 µm

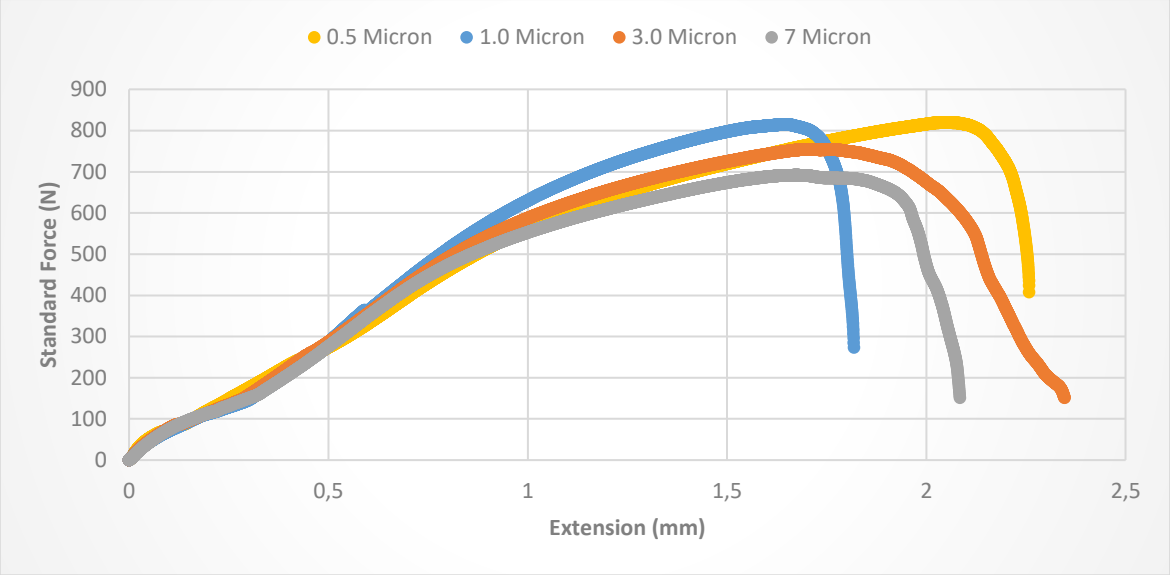

Figure 6-5 Force Extension graph when core was kept at 10 µm

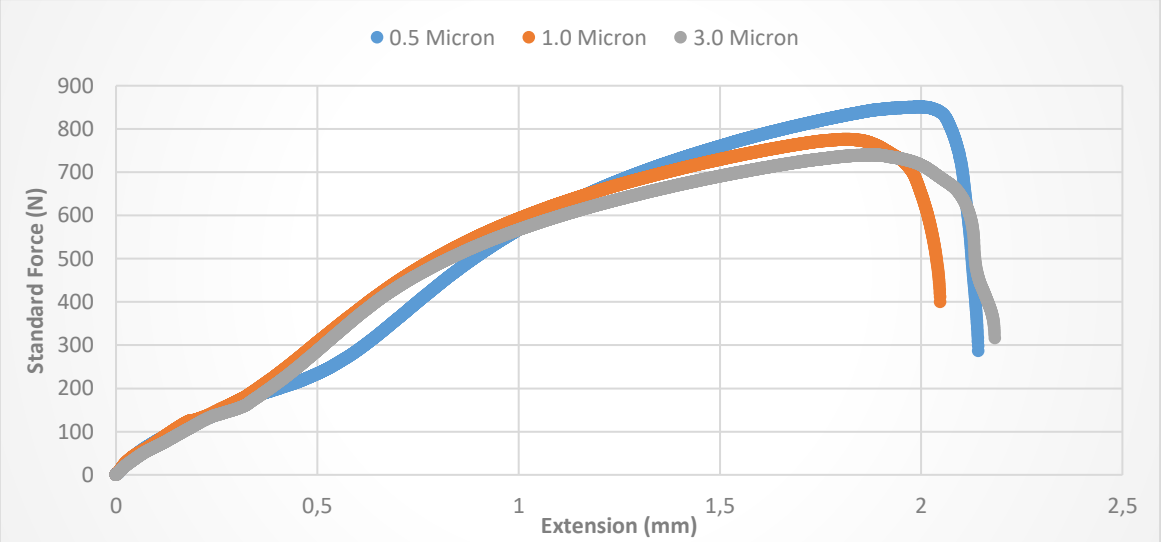

Figure 6-6 Force Extension graph when core was kept at 15 µm

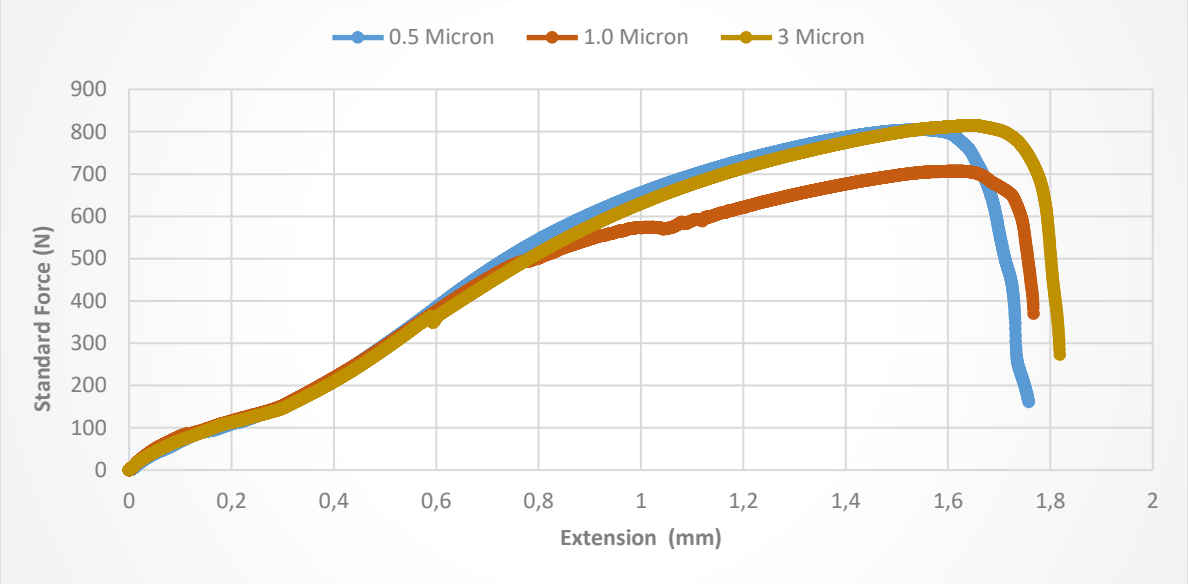

Figure 6-7 Force Extension graph when core was kept at 25 µm

The deformation force between the clad at 1 µm and the core at 10 µm obtained from the tensile shear test results was approximated to be 779 N. The design of the tensile shear test specimens had a small shear area of approximately 6.25 mm^2. According to the literature, the average force required to deform a bond was expected to increase with increasing surface roughness during roll bonding. However, in the tensile shear tests the average forces required to deform the bonds between the clad and the core were not consinstant. For instance, the deformation force required to deform a bond between the clad and the core when the clad was kept at 0.5 µm and bonded to the core (surface finish 7 µm - 25 µm) did not vary significantly. Another behaviour was observed when the clad was kept at 1 µm and bonded to the core (surface finish 7 µm - 25 µm): the deformation force required to break the bond was decreasing with increasing surface roughness. A compararison was made of each condition with the hulamin standard finish deformation force to obtain Δ f but no significant results were obtained as well. (See Table 6-2)

This was foreseen before the commencement of the tensile shear tests and, as a result, the tests were run in conjunction with the DIC. The DIC mapped the strain distribution during the tests. The detailed explanation of the results is shown in Chapter 7.

Table 6-2 Summarised Tensile shear test results

			Clad			
			0.5 µm	**1 µm**	**3 µm**	**7 µm**
Core	**7 µm**	UTS (N)	819	798	745	
		Extension(mm)	2.34	1.51	1.88	
		Δ F	40	19	-34	
	10 µm	UTS (N)	820	779	750	726
		Extension(mm)	2.04	1.74	1.79	1.86
		ΔF	41	0	-29	-53
	15 µm	UTS (N)	803	798	823	
		Extension(mm)	1.84	1.81	1.91	
		Δ F	24	19	44	
	25 µm	UTS (N)	804	705	823	
		Extension(mm)	1.74	1.62	1.84	
		Δ F	25	-74	44	

7 RESULTS AND ANALYSIS OF DIGITAL IMAGE CORRELATION

The *data* were presented in a way that showed the true strain at various intervals in the tests, namely at 0%, 50% and 75% prior to deformation and at the point just before fracture. The colour green indicated no visible strain localisation, the colours red and purple represented high magnitudes of strain localisation and the yellow-blue colour represented minimum strain localisation.

7.1 Strain Localisation Mapping

7.1.1 Core at 7.0 Micron

7.1.1.1 Core at 7 Micron and clad at 0.5 µm, 1 µm and 3 µm

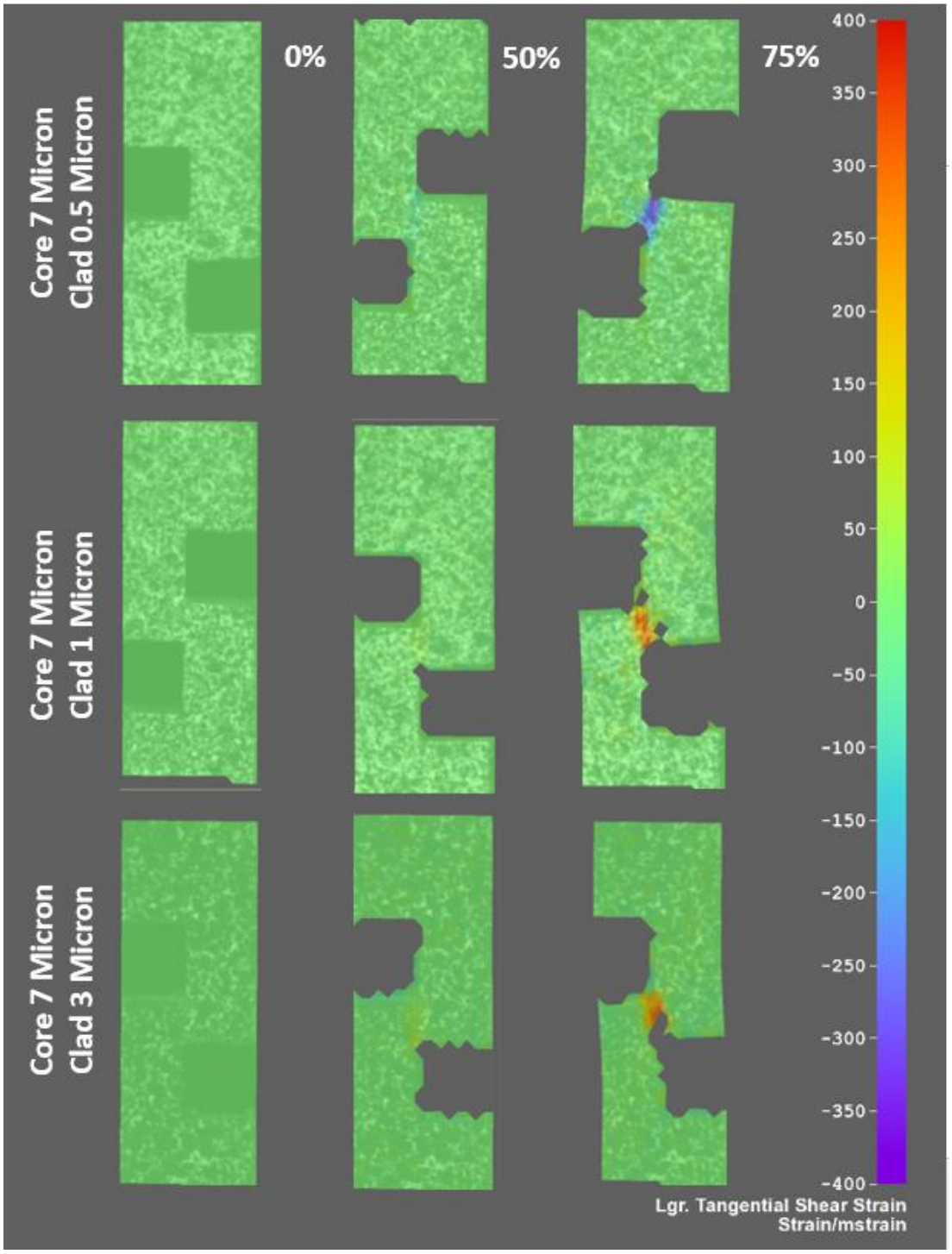

Figure 7-1 Strain map when core was kept at 7.0 µm using DIC

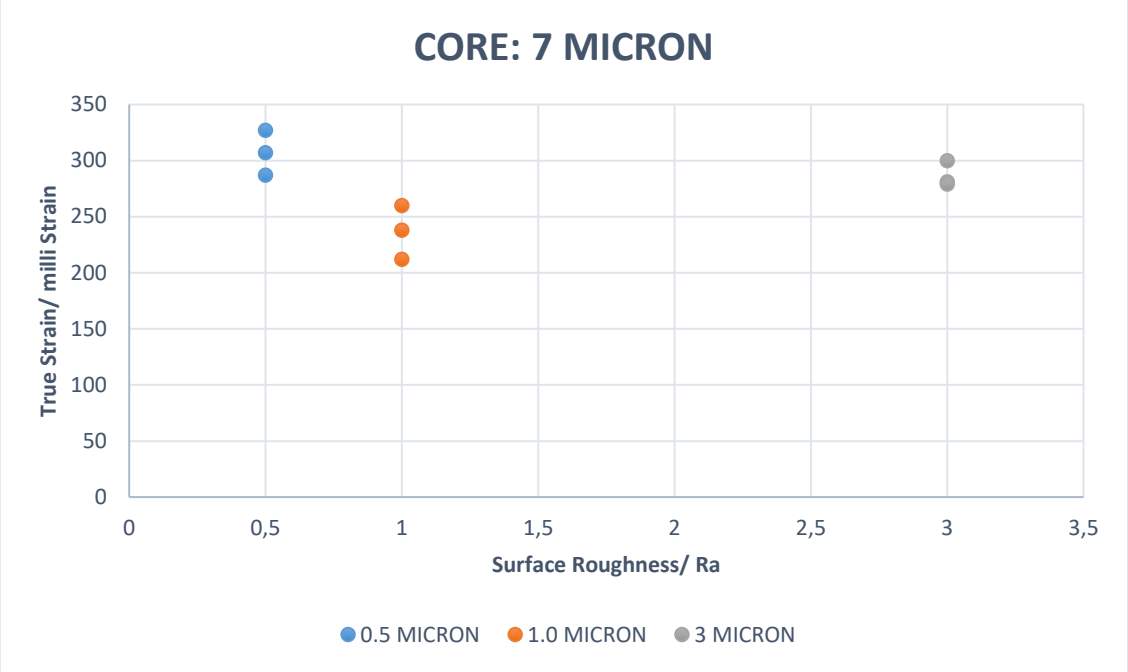

Figure 7-2 True Strain against surface roughness when core is at 7.0 µm

The strain map represented in Figure 7-1 shows the distribution of strain across each interface throughout the testing. The red and purple colours represent high magnitudes of strain, whereas the green colour represents low magnitudes of strain. To quantify the strain, three linescans were taken at 50% deformation and the strain results were plotted in Figure 7-2 . The trend was similar to previous results: true strain decreased with an increase in surface roughness. Here the strongest bond was obtained when the surface roughness of the clad was at 1µm. This increase in surface asperities associated with the relativ ely rough surface of 1 µm facilitated the breaking down of the oxide layer. However, a further increase in surface roughness, this time to 3.0 µm, resulted in a weaker bond, owing to the relatively deep scratches embedded in each specimen, these to some extent compromising the welding process during bond formation.

7.1.2 Core at 10 Micron

7.1.2.1 Core at 10 Micron and clad at 0.5 µm, 1 µm, 3 µm and 7 µm

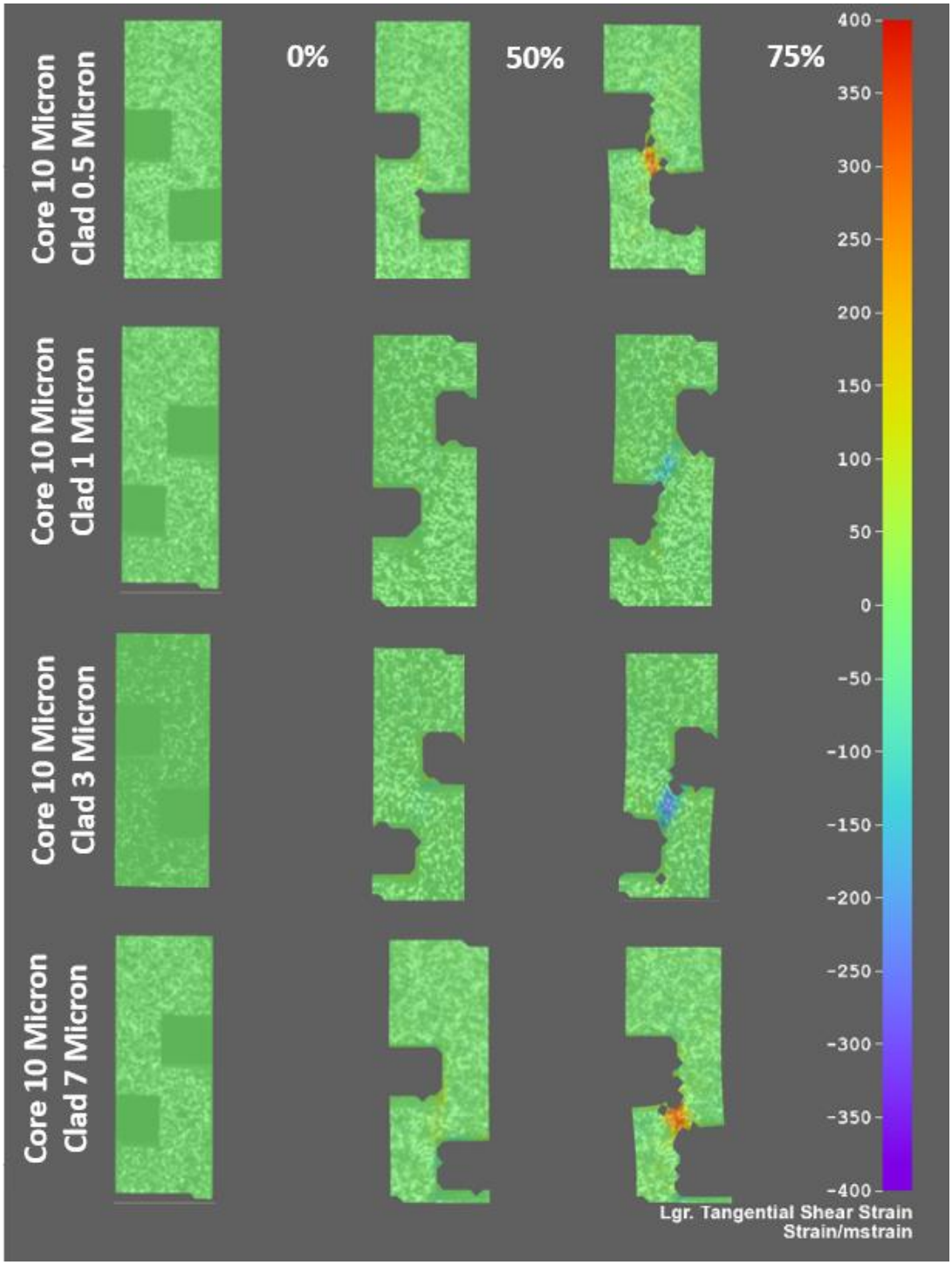

Figure 7-3 Strain Map when core was kept at 10 µm with DIC

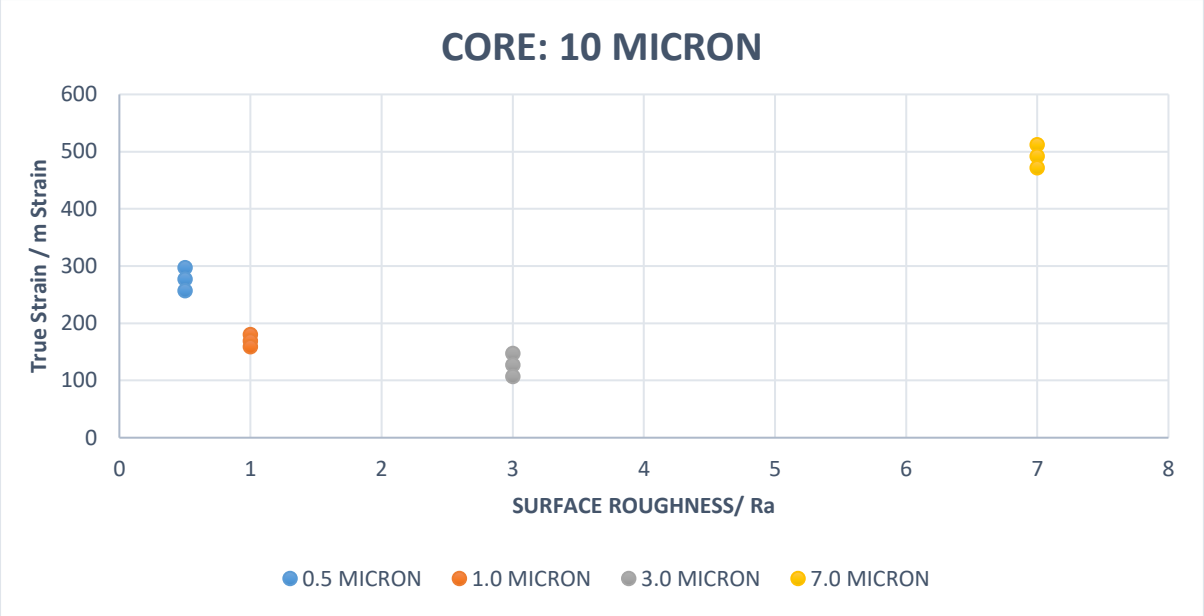

Figure 7-4 True strain against surface roughness

The Hulamin benchmark of surface preparation was set at core 10 µm and clad 1.0 µm. For these tests the level of surface roughness on the clad was varied from 0.5 µm to 7.0 µm. The trend was again observed whereby, as surface roughness was increased, strain localisation was reduced, thereby improving bond strength. At a point corresponding to a clad roughness of 3 µm, this trend was reversed and the bond strength deteriorated, indicating the presence of an optimal degree of surface roughness at approximately 3.0 µm. The average strain localisation using the Hulamin benchmark (core 10 µm and clad 1.0 µm) was approximately 169 ± 4 milli strain, as indicated in Figure 7-4. When the clad surface roughness was lowered to 0.5 µm the strain induced rose to 257 ± 4 milli strain, indicating a poor bond formation. This could be explained by the fact that a smooth surface finish would have fewer surface asperities, which are associated with improved bond strength. It can be seen in Figure 7-4 that as the surface roughness of the clad was increased to 3.0 µm there was an improvement in the bond strength, owing to the fact that the strain induced was reduced to 127 ± 4 milli strain. This improvement in bond strength could be explained by the fact that the surface oxides were being broken down, thereby exposing the virgin material, which would weld and set more effectively when the two alloys came into contact during roll bonding. However, a further increase in surface roughness resulted in increased strain and a weaker bond. The increase in the strain when the surface roughness was increased to 7 µm was as a result of the deep troughs that had formed in the surface that were caused by the rougher surface finish. When the two materials merged during roll bonding, the gaps in the deep troughs would persist, thereby inhibiting the formation of a

complete weld, this resulting in voids on each interface. These voids would become sites of strain localisation, as can be seen in Figure 7-4.

7.1.3 Core at 15 Micron

7.1.3.1 Core at 15 Micron and clad at 0.5 µm, 1 µm and 3 µm

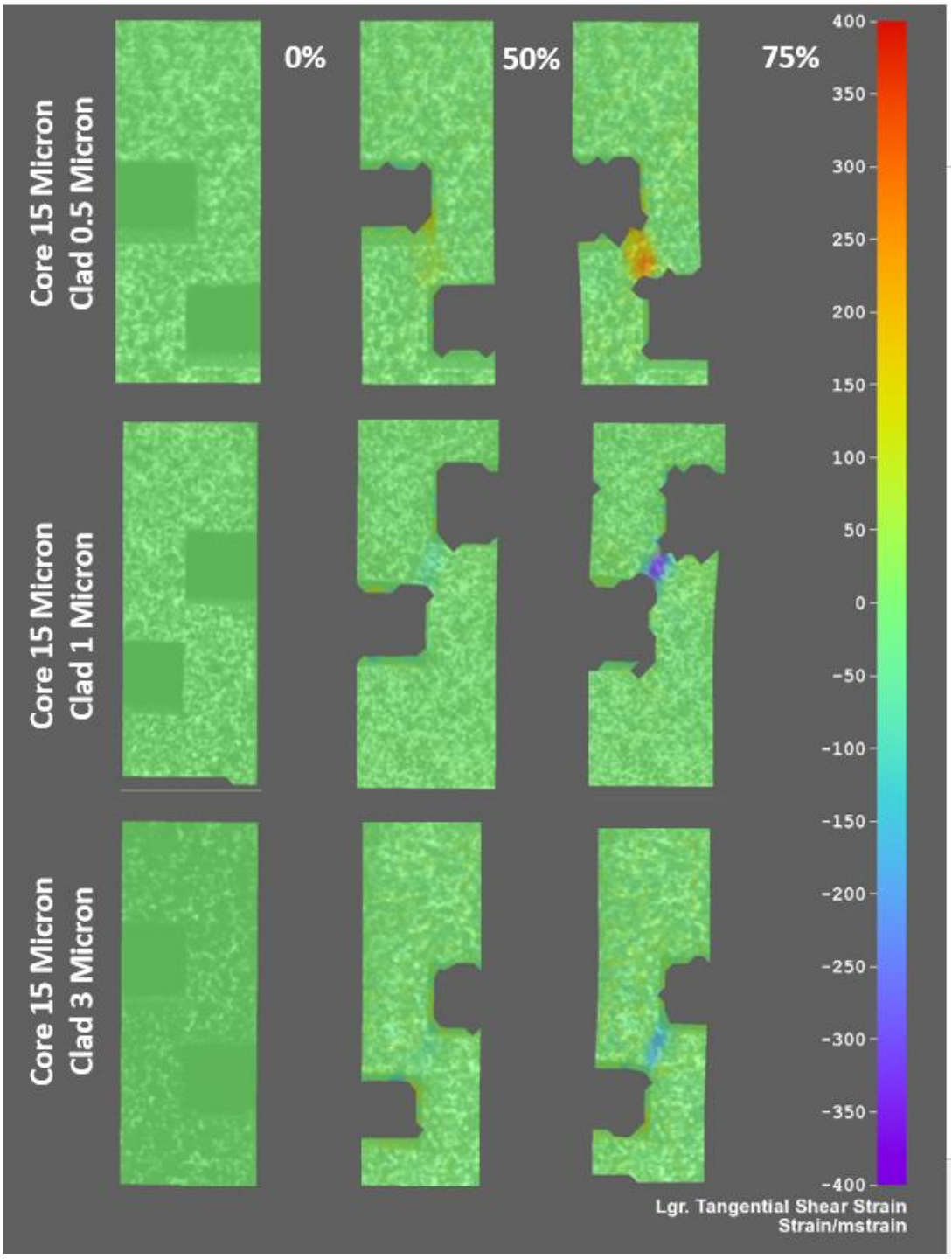

Figure 7-5 Strain Map when the core was kept at 15 µm using DIC

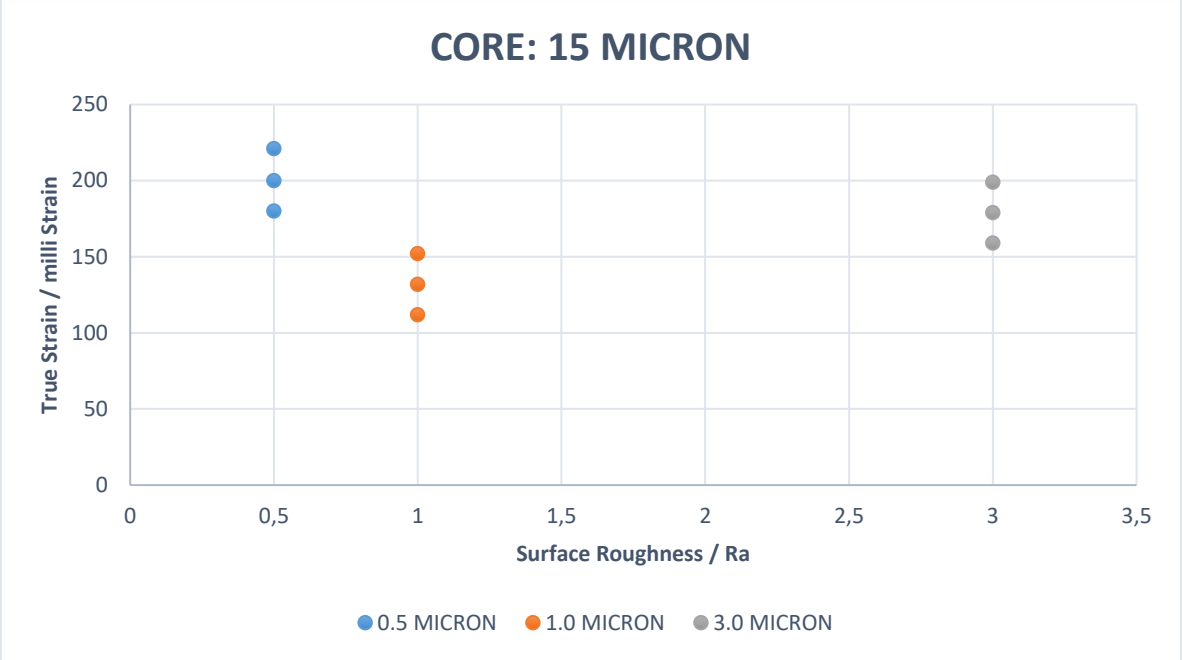

Figure 7-6 True strain against surface roughness

In the strain map at 50% deformation when the clad was at 0.5 µm in Figure 7-5, it could be seen that the specimen exhibited a high strain, which indicated the initiation of deformation. This was shown by the occurrence of a purple-red colour, representing very high levels of strain. In contrast, at 1.0 µm and 3.0 µm, the levels of strain were much lower, as indicated by the light blue colour, which represented low levels of strain. The strain induced was 200 ± 4 milli strain when the surface roughness was 0.5 µm. However, when the surface roughness was increased to 1.0 µm there was improvement in the bond strength as the strain induced was reduced to 132 ± 4 milli strain. At an increased surface roughness of 3.0 µm, the strain localisation rose to 179 ± 4 milli strain. Again, this could be explained by the further increase in surface roughness, resulting in deeper troughs in the surfaces of the bonding alloys. As stated in the Thin Film Theory, the surface asperities need to merge and form a weld. Instead, the deep troughs that had formed led to gaps in the interfaces, in turn leading to voids that compromised bond strength. Figure 7-6 shows that a better bond strength could be achieved during roll bonding when the core was at 15 µm and the clad at 1.0 µm, with the strain induced at approximately 132 ± 4 milli strain. This was an improvement on the Hulamin set benchmark, which was at 169 ± 4 milli strain.

7.1.4 Core at 25 Micron

7.1.4.1 Core at 25 Micron and clad at 0.5 µm, 1 µm and 3 µm

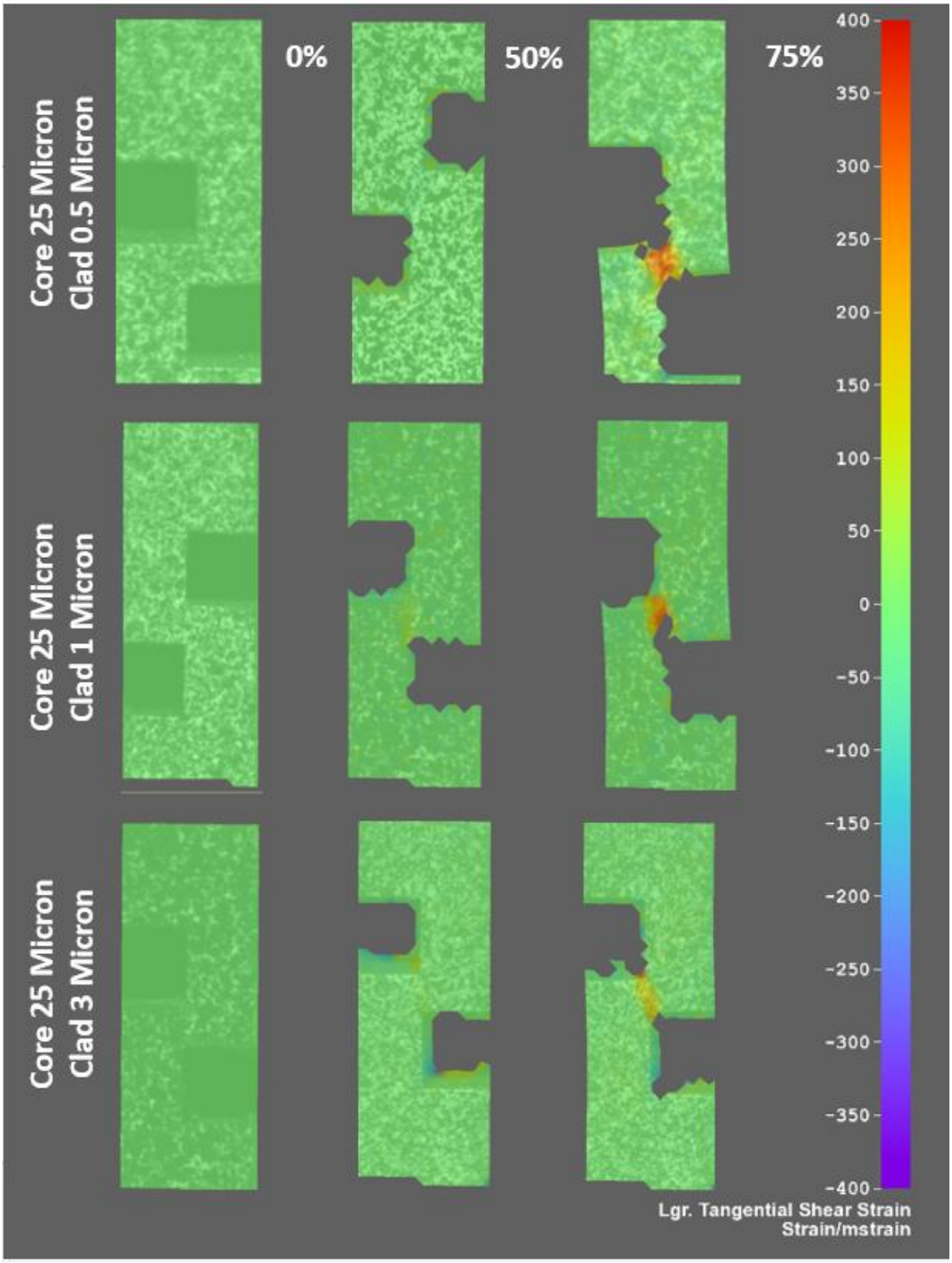

Figure 7-7 Strain map when the clad is kept at 25 µm using DIC

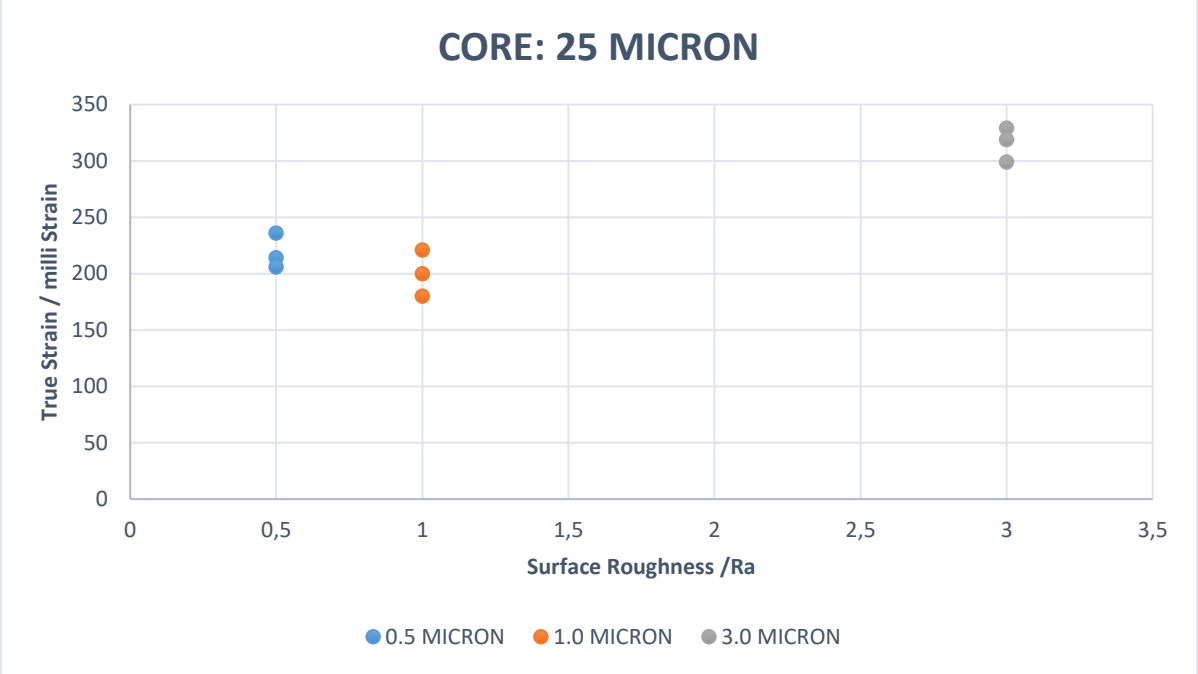

Figure 7-8 True Strain against roughness

Given that the Hulamin benchmark surface roughness of the core was 10 µm, a decision was made to test the bond strength with the core at a significantly higher level of surface roughness. Therefore, in this round of testing the core was roughened to 25 µm and kept constant, while the clad was at 0.5 µm, 1 µm and 3 µm. The observed trend was similar to that of previous tests in that an increase in surface roughness led to greater bond strength. However, beyond the optimal level of surface roughness, the bond strength was significantly compromised. Up to the optimal level of surface roughness, there was a decrease in strain from 214 ± 4 milli strain to 200 ± 4 milli strain, indicating a slight improvement in bond strength. However, after the optimal level of surface roughness had been reached there was a significant rise in strain, up to approximately 319 ± 4 milli strain, as is illustrated in Figure 7-8. It must be noted that this condition recorded the highest level of strain localisation during the entire process of testing. From this it can be deduced that very rough surfaces cause very deep troughs at the surfaces of both alloys, resulting in voids of such magnitude at each interface leading to severely compromised bond strength.

7.1.5 Core Roughness in Summary

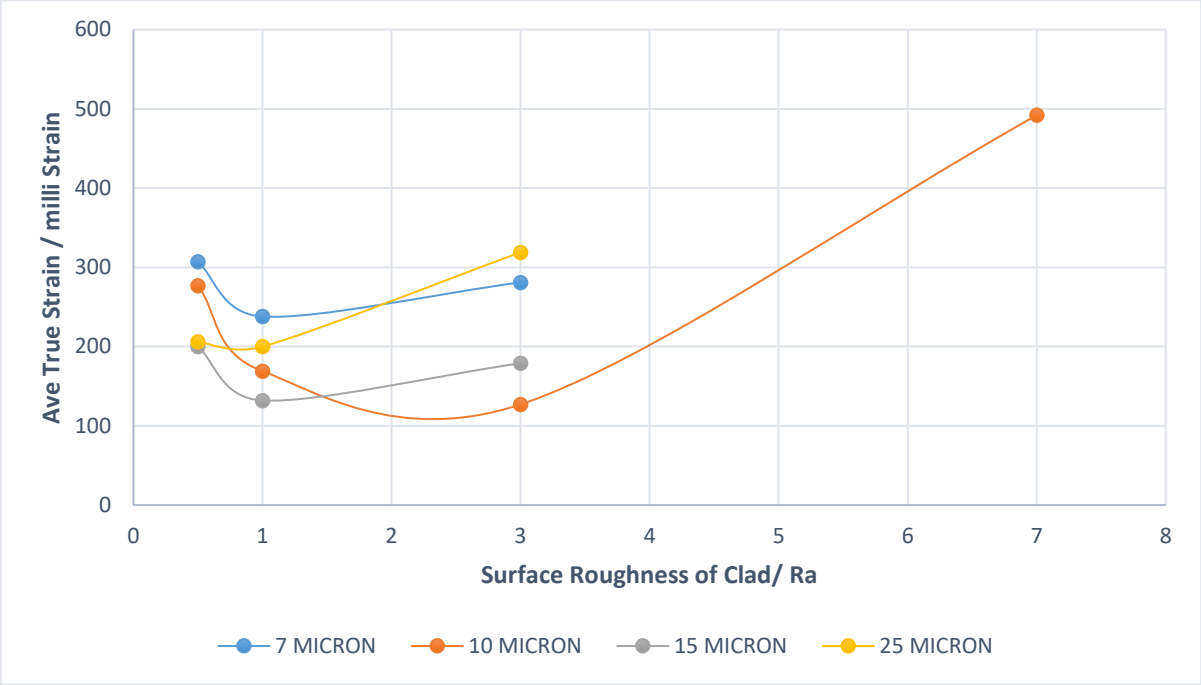

Figure 7-9 True strain against surface roughness for the core roughnesses of 7, 10, 15 and 25 micron

An analysis of the tensile shear testing results on samples designed according to a modified ASTM D3165 proved that surface roughness played a major role in bond strength when two materials were bonded together. Figure 7-9 shows that the weakest bond was obtained when a core with a surface roughness of 10 µm was bonded with the clad at 7 µm. The Hulamin benchmark was set at 10 µm for the core and 1 µm for the clad. A slight improvement on the Hulamin bond strength was obtained when the surface finish of the clad was increased to 3 µm, but a further increase in the surface roughness of the clad to 7 µm led to a weakening of the bond. The main reason for this was that as the surface finish became rougher, the troughs embedded in the surface of the material become deeper, thus compromising the weld. This phenomenon will be explained in detail in Chapter 9 when the SEM micrographs are correlated with the strain map results.

From the results in Figure 7-9, it is apparent that the best combination for bond strength is when the surface roughness of the core is at 10 µm and the surface roughness of the clad is at 3 µm, closely followed by a combination of 15 µm core and 1.0 µm clad roughness. Therefore, the Hulamin surface preparation can be slightly improved upon to give a better bond strength.

8 RESULTS AND ANALYSIS OF THE MICROSTRUCTURE FEATURES

Microstructural analysis was necessary to validate the shear test results through the characterisation of the bond. A selected number of samples were analysed, using optical microscopy to investigate whether melting had occurred at the interface during the Gleeble roll bond testing, using Scanning Electron Microscopy (SEM) to investigate the presence of porosity at the interface of the bond and using energy dispersive x-ray spectroscopy (EDS) to characterise the silicon distribution across the bond.

8.1 Optical Microscopy

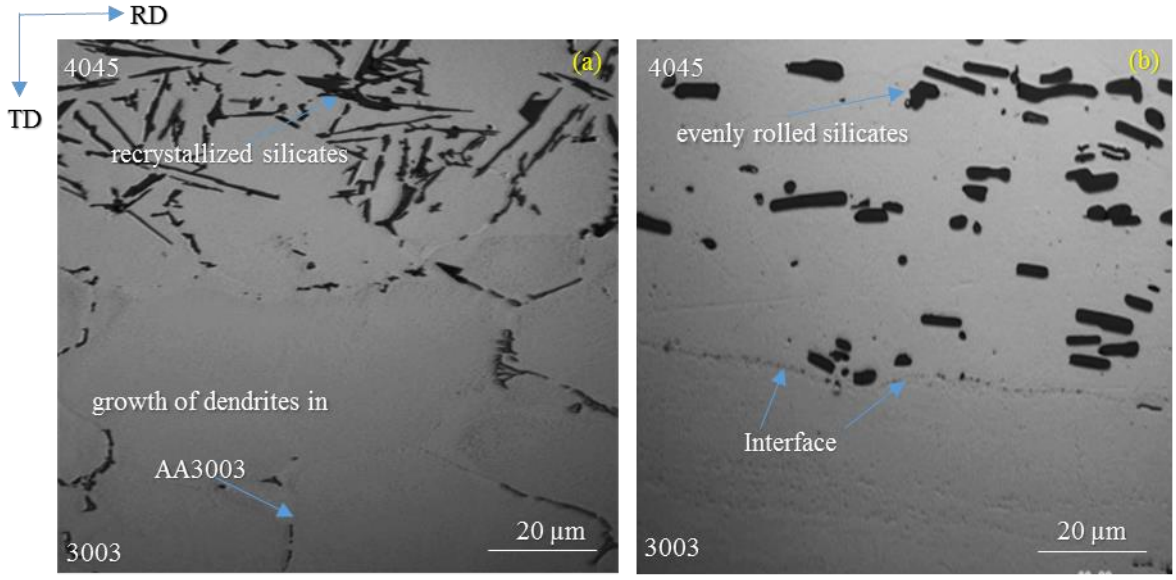

Figure 8-1Optical micrographs (a) melted sample (b) umelted sample

The Gleeble 3800 uses resistive heating to achieve deformation temperature. The anvils were lubricated with tantalum to avoid localised heating but, in spite of this precaution, eleven of the 39 specimens melted and these tests had to be repeated. In the melted samples, as can be seen in Figure 8-1 (a), the silicates had recrystallised and solidification had taken place, as evidenced in the flake-like structure that prevented the establishment of an interface between the two alloys. The micrograph in Figure 8-1 (b), shows the results of a successful test whereby the interface between the two alloys is well defined and the silicon particles are in their as-rolled morphology and are distributed fairly uniformly in the clad plate. The optical micrographs could not be used to illustrate the sizes of the voids present at each interface. As is illustrated in Figure 8-1 (b), the interface was visible but the voids at the interface could not

be quantified as they were very small. SEM had to be performed at high magnification so that the voids present at the interface could be identified and quantified.

8.2 SEM Micrographs

The results from the DIC indicated that the strain distribution across the interface had decreased as the surface roughness was increased. The tests that had low strain induced at the interface indicated good bond strength, thus better bond quality. Relating to the microstructure, a good bond would have a smooth interface that was free of voids [33]. The micrographs were taken using the FEI NovaNano SEM microscope, with a backscatter detector. The sizes of the voids were quantified using ImageJ software and the size of the voids per condition had a standard deviation of ± 0.05 µm.

8.2.1 Core at 7 Micron

8.2.1.1 Core at 7 Micron and clad at 0.5 µm, 1 µm and 3 µm

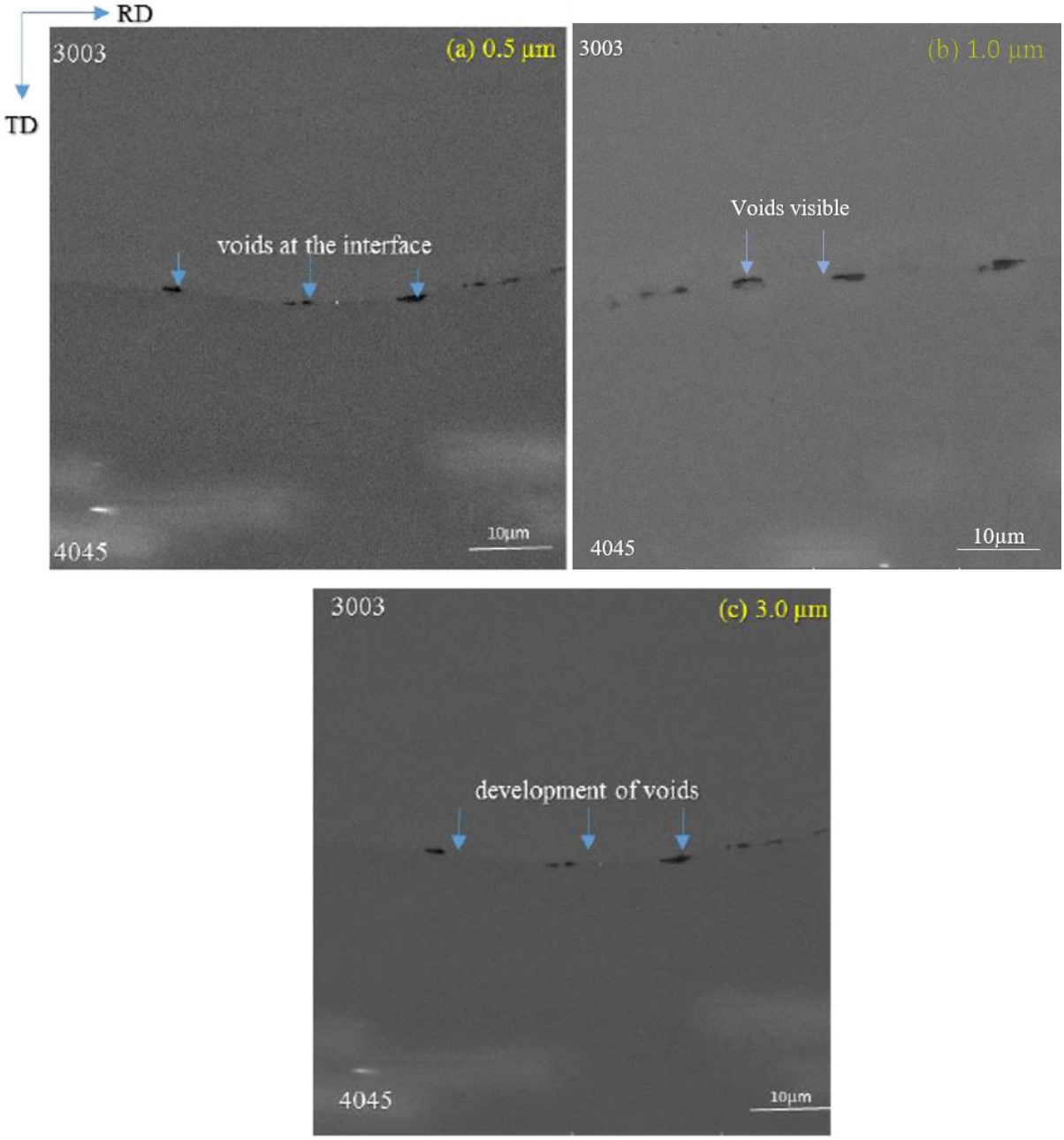

Figure 8-2 SEM micrographs when the core at 7.0 µm was bonded with the clad at (a) 0.5 µm (b) 1 µm (c) 3 µm

When the core at 7 µm was bonded to the clad at 0.5 µm, 1 µm and 3 µm, a trend similar to those of previous tests was observed: void sizes decreased with each increase in surface roughness, but once the optimal level of surface roughness had been exceeded, the void sizes increased significantly. [See Figure 8-2, (a) to (c)] This was is in line with the results presented in Figures 7-8 and 7-9, where the strain was shown to have reduced with increases in surface roughness but, once the optimal level of surface roughness at this condition had been exceeded, the strain increased significantly. The voids were approximately 0.44 ± 0.05 µm in size when

the core at 7 µm was bonded to the clad at 0.5 µm. At 1 µm the void size was further reduced to approximately 0.253 ±0.05 µm, but at 3 µm the void size was shown to have increased to approximately 0.316 ±0.05 µm.

In an analysis of the micrographs when the core at 7 µm was bonded to the clad at 1.0 µm, a smooth interface was observed, with smaller, more refined voids being identified, which indicated that a good bond had formed. However, when the bond was formed with the clad at 3 µm, the bond strength did not improve. Instead, it deteriorated, owing to the deep troughs induced in each specimen where the level of surface roughness had been increased to 3 µm. There was an incomplete fusion of the two materials and for this reason voids were created. This clearly indicated that there was an optimal level of surface roughness for every condition and if this level was exceeded, large voids would develop, causing weakening of the bond through delamination.

8.2.2 Core at 10 Micron

8.2.2.1 Core at 10 Micron and clad at 0.5 µm, 1 µm, 3 µm and 7 µm

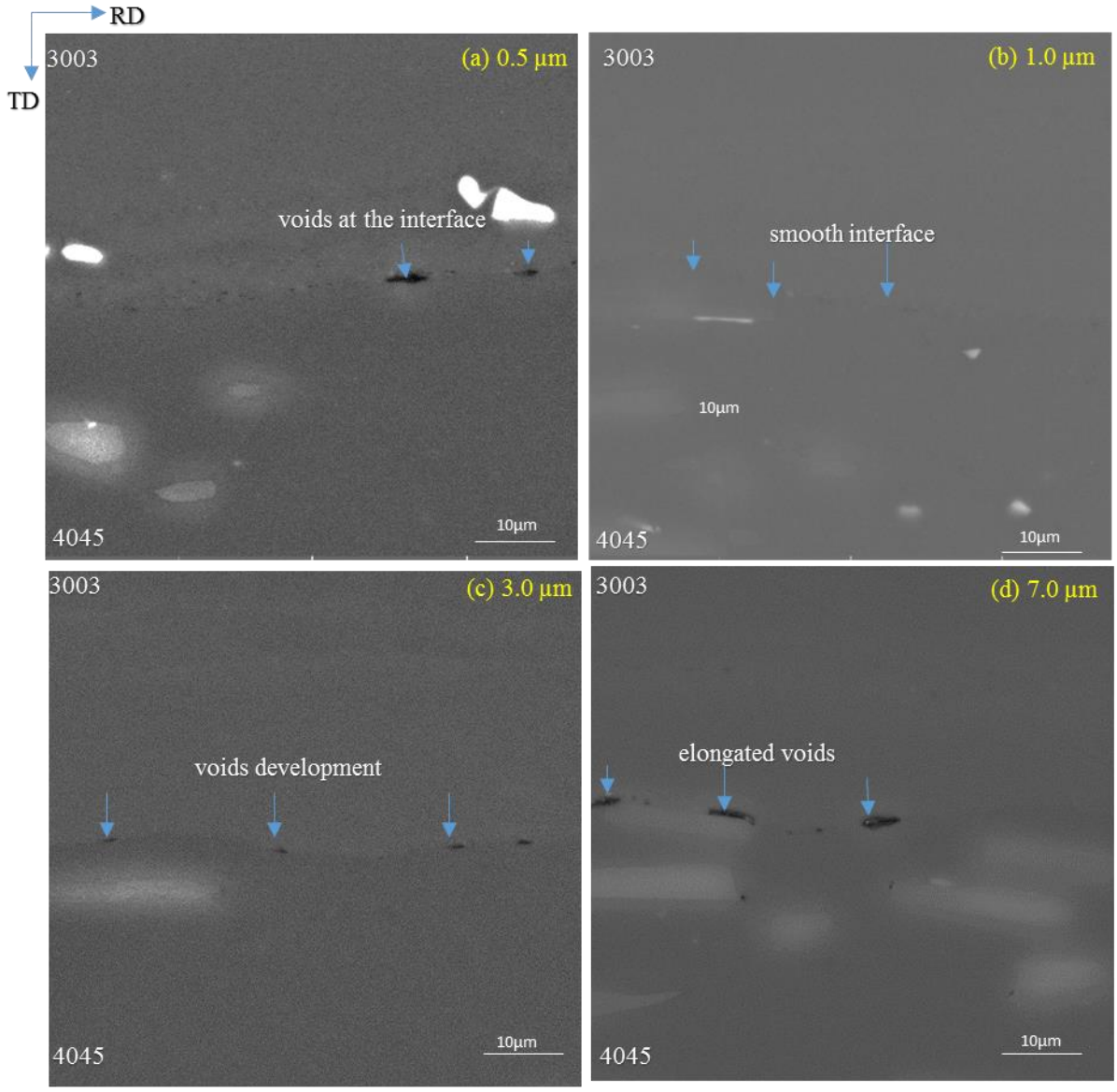

Figure 8-3 SEM micrographs when the core at 10 µm was bonded with the clad at (a) 0.5 µm (b) 1 µm (c) 3 µm (d) 7 µm

The Hulamin surface preparation standard was used as the benchmark for these test results. The current surface roughness preparation at Hulamin has the roughness of the core at 10 µm and the clad at 1 µm. In this section, the surface roughness of the core was kept at 10 µm and the surface roughness of the clad was varied, from 0.5 µm, through 1 µm and 3 µm, to 7 µm. Comparing the two micrographs in Figure 8-3, (a) and (b), it is clearly evident that the voids were significantly larger at 0.5 µm than at 1.0 µm. This was confirmed when the voids were measured using Image J software, where they were found to be approximately 0.138 ± 0.05 µm and 0.1 ± 0.05 µm respectively. Figure 8-3 confirmed the trend whereby the voids were

reduced in size with increased surface roughness, but also showed that when the optimal level of roughness had been exceeded, the void sizes increased to approximately 0.214 ± 0.05 µm for the clad at 3 µm and approximately 0.44 ± 0.05 µm for the clad at 7 µm. These findings validated the results obtained from the DIC in Figure 7-3 and Figure 7-4, where the strain localisation was shown to have decreased with increased surface roughness, but once the optimal level of surface roughness had been exceeded, strain localisation increased. Voids on the interface were the sites of strain localisation and the larger the void, the weaker the bond.

8.2.3 Core at 15 Micron

8.2.3.1 Core at 15 Micron and clad at 0.5 µm, 1 µm and 3 µm

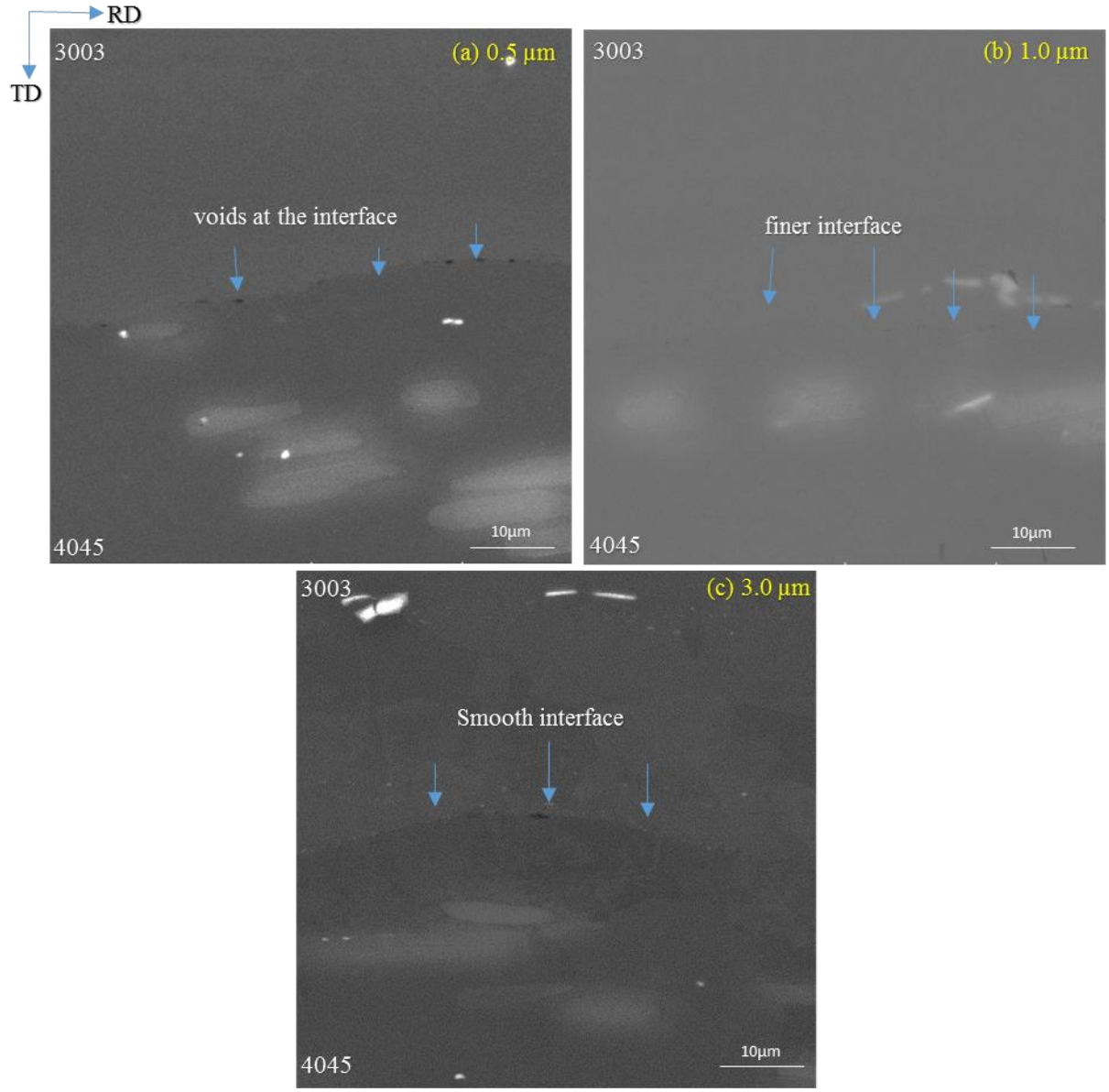

Figure 8-4 SEM micrographs when the core at 15 µm was bonded with the clad at (a) 0.5 µm (b) 1 µm (c) 3µm

Figure 7-5 and Figure 7-6 show the strain induced at the interface when the core at 15 µm was bonded to the clad at 0.5 µm, 1.0 µm and 3 µm, With the clad at 0.5 µm the bond was marginally weaker than with the clad at 1.0 µm, with slightly larger voids of approximately 0.388 ± 0.05 µm. But with the clad at 3 µm, the bond was weaker still, with voids of approximately 0.161 ± 0.05 µm. Therefore, the optimal surface roughness at this condition was determined to be when the core was bonded to the clad at 1 µm.

8.2.4 Core at 25 Micron

8.2.4.1 Core at 25 Micron and clad at 0.5 µm, 1 µm and 3 µm

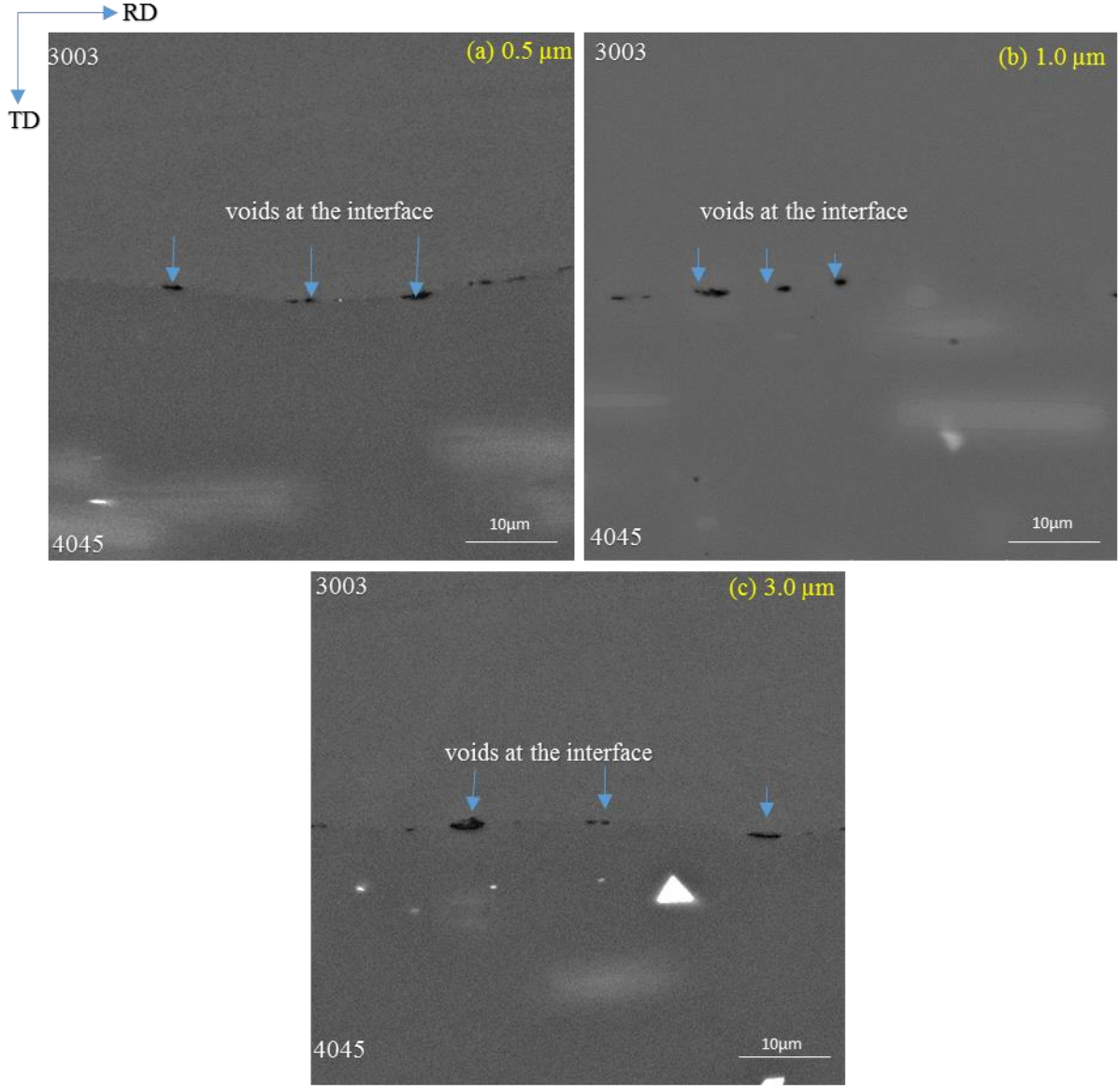

Figure 8-5 SEM micrographs when the core at 25µm was bonded with the core at (a) 0.5 µm (b) 1 µm (c) 3µm

Given that the Hulamin benchmark surface roughness of the core was 10 µm, a decision was made to test the bond strength with the core at a significantly higher level of surface roughness. Thus, in this round of testing the core was roughened to 25 µm and kept constant, while the clad was varied to 0.5 µm, 1 µm and 3 µm. The trend evident in the micrographs in Figure 8-8, a to c, corroborated the results of the tensile shear tests shown in Figures 7-7 and 7-8, in that an increase in surface roughness led to greater bond strength but beyond the optimal level of surface roughness the bond strength was compromised. However, in this set of tests, because of the very high level of roughness of the core (25 µm), while following the above trend, the overall bond strengths were significantly lower in comparision with all other tests performed for the purposes of this research.

With reference to Figure 8-5, the void sizes showed little variation along each interface (ranging from approximately 0.388 ± 0.05 µm to approximately 0.412 ± 0.05 µm). This comparative uniformity was due to the uniformly deep troughs on the surface of the specimens, caused by the more extreme roughening process at all three conditions. As was mentioned previously, the presence of these larger voids would become sites of strain localisation, with resultant delamination at these points. This behaviour was in line with the Thin Film Theory [2].

8.2.5 Summary

The microstructural analysis of the voids revealed that the level of surface roughness did play a major role in the bond strength during roll bonding. This was indicated by the range of void sizes that were quantified when the surface roughness ranged from low to very high. Smaller voids were associated with good quality bonds, whereas larger voids were associated with poorer bond quality. The SEM micrographs verified that the Hulamin benchmark, set at core 10 µm and clad 1 µm, and yielding voids with an approximate size of 0.10 ± 0.05 µm, could be slightly improved upon if the surface roughening of the core were increased to 15 µm, while the clad was kept at 1 µm. The void size would be less than 0.10 µm. Table 8-1 summarises the average void sizes for each of the surface roughness combinations. Included in the table is the average strain value, as determined from DIC (Chapter 7). Previously it was shown that the lowest strain value represented the best bond. In order to identify which of the combinations exhibited the smallest void size, associated with the best bond, as well as the lowest strain, these values have been summarised in Table 8-1 and the two lowest strain values and two smallest void sizes have been highlighted. The combination that exhibited low values of both strain and void size would represent the most favourable surface roughness

combination. This was shown to be a surface roughness of 15 µm on the core and 1 µm on the clad layers.

The SEM micrographs also verified that deep troughs in the surfaces of the material, induced by comparatively rougher surface finishes, would result in large voids at each interface, because the deformed material would cause incomplete fusion in the bonding process. This is illustrated in the sketch in Figure 8-6, where Image (a) shows two materials with similar surface finishes and Image (b) shows an even surface finish in one material and a rougher surface finish that has deep troughs in the second material. The gaps between the troughs would result in voids when the two materials were brought together, as explained previously.

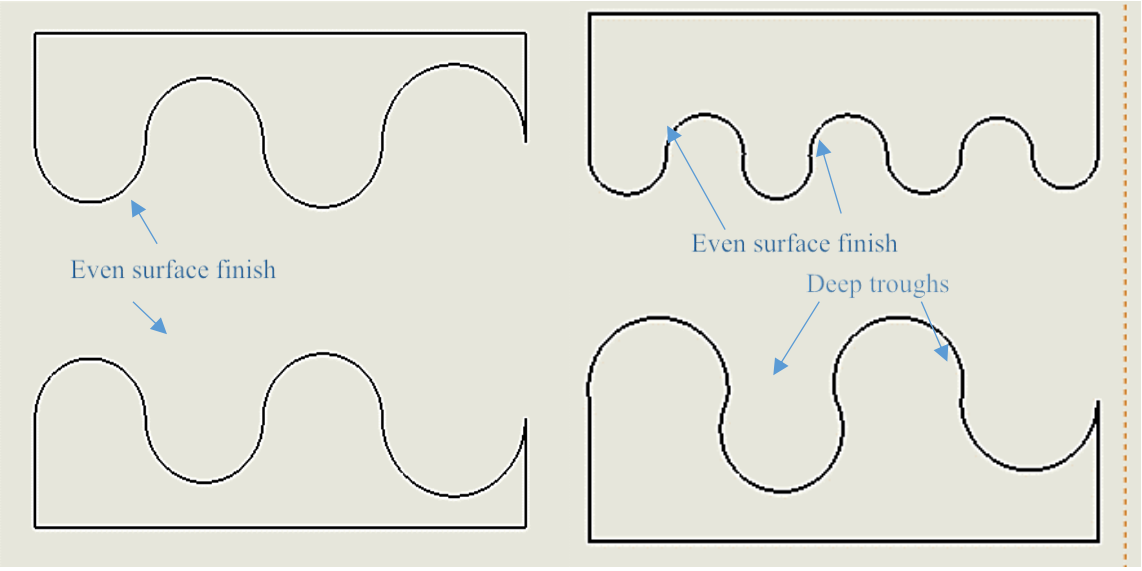

Figure 8-6 Metallurgical bond formation

Table 8-1 Summary of void sizes and DIC strain for the various surface roughness combinations

Core	Clad	Void size (µm)	Strain ($\mu\varepsilon$)
7 µm	0.5 µm	0.44 ± 0.05	287
	1 µm	0.253 ± 0.05	212
	3 µm	0.316 ± 0.05	279
10 µm	0.5 µm	0.318 ± 0.05	277
	1 µm	0.100 ± 0.05	169
	3 µm	0.214 ± 0.05	127

	7 µm	0.440 ± 0.05	472
15 µm	0.5 µm	0.388 ± 0.05	180
	1 µm	0.100 ± 0.05	132
	3 µm	0.151 ± 0.05	179
25 µm	0.5 µm	0.388 ± 0.05	214
	1 µm	0.316 ± 0.05	180
	3 µm	0.412 ± 0.05	319
Note: Cells are highlighted for two lowest strain values and two smallest porosity sizes. The combination which exhibits the lowest strain and smallest pore size represents best possible combination.			

8.3 Energy-Dispersive X-ray spectroscopy (EDS)

EDS is a method used for qualitative and quantitative purposes to determine the compositions of elements in any material. As mentioned in the literature, the concept of roll bonding can be explained in two ways: firstly, according to the Thin Film Theory and secondly, in terms of diffusion bonding [2]. (See Chapter 2.) The relevance of the Thin Film Theory has already been ascertained in this research. In this section, the diffusion of silicon from the clad layer into the core during roll bonding will be analysed. This was achieved using the EDS technique.

Because diffusion bonding is highly temperature- and holding-time dependent, surface preparation is crucial in the diffusion of atoms across an interface during roll bonding [55]. The two alloys analysed in this research had different compositions and thus the elements had different diffusion coefficients, with Si having a higher diffusion coefficient than Mn, thus Si was the element that diffused into AA3003, with lower Si content of 0-0.6 wt% Si, from AA4045, with a higher Si content of 9-11 wt% Si. EDS linescans were performed on samples with the clad surface roughness at a constant 1.0 µm, while the core surface roughness varied from 7 µm, through 10 µm and 15 µm, to 25 µm. Three linescans were performed across each interface per condition and each linescan represented 20 points, where Point 1 was the starting point and Point 20 was the ending point of the line. The starting point of the linescans were on the AA3003 and progressed into the AA4045.

8.3.1 Core at 7 Micron

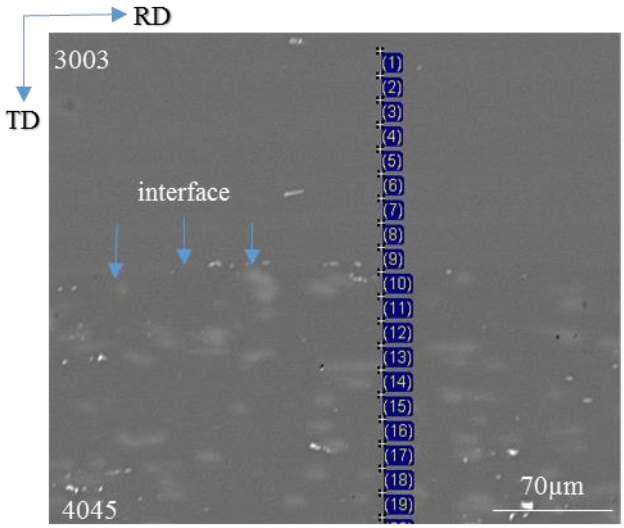

Figure 8-7 EDS line scan taken when the core was set at 7µm and clad at 1µm across the interface

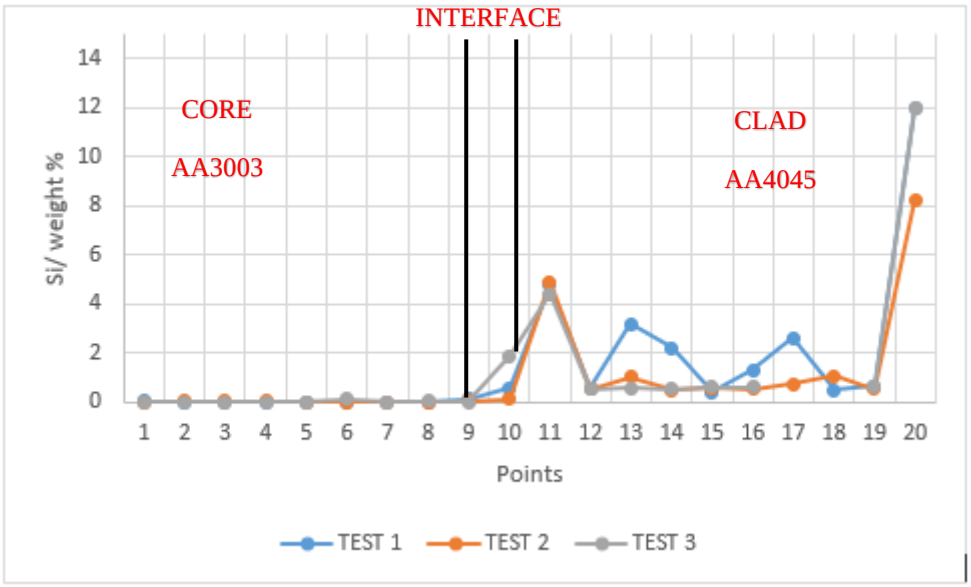

Figure 8-8 Silicon diffusion profile when core is at 7µm and clad at 1µm

From the literature it was established that when two dismilliar alloys were roll bonded there existed an atomic diffusion gradient during the formation of the metallurgical bond, owing to the different diffusion coefficents of the two alloys [53]. This promoted the diffusion of one alloy into another. The success of this process, where a smooth diffusion profile was achieved, was dependent on the following conditions: holding temperature, holding bonding time, pressure and surface condition [53]. In Figure 8-7, with the the core set at 7 µm and clad at 1µm, the diffusion profile was not smooth. Points 1 to 8 refer to AA3003, Points 9 to 11 refer to the passage through the interface and Points 12 to 20 refer to AA4045. The line scan was

taken from AA3003 into AA4045, this accounting for the depletion of the silicon from Point 20 to Point 1. Considering the region of transition from AA4045 to AA3003, there was a spike in the Si concentration to approximately 4.9 ± 1 w%. This spike could be due to the presence of voids situated at the interface (See Figure 8-8) and also could be associated with the EDS spot being on a Si-containing intermetallic particle, hence the non-uniformity in the diffusion profile, resulting in a weaker bond, as indicated by the tensile shear tests.

8.3.2 Core at 10 Micron

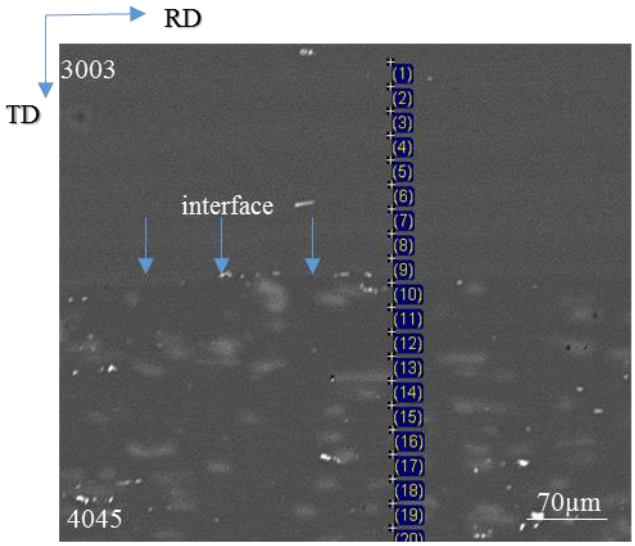

Figure 8-9 EDS line scan taken when the core was set at 10µm and clad at 1 µm

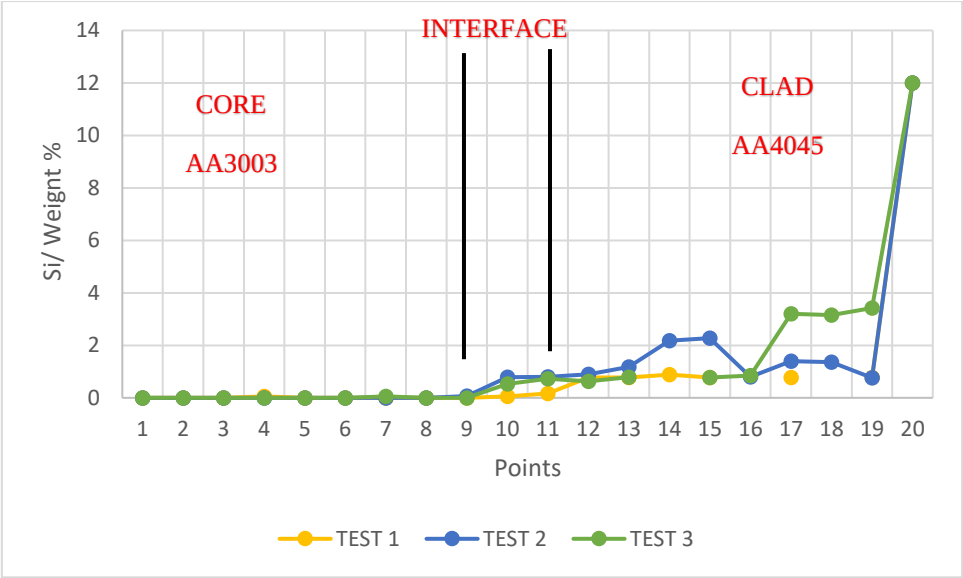

Figure 8-10 Silicon diffusion profile when core is at 10µm and clad at 1µm

In this phase of the testing, the surface roughness of the core was increased from 7 µm to 10 µm, with the clad surface roughness kept constant at 1 µm. This resulted in an interface with smaller voids, than that obtained when the core surface roughness was at 7 µm. An EDS line scan was performed at this condition and a much smoother diffusion profile was obtained. Further roughnening of the core disrupted the oxide layer that existsed on the surface of the alloys that would have impeded the diffusion of Si [53]. This was indicated by the depletion of Si as it diffused into AA3003. (See Figure 8-10) This then resulted in a bond with better bond strength, as indicated by the tensile shear test results.

8.3.3 Core at 15 Micron

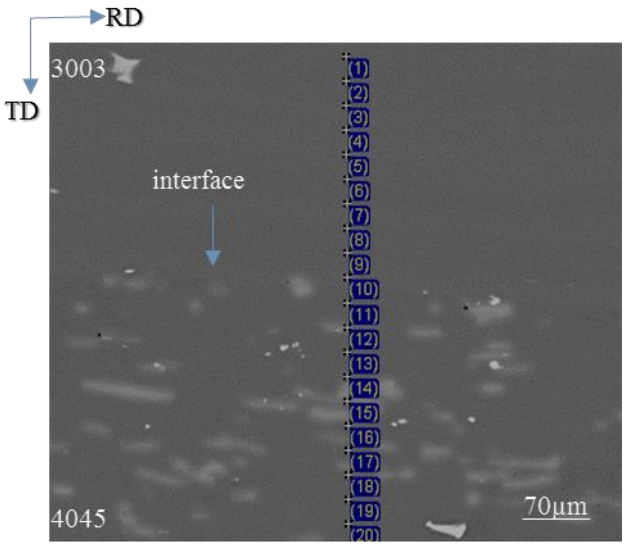

Figure 8-11 EDS line scan taken when the core was set at 15 µm and clad at 1µm

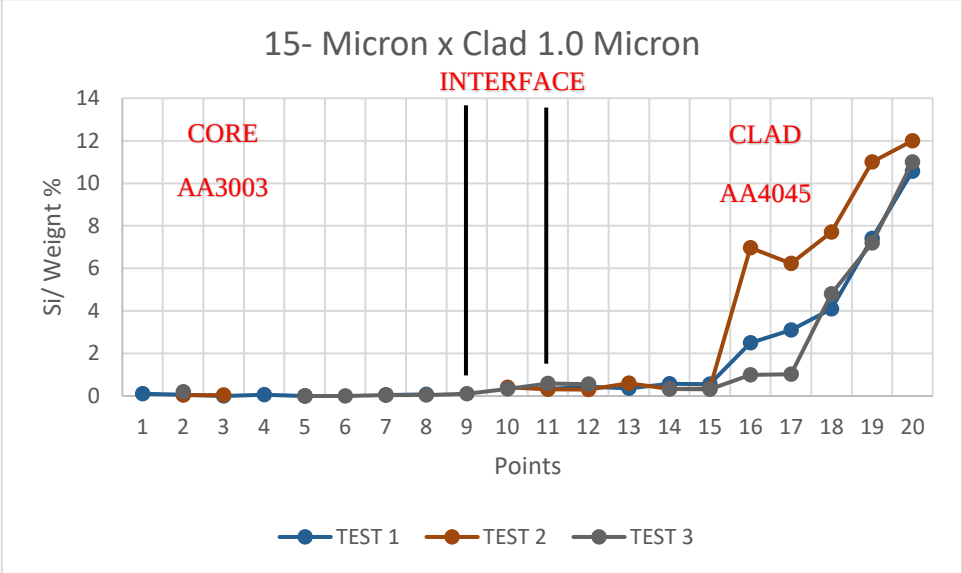

Figure 8-12 Silicon diffusion profile when core is at 15µm and clad at 1µm

In this phase of the testing, the surface roughness of the core was increased from 10 µm to 15 µm, while keeping the clad surface roughness constant at 1 µm. This resulted in a slightly more refined interface than the one shown when the core was at 10 µm, indicating further disruption of the aluminium oxide layer, hence promoting the diffusion of Si across the interface into the clad. In consequence, a much more better bond than before was obtained [53].

The sudden increase in the Si weight % at Point 16 indicates an intermetallic that was formed in the clad. The intermetallic might have resulted from fluctuating temperature during the PSC test. (See Figure 8-12)

8.3.4 Core at 25 Micron

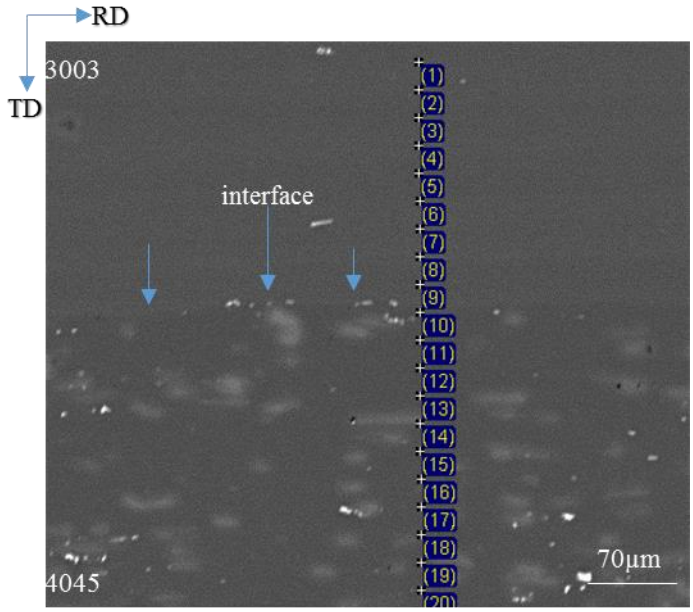

Figure 8-13 EDS line scan taken when the core was set at 25 µm and the clad at 1µm

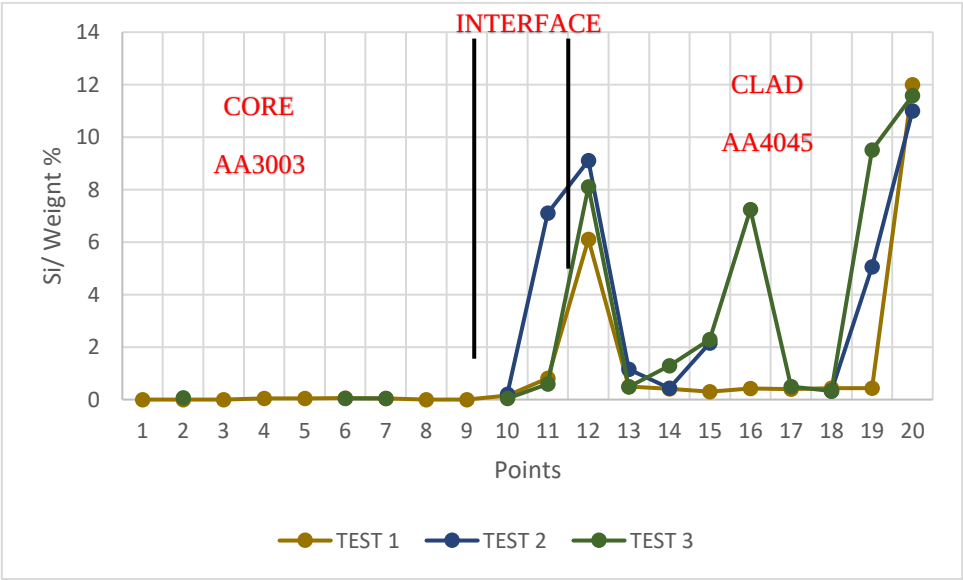

Figure 8-14 Silicon diffusion profile when core is at 25µm and clad at 1µm

In this phase of the testing, the surface roughness of the core was increased from 15 µm to 25 µm, with the clad surface roughness kept constant at 1 µm. This substantial increase in surface roughness resulted in a significantly weaker bond, owing to the presence of large voids that were formed at the interface. (See Figure 8-13 and Figure 8-14) The deep troughs caused by the roughening process had compromised the formation of a strong metallurgical bond, leading to the formation of these voids. It is higly possible that the presence of the voids and the intermetallic present could have caused the peaks seen in Figure 8-14, these impeding the diffusion of Si and resulting in a weaker bond. This was corroborated by the shear test results.

8.3.5 Summary

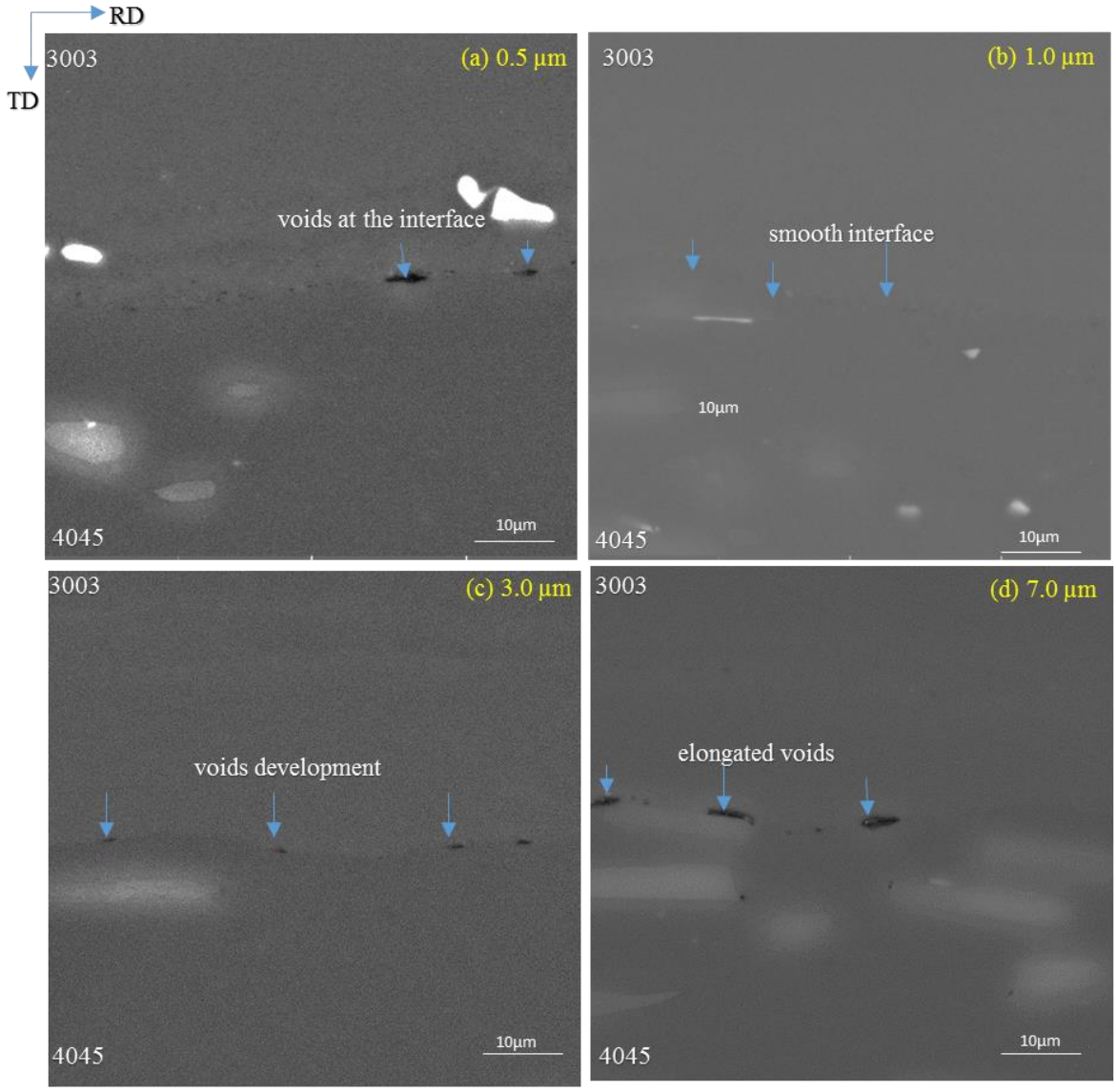

Figure 8-15SEM micrographs when the clad at 1.0µm was bonded with the core at (a) 7 µm (b) 10 µm (c) 15 µm (d) 25 µm

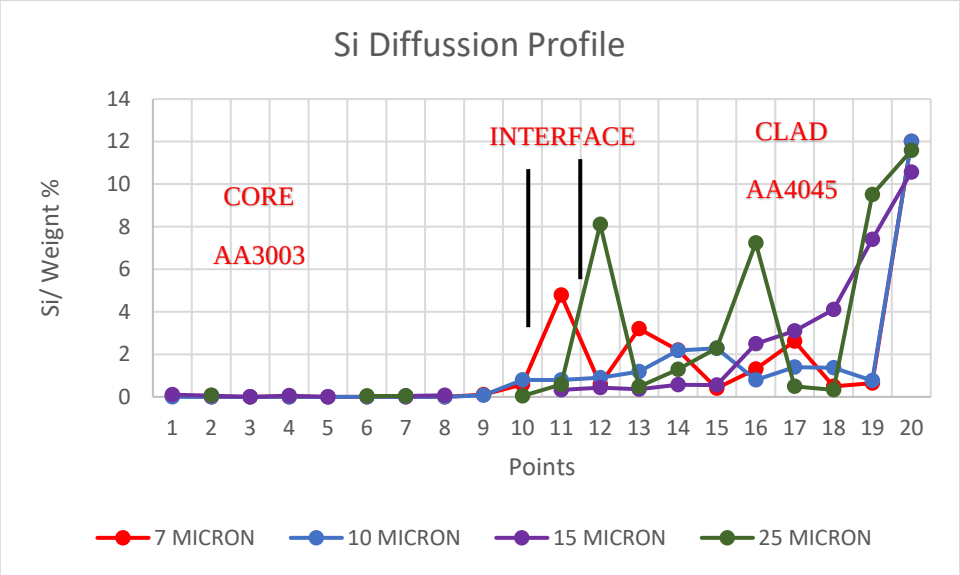

Figure 8-16 Si Diffusion Profile of the core at 7 µm, 10 µm, 15 µm and 25 µm, where the clad was kept at 1µm.

In summary, it can be concluded that, in addition to the role of temperature and holding time in diffusion bonding, surface roughness is a significant consideration in diffusion bonding. Increase in the surface roughness favours the diffusion of Si across the interface since the disruption of the aluminum oxide layers of Aluminium [53]. The optimal level of surface roughness was found to exist somewhere between 10µm and 15 µm, since these conditions both favoured the smooth diffusion of Si, owing to the relatively small voids present at their respective interfaces. (See Figure 8-16)

9 CONCLUSIONS

The main conclusion that can be drawn is that surface roughness plays a major role in the bond strength between the two aluminium alloys, AA3003 and the AA4045, during roll bonding simulation. The critical presence of surface asperities is induced by rougher surface finishes. During bonding at intense pressures and at a high temperature the surface asperities merge and form a weld, thus forming a metallurgical bond. Ideally, this metallurgical bond should exhibit limited voids of very small size at the interface and the strain during tensile shear testing should be as low as possible.

This overall conclusion was made based on the conclusions below:

- While simulation of roll bonding was achieved successfully using PSC on the Gleeble 3800, the testing process itself revealed that good contact between anvils and samples is critical during testing in order to avoid heat localisation, which induces the localised melting of material. Good contact is achieved with the use of tantalum as a barrier layer.
- The most valuable methodology that can be used to differentiate between different surface roughness combinations in the core and clad layers is through analysis of the strain distribution *data* attained through DIC during tensile shear testing. Strain distribution *data* showed that the weakest bond is obtained when a core with a surface roughness of 10 µm is bonded with the clad at 7 µm, while the best combination for bond strength is when the surface roughness of the core is at 15 µm and the surface roughness of the clad is at 1 µm. This produces a slightly better result than the combination of surface roughnesses of 10 µm (core) and 1.0 µm (clad).
- The microstructural characterisation process revealed the presence of voids and, when correlated with the strain distribution results, the microstructural analysis showed that smaller voids are associated with good quality bonds, while larger voids are associated with poorer quality bonds. An optimal surface roughness combination was determined by identifying the combinations that exhibited both the smallest void size and a low strain value attained from DIC. The optimal roughness combination for the best bond strength was seen with the core at 15 µm and the clad at 1 µm, with a void size of approximately 0.10 ± 0.05 µm and a strain of 132 micro strain. This was closely followed by: the core at 10 µm and the clad at 1 µm (the Hulamin standard), with a void size of approximately 0.10 ± 0.05 µm and a strain of 169 micro strain.

- The SEM micrographs also verified that deep troughs in the surfaces of the material, associated with rougher surface finishes, would result in large voids at each interface, as a result of incomplete fusion in the bonding process. The relative sizes of the surface asperities associated with the different roughness values are critical for the metallurgical bonding and the porosity that results at the interfaces.
- Surface roughness also plays a role in the diffusion of Si across the bond during roll bonding although it is highly dependent on temperature. The optimal level of surface roughness was found to exist somewhere between 10µm and 15 µm, since both these conditions favoured the smooth diffusion of Si across the interface.
- There is an optimal surface finish that exists between the two alloys to obtain a better metallurgical bond since, if the optimum finish is exceeded, the strain level increases during tensile shear testing, with the voids that are induced increasing in size and the Si diffusion across the interface decreasing. These factors point to a compromise in the quality of the bond.
- The Hulamin benchmark surface preparation, which is currently set at 10 µm (core) and 1µm (clad), can be improved by increasing the surface roughness of the core to 15µm, while keeping the clad surface finish constant.

10 FUTURE WORK AND RECOMMENDATIONS

Based on the experimental work and the results attained during this limited investigation, it is recommended that the following topics be explored in connection with future work on this project.

- During surface preparation, differing degress of surface roughness were considered. However, surface waviness also plays a major role in roll bonding. Owing to the limitations in the experimental matrix size of this study, surface waviness was not taken into account. There should be an investigation into the context of porosity at the interface associated with waviness.
- The sizes of the grains are significant in the determination of bond strength, as grain refinement correlates with better material strength. A technique that could be used to evaluate the grain sizes on either side of the interface is electron backscatter diffraction (EBSD). It could also be used to identify dendritic growth in areas where localised melting may have occurred.
- Fractography can also be performed in SEM to view the surfaces of the bond interface after tensile shear testing.
- Equipment with induction heating, rather than electrical resistance heating (as used in this project), may be more suitable to this type of roll bonding simulation. It is suggested that a matrix of tests be performed on a machine with induction heating to eliminate temperature gradients and localised melting owing to arcing.

LIST OF REFERENCES

[1] U. States, "(12) Patent Application Publication (10) Pub. No.: US 2014/0272463 A1," 2014.

[2] J. Kuśnierz and J. Bogucka, "Accumulative roll-bonding (ARB) of A199.8%," *Archives of Metallurgy and Materials*, vol. 50, no. 1. pp. 219–230, 2005.

[3] M. J. F. Gándara, "Aluminium: The metal of choice," *Mater. Tehnol.*, vol. 47, no. 3, pp. 261–265, 2013.

[4] H. M. King, "Bauxite: The principal ore of aluminum." 2017.

[5] J. Davis, "Alloying: understanding the basics-Light Metals and Alloys," *Mater. Sci. Technol.*, pp. 192–203, 2001, doi: 10.1361/autb2001p351.

[6] "Aluminium's Lifecycle | About | Hulamin, South Africa." .

[7] A. W. Brace, "'Surface treatment and finishing of aluminium,'" *Br. Corros. J.*, vol. 23, no. 3, pp. 156–156, 1988, doi: 10.1179/000705988798270884.

[8] F. . Campbell, "Aluminum," in *Elements of Metallurgy and Engineering Alloys*, AS International, 2008, pp. 487–508.

[9] L. J. Barker and assignor to, "United States Patent Office Heat Treatment of Aluminumalloys," p. 845, 1953.

[10] "Data Book November 2014 Edition 18," no. November, 2014.

[11] "Aa 3003 - h14," p. 3312182.

[12] S. W. Nam and D. H. Lee, "The effect of Mn on the mechanical behavior of Al alloys," *Met. Mater. Int.*, vol. 6, no. 1, pp. 13–16, 2000, doi: 10.1007/BF03026339.

[13] A. Rawal, R. Kumar, and H. Saraswat, "Tensile mechanics of braided sutures," *Text. Res. J.*, vol. 82, no. 16, pp. 1703–1710, 2012, doi: 10.1177/0040517512445340.

[14] N. A. Belov, D. G. Eskin, and A. A. Aksenov, "Multicomponent Phase Diagrams: Applications for Commercial Aluminum Alloys," *Multicomponent Phase Diagrams Appl. Commer. Alum. Alloy.*, pp. 12–15, 2005, doi: 10.1016/B978-0-08-044537-3.X5000-8.

[15] Y. J. Li and L. Arnberg, "Evolution of eutectic intermetallic particles in DC-cast AA3003 alloy during heating and homogenization," *Mater. Sci. Eng. A*, vol. 347, no. 1–2, pp. 130–135, 2003, doi: 10.1016/S0921-5093(02)00555-5.

[16] Y. J. Li and L. Arnberg, "Quantitative study on the precipitation behavior of dispersoids in DC-cast AA3003 alloy during heating and homogenization," *Acta Mater.*, vol. 51, no. 12, pp. 3415–3428, 2003, doi: 10.1016/S1359-6454(03)00160-5.

[17] I. Company, "AL 4147 (BAlSi-9)," pp. 1–2.

[18] A. Kłyszewski *et al.*, "New rolled aluminium alloy products for the automotive industry," *Arch. Metall. Mater.*, vol. 59, no. 1, pp. 393–396, 2014, doi: 10.2478/amm-2014-0065.

[19] A. Sharma, Y. S. Shin, and J.-P. Jung, "Influence of Various Additional Elements in Al Based Filler Alloys for Automotive and Brazing Industry," *J. Weld. Join.*, vol. 33, no. 5, pp. 1–8, 2015, doi: 10.5781/jwj.2015.33.5.1.

[20] M. Haghshenas and J. Jamali, "Assessment of circumferential cracks in hypereutectic Al-Si clutch housings," *Case Stud. Eng. Fail. Anal.*, vol. 8, pp. 11–20, 2017, doi:

10.1016/j.csefa.2016.11.003.

[21] R. TIMSIT and B. JANEWAY, “A novel brazing technique for aluminum,” *Weld. J.*, vol. 73, no. 6, p. 119, 1994.

[22] “23 Aluminium Brazing – News, Knowledge & Technology.” .

[23] H. Engstroem and L. O. Gullman, “Multilayer clad aluminum material with improved brazing properties,” *Weld. J. (Miami, Fla)*, vol. 67, no. 10, pp. 222–226, 1988.

[24] *Surface Characterization An Overview Techniques :*, no. July 2002. 2017.

[25] Y. Wang, F. Xie, S. Ma, and L. Dong, “Review of surface profile measurement techniques based on optical interferometry,” *Opt. Lasers Eng.*, vol. 93, no. January, pp. 164–170, 2017, doi: 10.1016/j.optlaseng.2017.02.004.

[26] M. K. Saha and S. Das, “A Review on Different Cladding Techniques Employed to Resist Corrosion,” *J. Assoc. Eng. India*, vol. 86, no. 1–2, p. 51, 2016, doi: 10.22485/jaei/2016/v86/i1-2/119847.

[27] H. Singhbedi, H. Arora, and M. Bansal, “Microstructure , Mechanical Properties & Corrosion Behavior of Duplex 2209 in Electro-Slag Strip Cladding over low carbon steel substrate : a Review Paper,” vol. 5, no. 3, pp. 72–73, 2015.

[28] Y. Kumar and S. Kumar, “Advances in Material Forming and Joining,” no. January, pp. 29–47, 2015, doi: 10.1007/978-81-322-2355-9.

[29] M. Cheepu *et al.*, “Fabrication and Analysis of Accumulative Roll Bonding Process between Magnesium and Aluminum Multi-Layers,” *Appl. Mech. Mater.*, vol. 877, no. February, pp. 183–189, 2018, doi: 10.4028/www.scientific.net/amm.877.183.

[30] L. Da Silva, M. El-Sharif, C. Chisholm, and S. Laidlaw, “A review of the cold roll bonding of AlSn alloy/steel bimetal strips,” *Met. 2014 - 23rd Int. Conf. Metall. Mater. Conf. Proc.*, no. May, pp. 274–284, 2014.

[31] “Rolling Aluminum : From the Mine Through the Mill on the Sheet and Plate Division ’ s Technology Committee .”

[32] M. H. Khan, O. A. Gali, A. Edrisy, and A. R. Riahi, “Effect of oxidation and surface roughness on the shear strength of single - lap - joint adhesively bonded metal specimens by tension loading,” *Appl. Adhes. Sci.*, pp. 1–17, 2016, doi: 10.1186/s40563-016-0077-1.

[33] J. Liu, M. Li, S. Sheu, M. E. Karabin, and R. W. Schultz, “Macro- and micro-surface engineering to improve hot roll bonding of aluminum plate and sheet,” vol. 479, pp. 45–57, 2008, doi: 10.1016/j.msea.2007.06.022.

[34] L. Li, K. Nagai, F. Yin, L. Li, K. Nagai, and F. Yin, “Progress in cold roll bonding of metals,” vol. 6996, 2008, doi: 10.1088/1468-6996/9/2/023001.

[35] D. S. Inc, *GLEEBLE SYSTEMS AND APPLICATIONS*. New York, 2012.

[36] N. Sae-eaw and Y. Aue-u-lan, “ScienceDirect Mechanical property determination for combined sheet and bulk metal forming process by plane strain compression test,” *Mater. Today Proc.*, vol. 5, no. 3, pp. 9376–9383, 2018, doi: 10.1016/j.matpr.2017.10.113.

[37] M. S. Loveday *et al.*, “Measurement of flow stress in hot plane strain compression tests,” vol. 23, no. 2, pp. 85–118, 2006.

[38] “39 Mechanical metallurgy - Dieter_ George Ellwood.pdf.” .

[39] T. A. Strip, J. Specimen, T. Results, C. S. Plate, C. Quality, and R. Bar, “Standard Test Method for Strength Properties of Adhesives in Shear by Tension Loading of Single-Lap-Joint Laminated Assemblies 1,” pp. 48–51, 2019.

[40] Y. Shen, “Deformation analysis of lap-shear testing of solder joints,” vol. 53, pp. 2633–2642, 2005, doi: 10.1016/j.actamat.2005.02.024.

[41] S. T. Method, “Standard Test Method for Peel Resistance of Adhesives (T-Peel Test) 1,” vol. 03, pp. 4–6, 2008.

[42] J. Kosmann, O. Völkerink, M. J. Schollerer, D. Holzhüter, and C. Hühne, “International Journal of Adhesion and Adhesives Digital image correlation strain measurement of thick adherend shear test specimen joined with an epoxy fi lm adhesive,” *Int. J. Adhes. Adhes.*, vol. 90, no. January, pp. 32–37, 2019, doi: 10.1016/j.ijadhadh.2019.01.024.

[43] V. Saouma, “Strain Measurements with Digital Image Correlation System Vic-2D NEES at CU Boulder Strain Measurements with the Digital Image Correlation System Vic-2D By University of Puerto Rico , Mayagüez,” no. January 2008, 2015.

[44] Y. Jing, Y. Qin, X. Zang, and Y. Li, “Journal of Materials Processing Technology The bonding properties and interfacial morphologies of clad plate prepared by multiple passes hot rolling in a protective atmosphere,” *J. Mater. Process. Tech.*, vol. 214, no. 8, pp. 1686–1695, 2014, doi: 10.1016/j.jmatprotec.2014.03.019.

[45] A. International, “Metals and alloys in the Unified Numbering System,” *Jt. Publ. ASTM Int. SAE Int.*, 2012.

[46] “47 Diamond Compounds.” .

[47] “48 Tensile test Engineers Gallery.” .

[48] B. Hafner, “Energy Dispersive Spectroscopy on the SEM :”

[49] “51 What is FEA Finite Element Analysis — SimScale Documentation.” .

[50] G. Cent and M. Engineering, “ity of e To w ve rs ity e To w,” 2015.

[51] M. Abbasi and M. R. Toroghinejad, “Journal of Materials Processing Technology Effects of processing parameters on the bond strength of Cu / Cu roll-bonded strips,” vol. 210, pp. 560–563, 2010, doi: 10.1016/j.jmatprotec.2009.11.003.

[52] “54 Mechanics of Materials 1 3rd Ed Hearn section 4 bending stress.pdf.” .

[53] “56 Effect of Alloying Elements Gradient on Solid-State Diffusion Bonding between Aerospace Aluminum Alloys.” .

11 APPENDIX

APPENDIX A PSC TESTS

Core 7.0µm x clad 0.5µm | A1xB1| Target Temp = 450ºC|TEST 1-3|

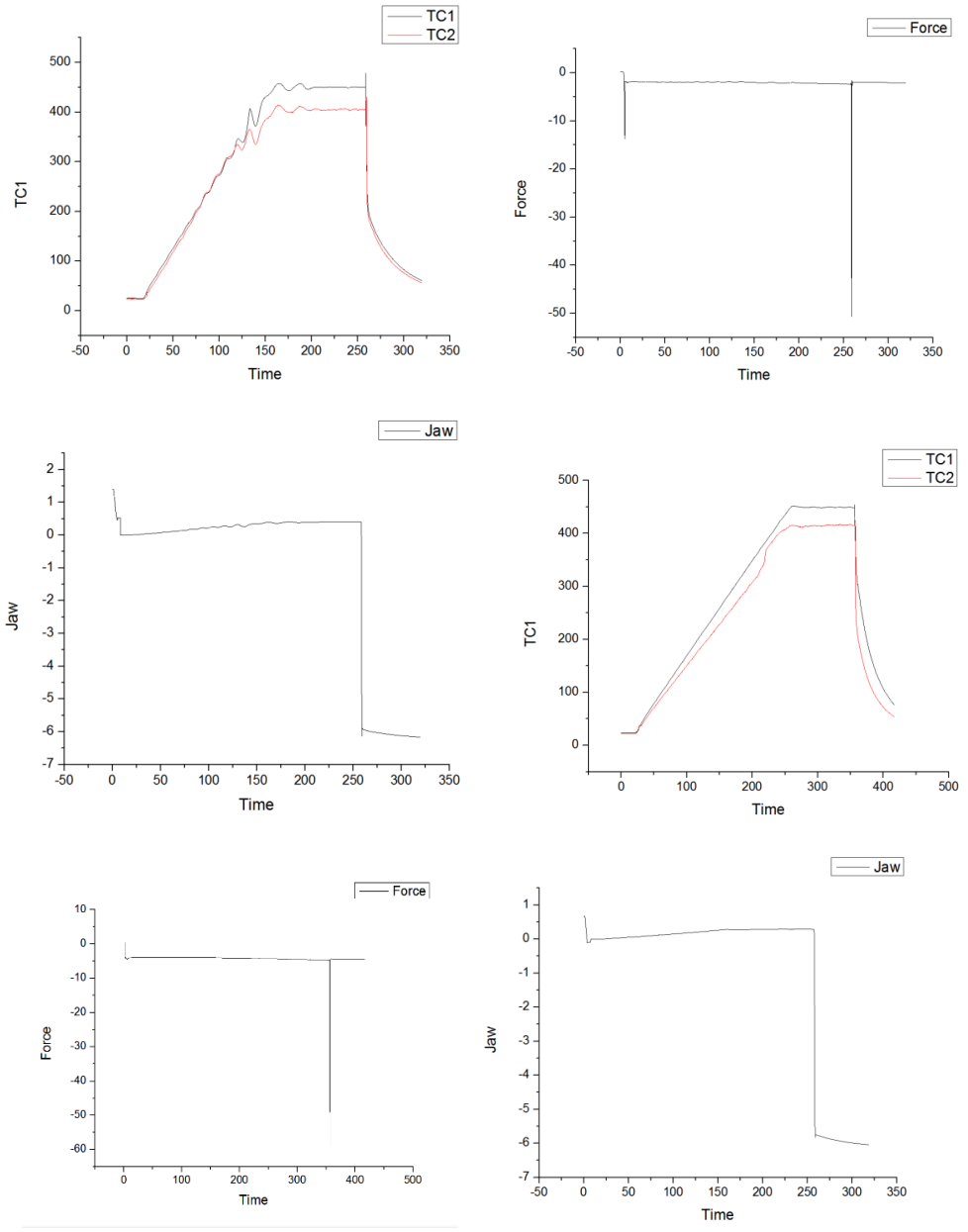

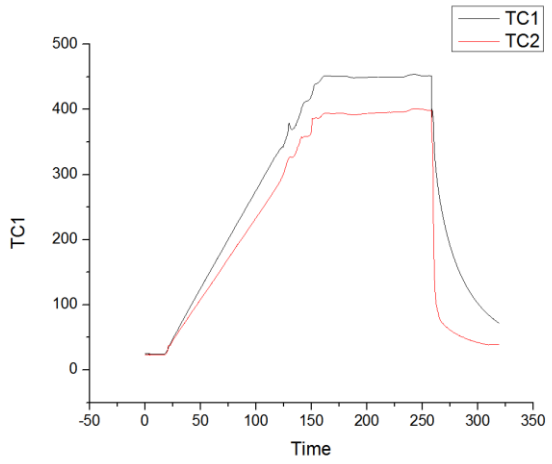
TC1
TC2
TC1
Time

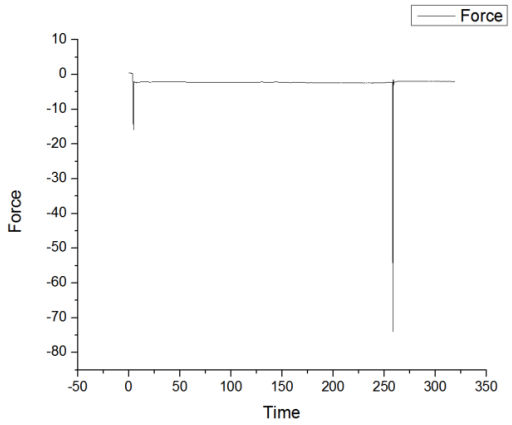
Force
Force
Time

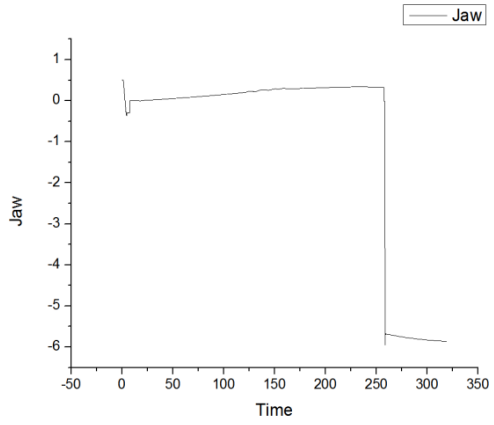
Jaw
Jaw
Time

Core 7.0µm x clad 1.0µm | A1xB2| Target Temp = 450ºC|TEST 1-3|

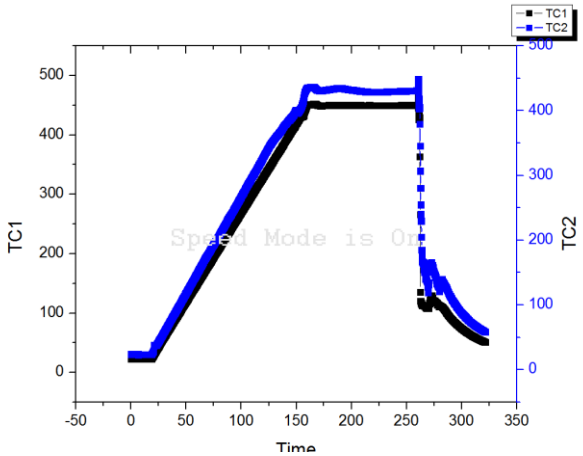

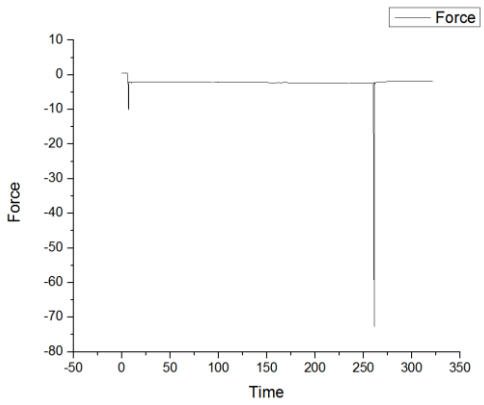

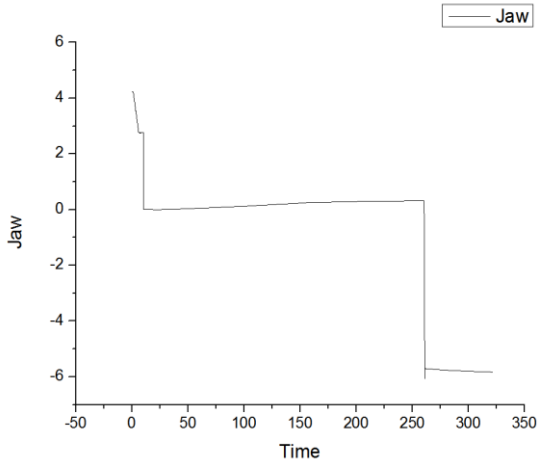

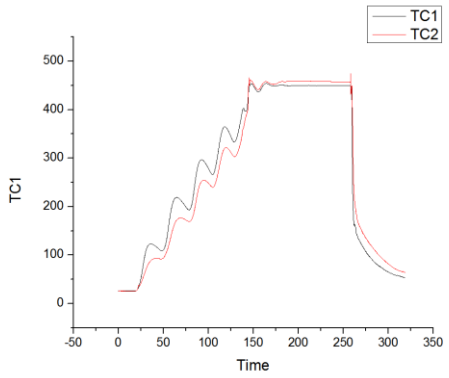

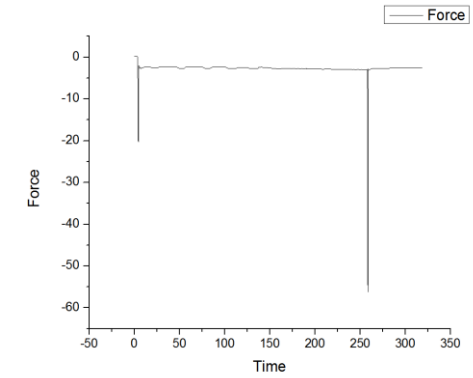

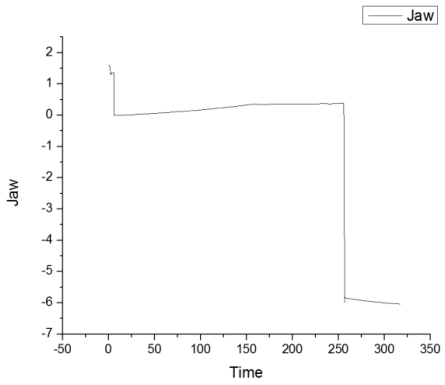

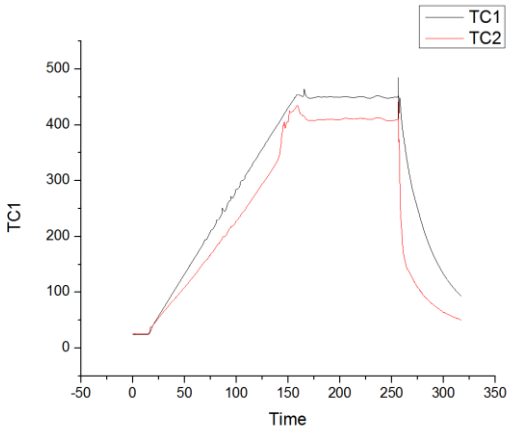
TC1
TC2
TC1
Time

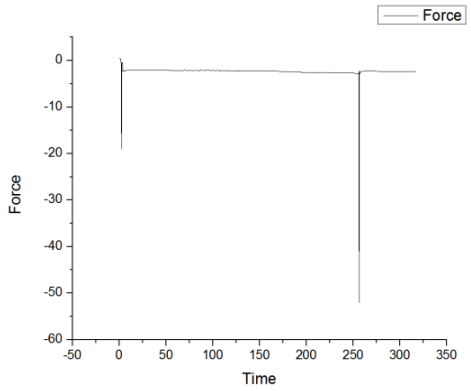
Force
Force
Time

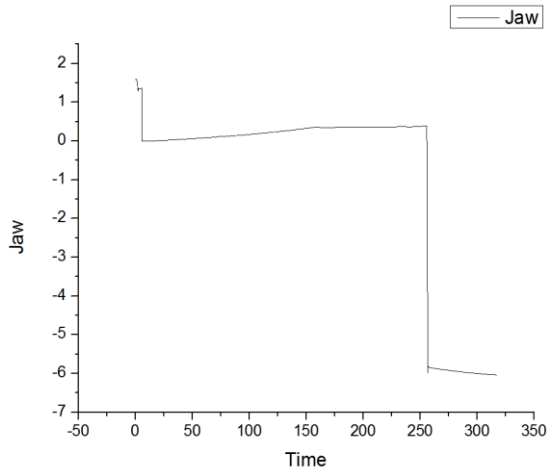
Jaw
Jaw
Time

Core 7.0µm x clad 3.0µm | A1XB3| Target Temp = 450ºC|TEST 1-3|

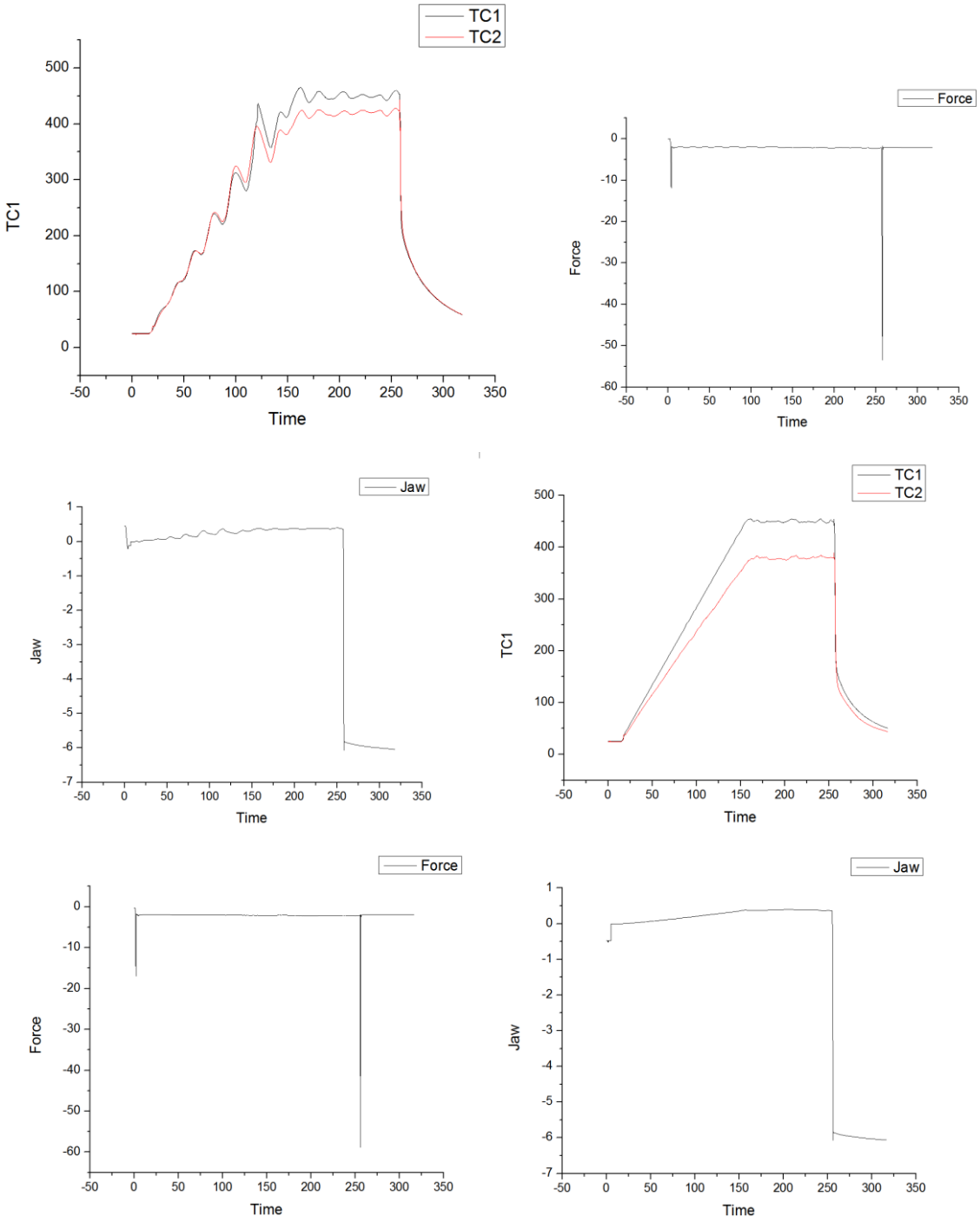

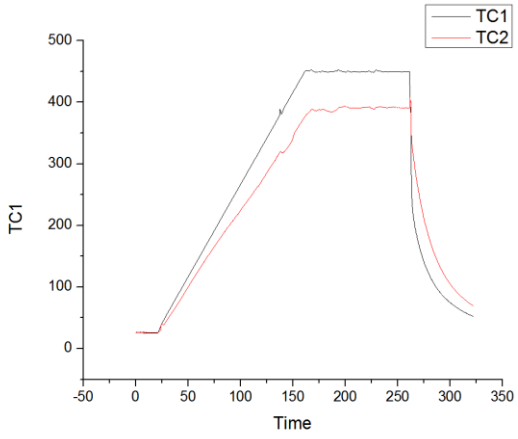
TC1
TC2
TC1
Time

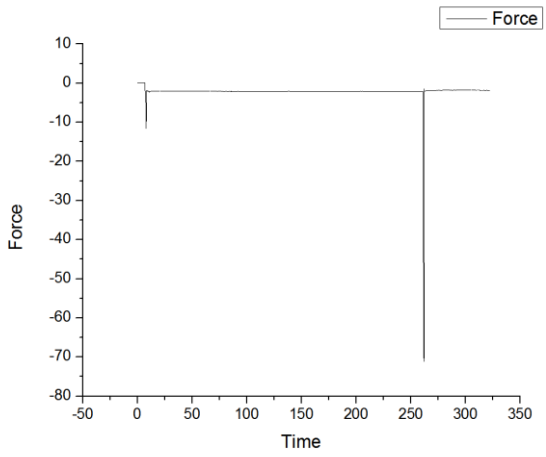
Force
Force
Time

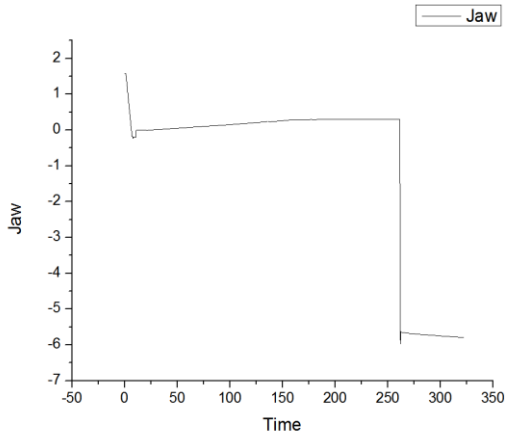
Jaw
Jaw
Time

Core 10µm x clad 3µm | A2XB2| Target Temp = 450ºC|TEST 1-3|

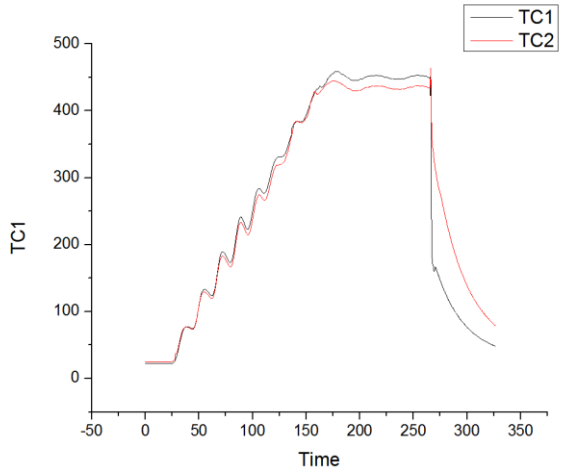

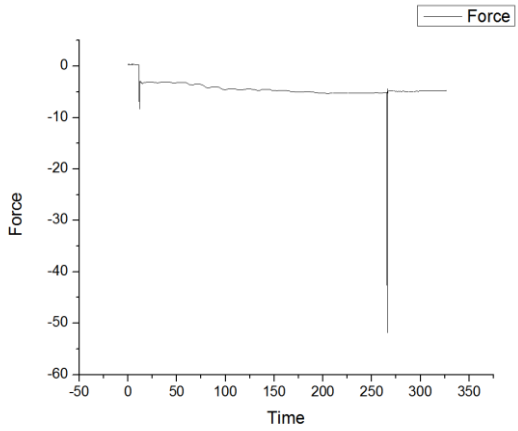

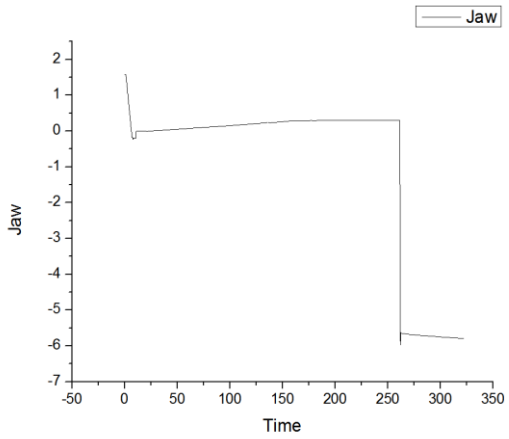

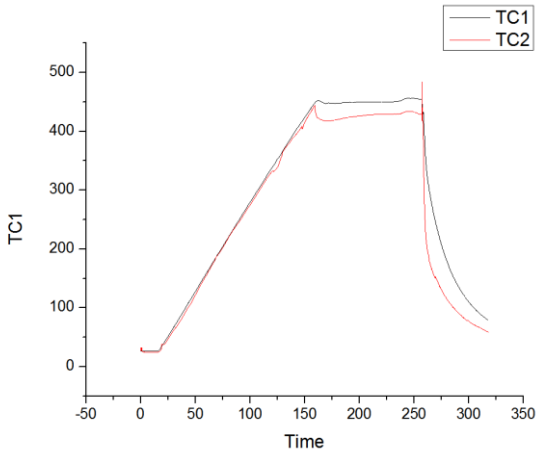

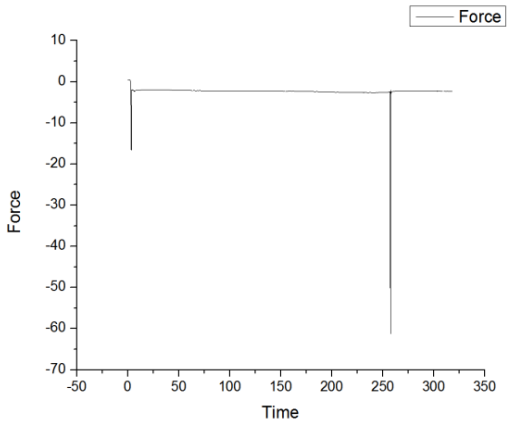

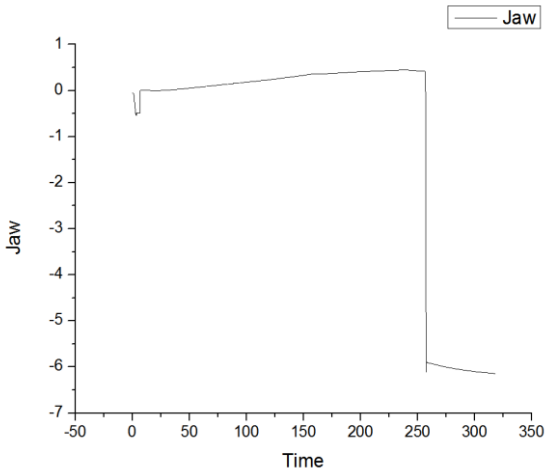

Core 10µm x clad 3 µm | A2XB3| Target Temp = 450ºC|TEST 1-3|

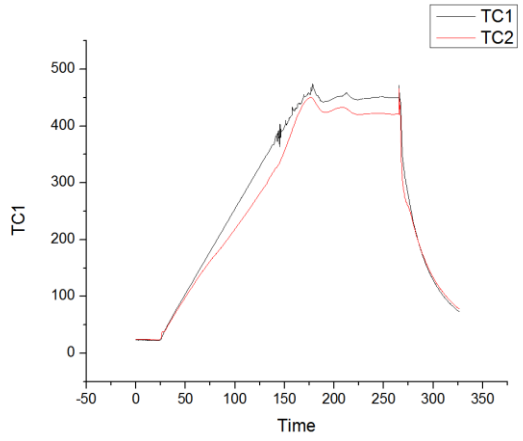

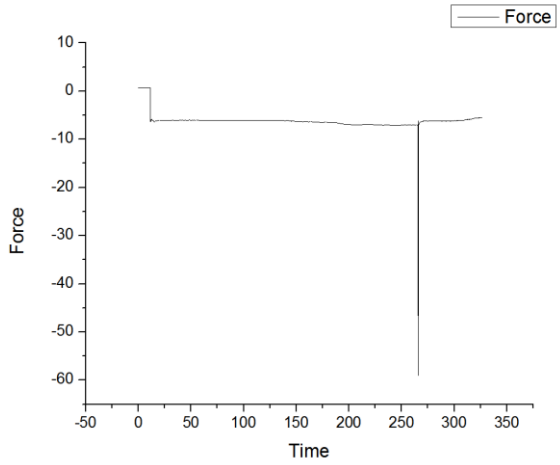

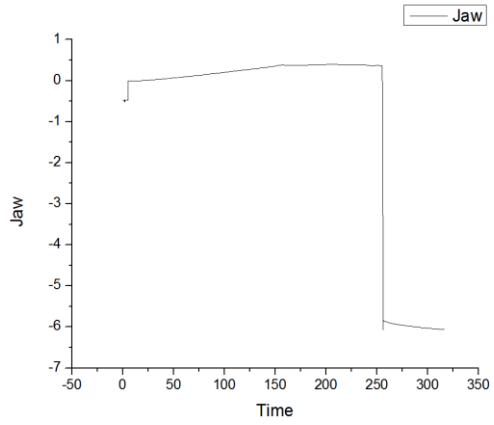

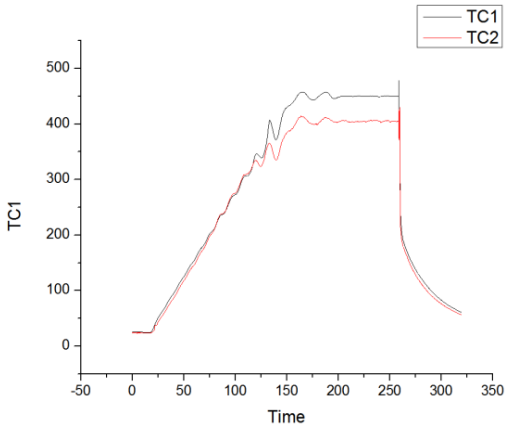

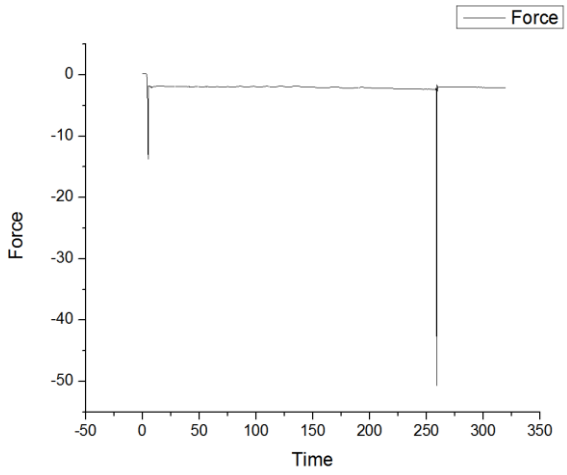

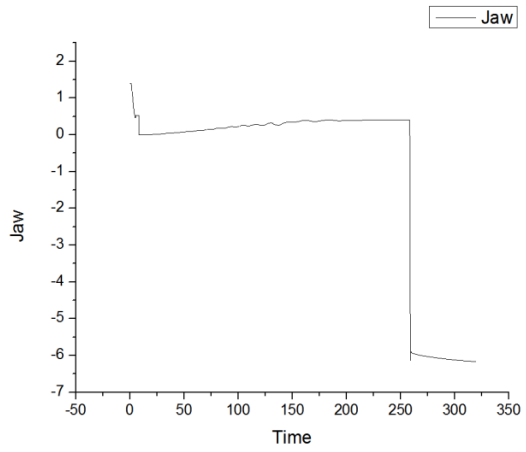
Jaw
Jaw
Time

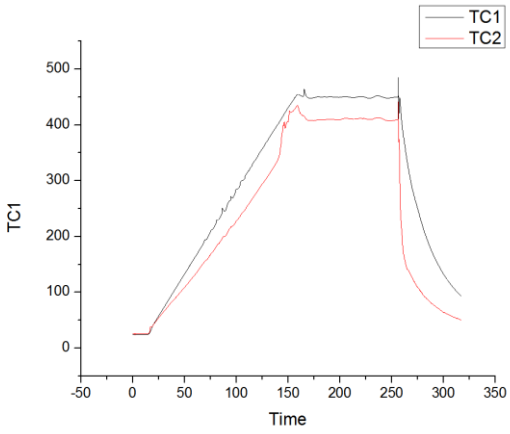
TC1
TC2
TC1
Time

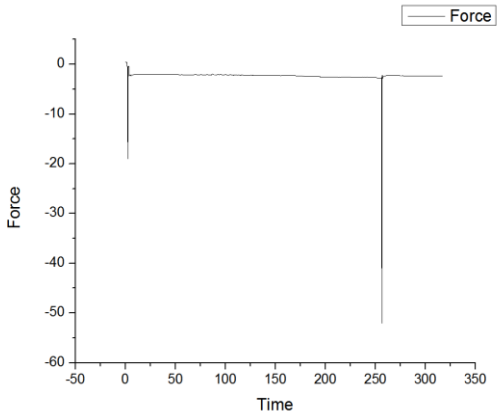
Force
Force
Time

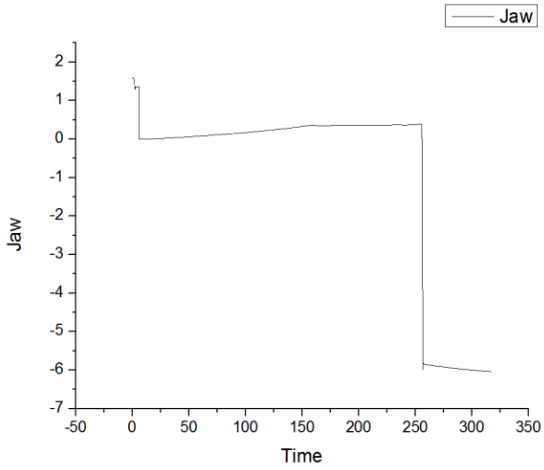
Jaw
Jaw
Time

Core 15µm x clad 0.5µm | A3XB1| Target Temp = 450ºC|TEST 1-3|

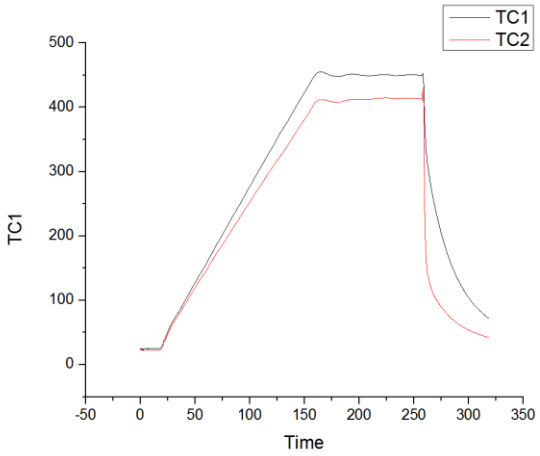

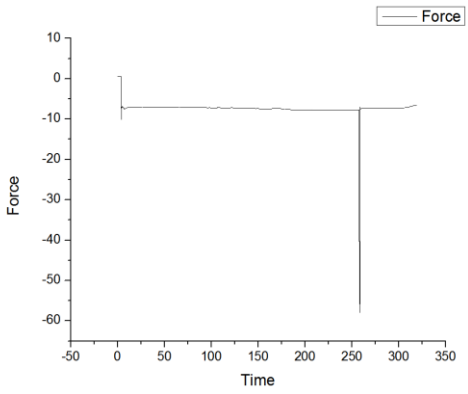

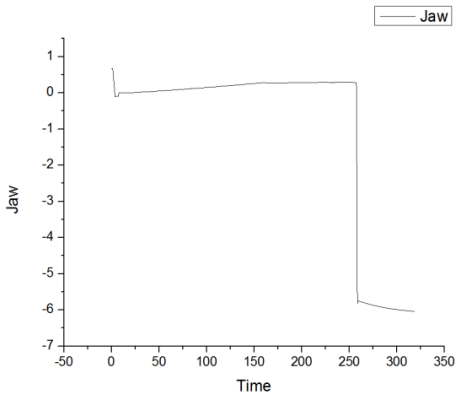

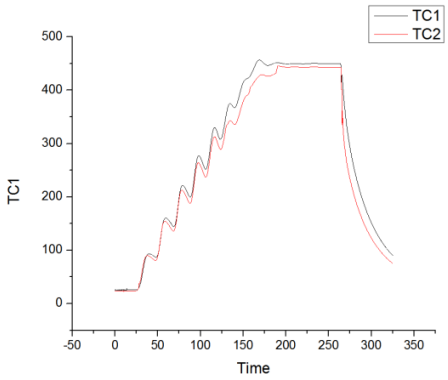

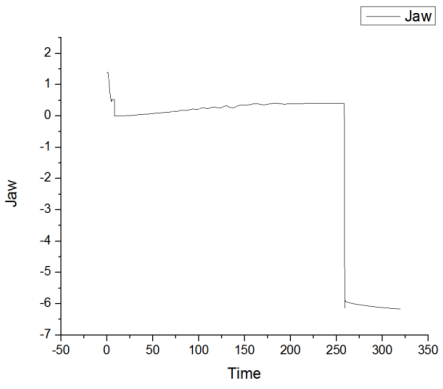

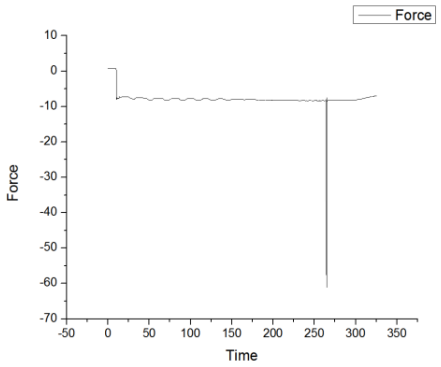

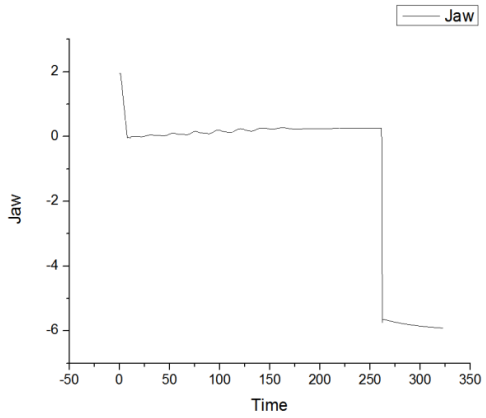
Jaw
Jaw
Time

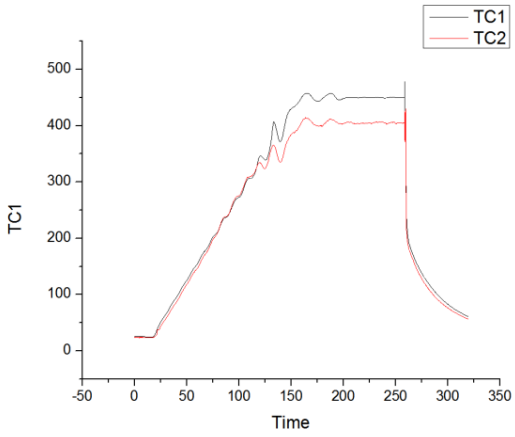
TC1
TC2
TC1
Time

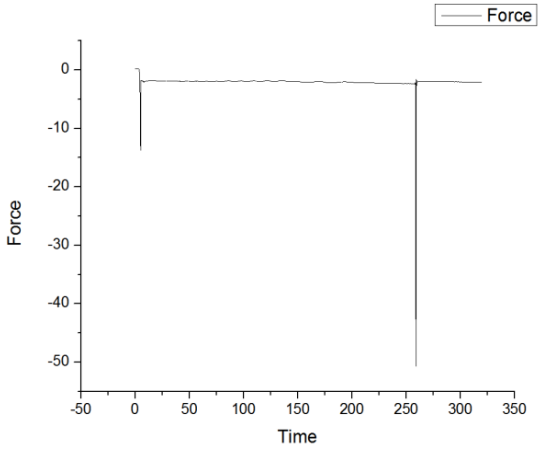
Force
Force
Time

Core 15µm x clad 1.0µm | A3XB2| Target Temp = 450ºC|TEST 1-3|

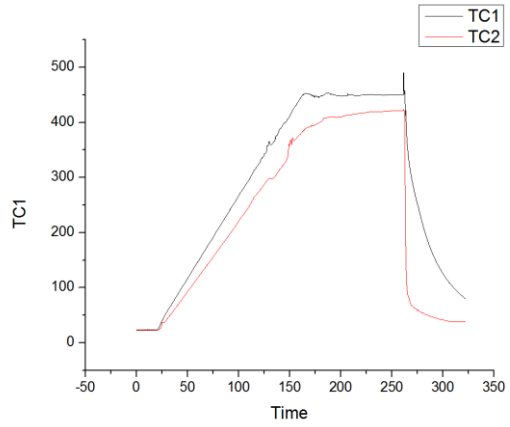

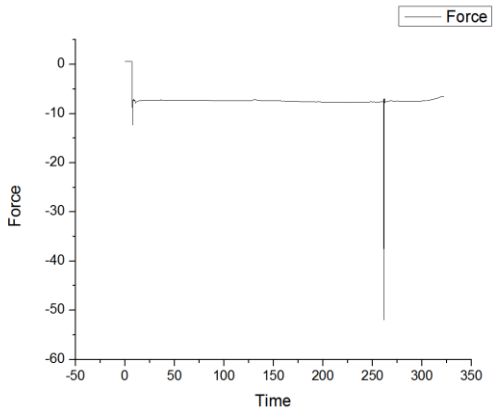

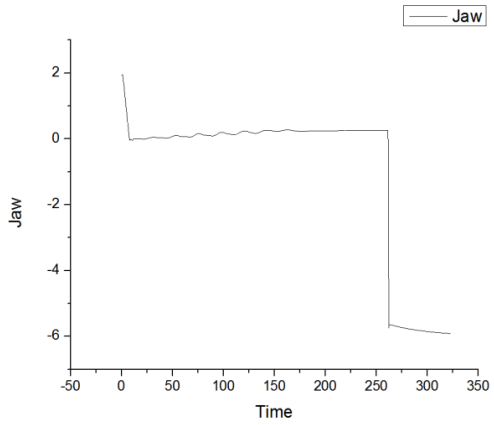

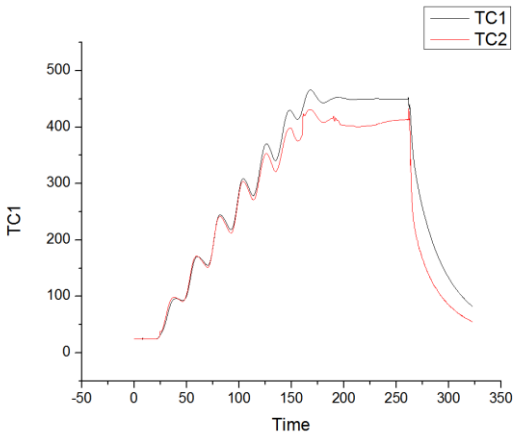

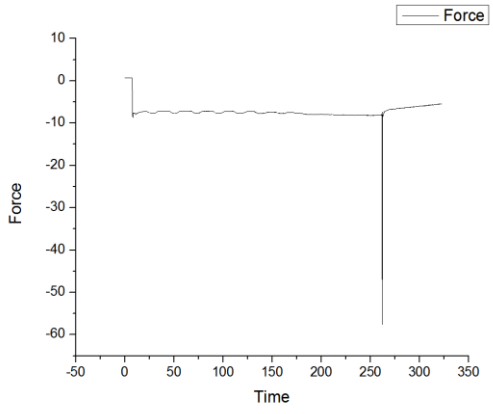

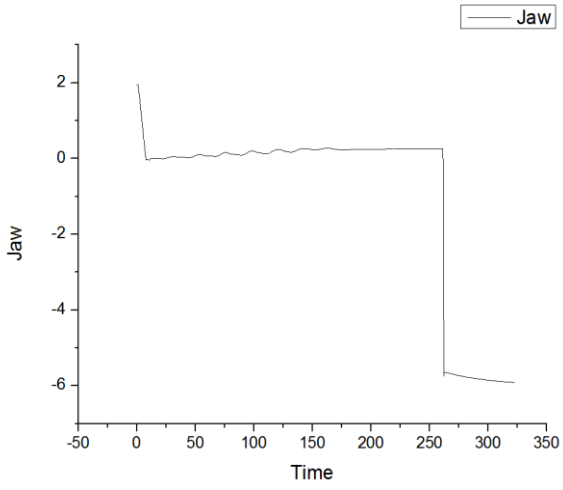

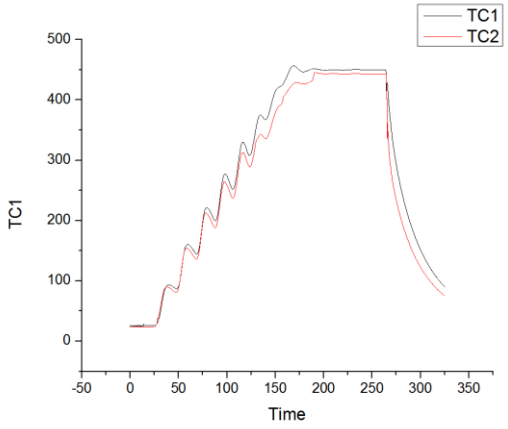
TC1
TC2
TC1
Time

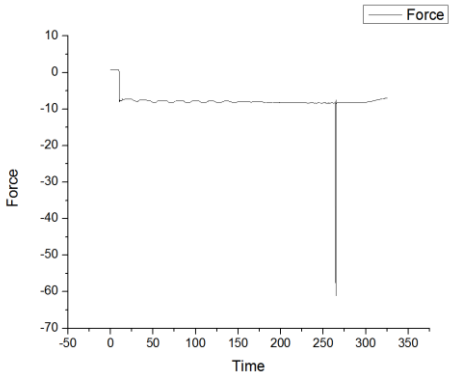
Force
Force
Time

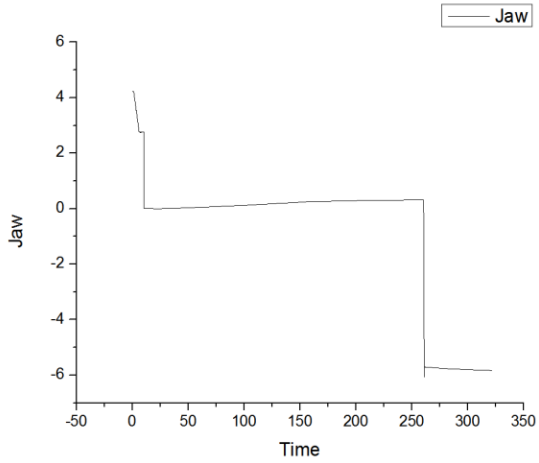
Jaw
Jaw
Time

Core 15µm x clad 3.0µm | A3XB3| Target Temp = 450ºC|TEST 1-3|

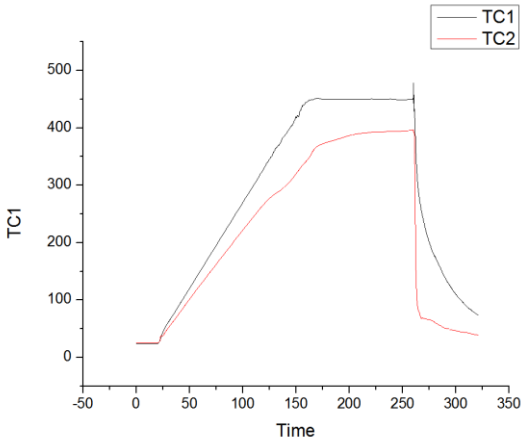

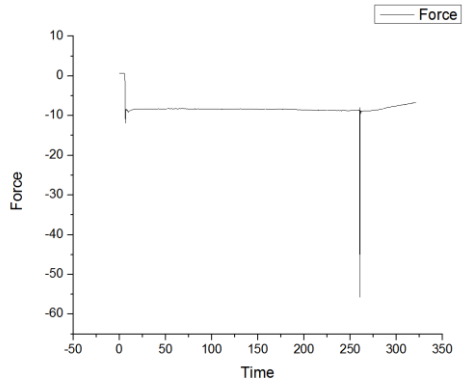

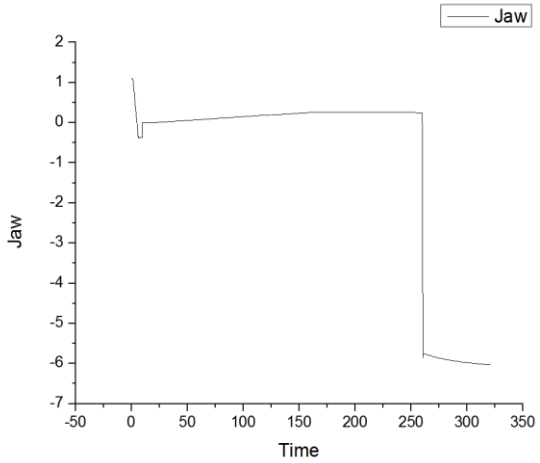

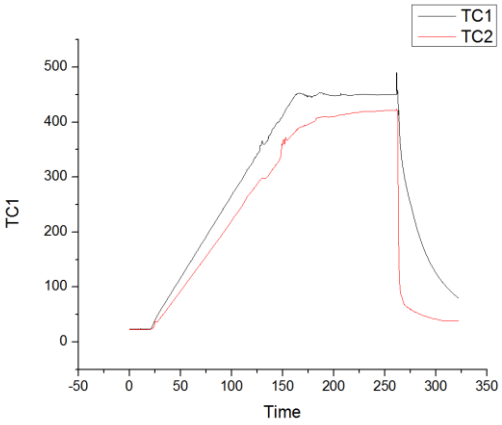

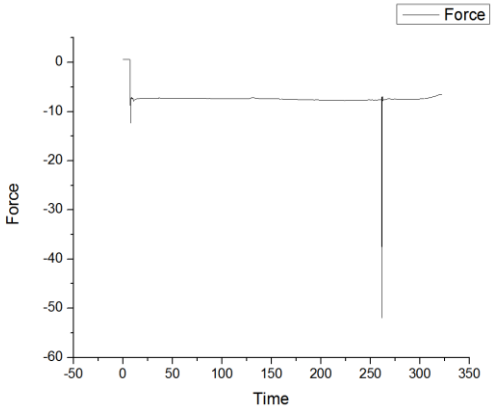

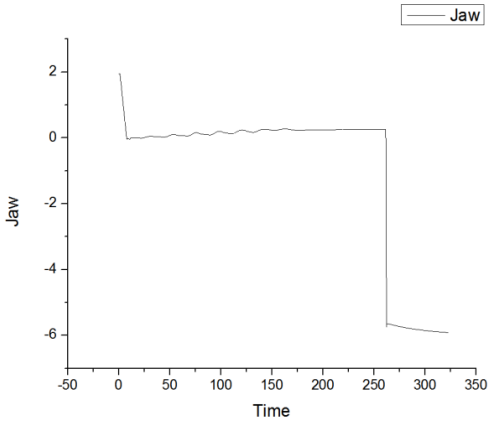

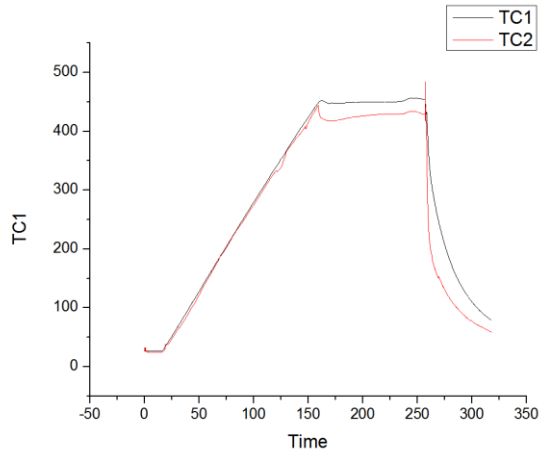
TC1
TC2
TC1
Time

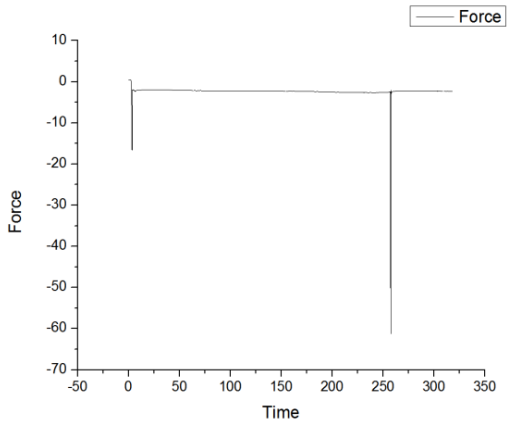
Force
Force
Time

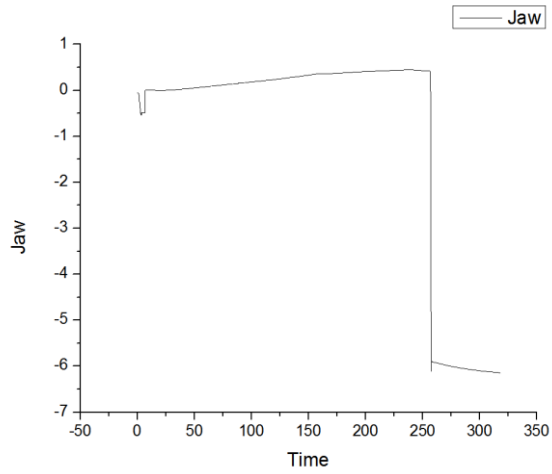
Jaw
Jaw
Time

Core 25µm x clad 0.5µm | A4XB1| Target Temp = 450ºC|TEST 1-3|

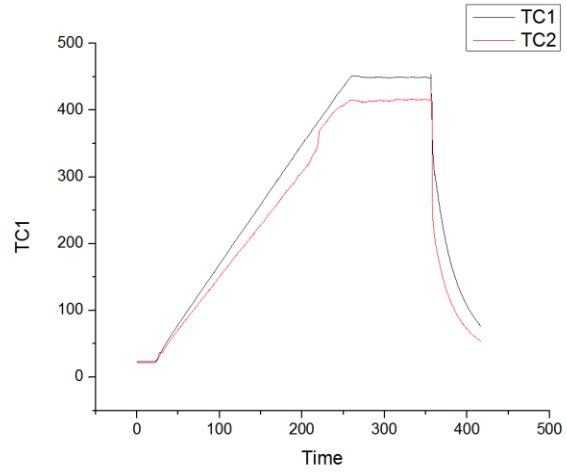

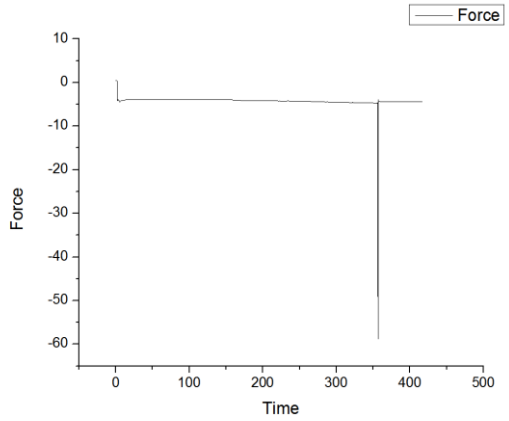

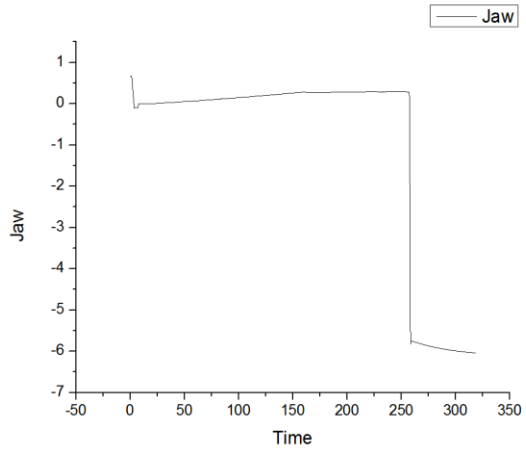

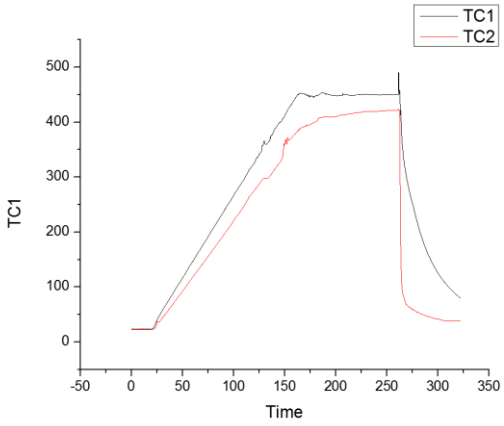

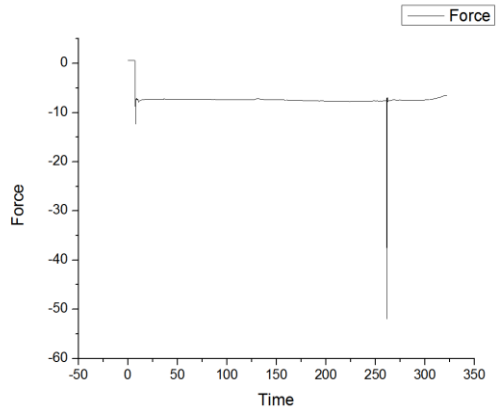

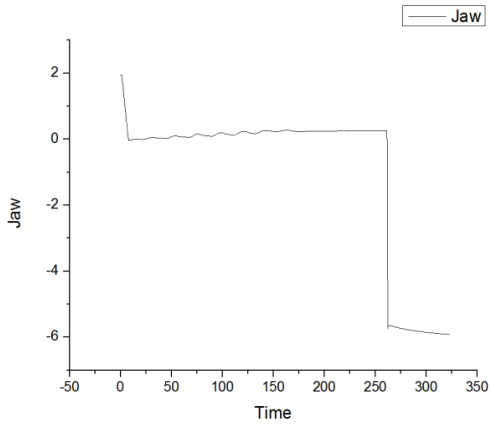

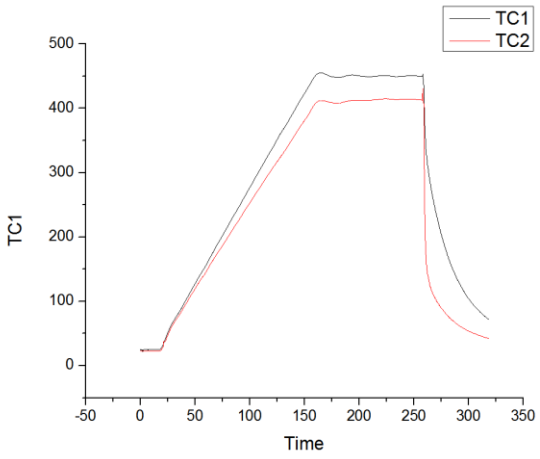
TC1
TC2
TC1
Time
500
400
300
200
100
0
-50
0
50
100
150
200
250
300
350

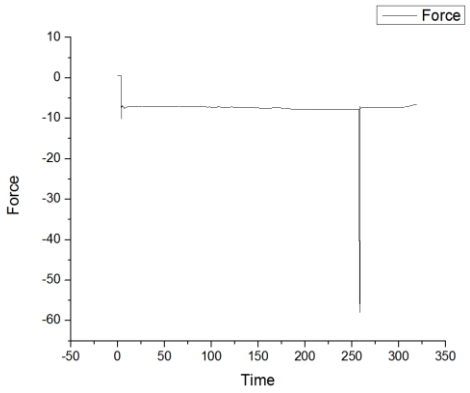
Force
Force
Time
10
0
-10
-20
-30
-40
-50
-60
-50
0
50
100
150
200
250
300
350

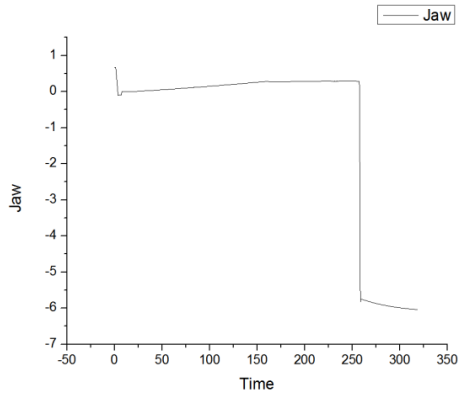
Jaw
Jaw
Time
1
0
-1
-2
-3
-4
-5
-6
-7
-50
0
50
100
150
200
250
300
350

Core 25µm x clad 1.0µm | A4XB2| Target Temp = 450ºC|TEST 1-3|

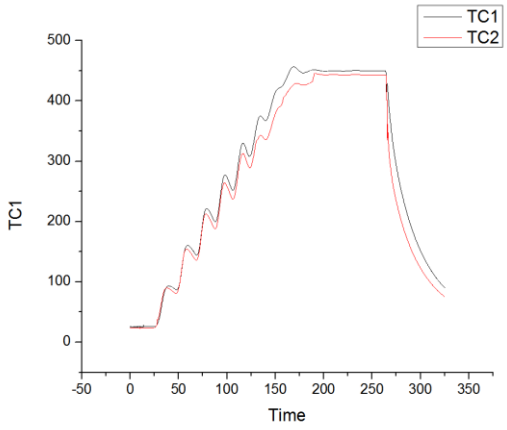

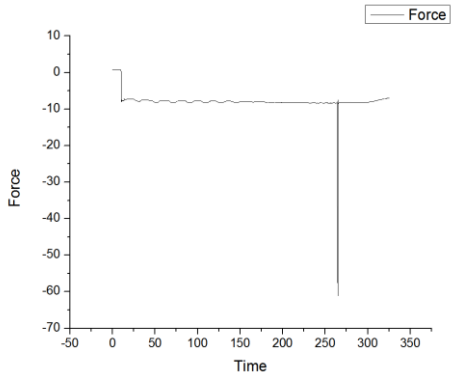

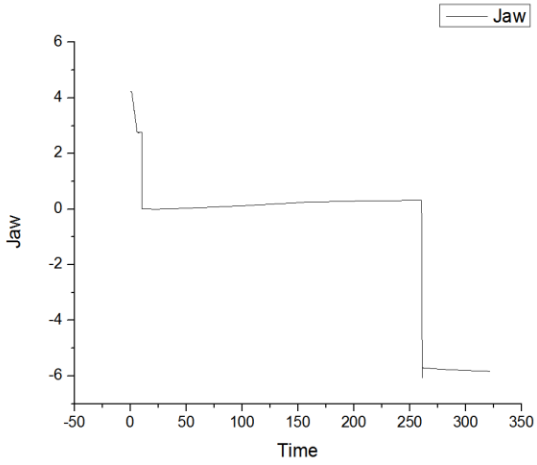

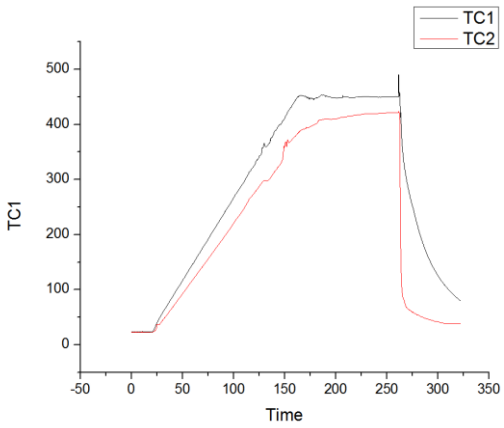

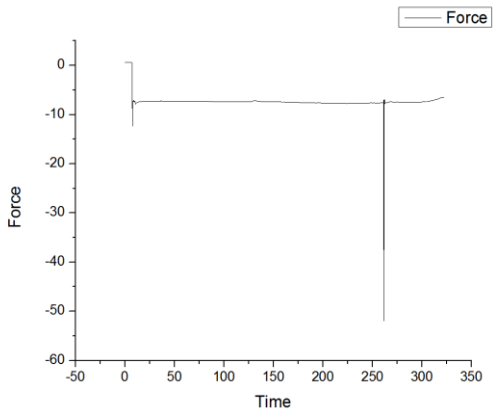

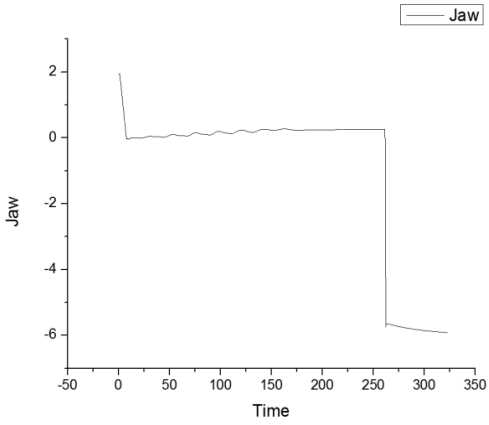

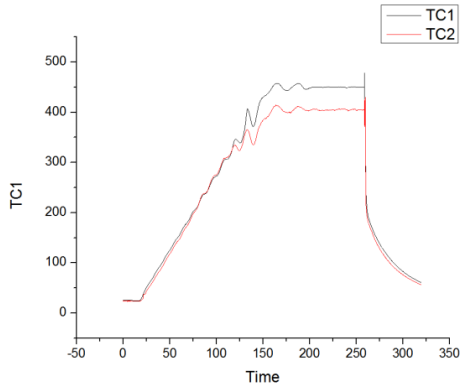
TC1
TC2
TC1
Time

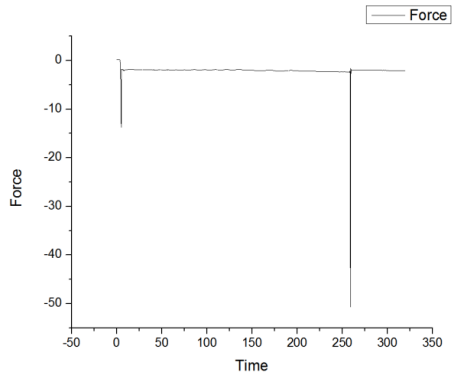
Force
Force
Time

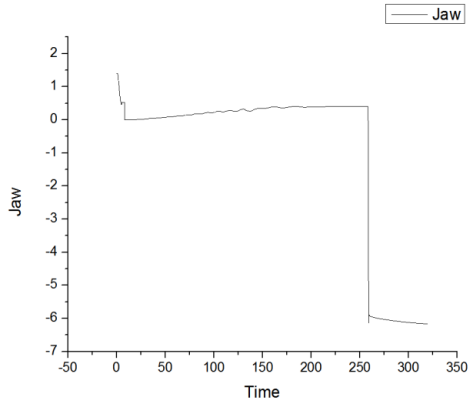
Jaw
Jaw
Time

Core 25µm x clad 3.0µm | A4XB3| Target Temp = 450ºC|TEST 1-3|

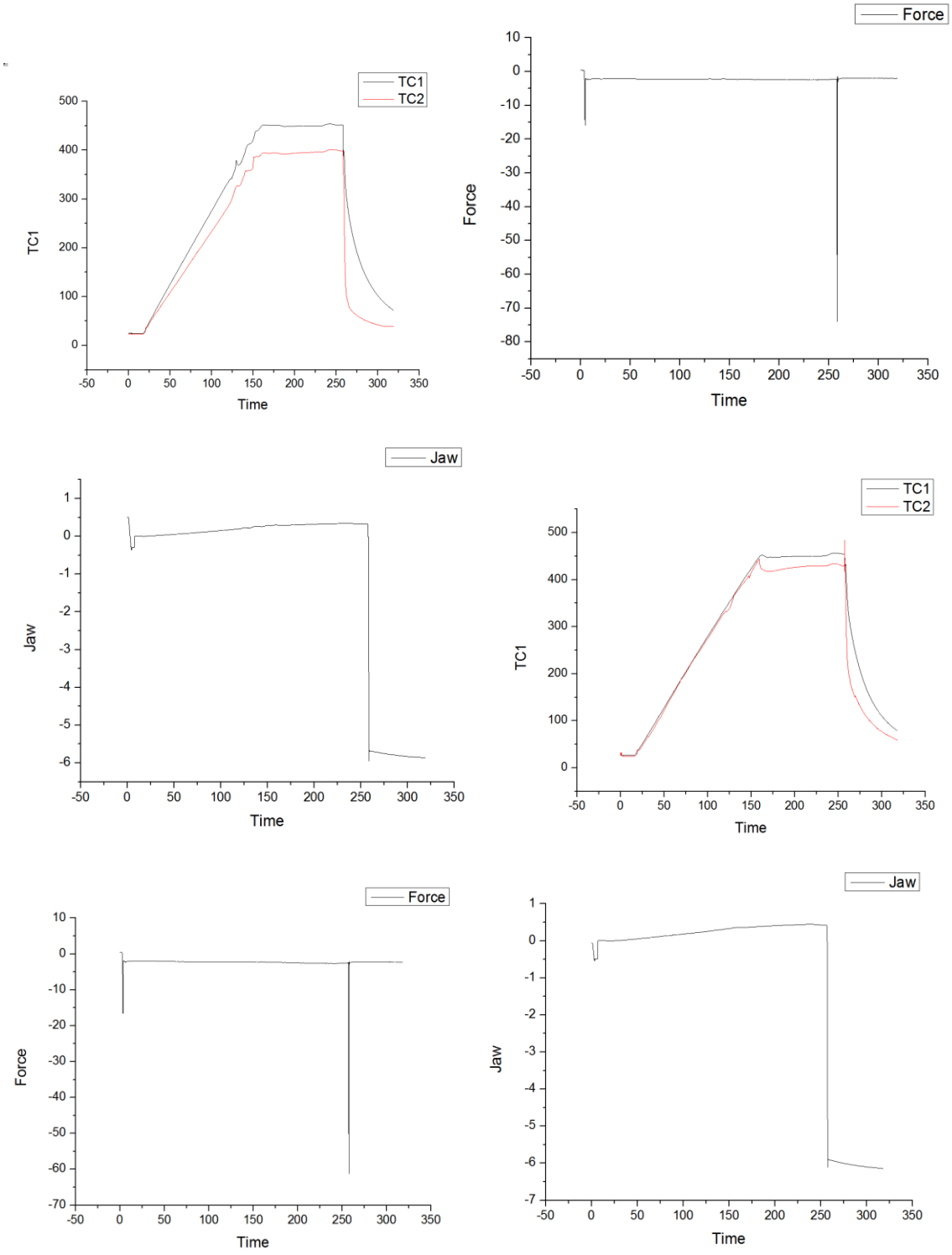

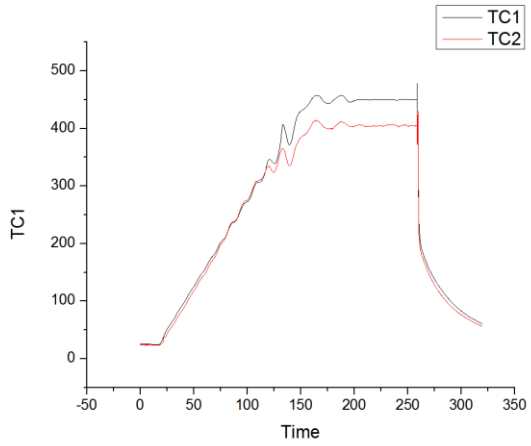
TC1
TC2
TC1
Time

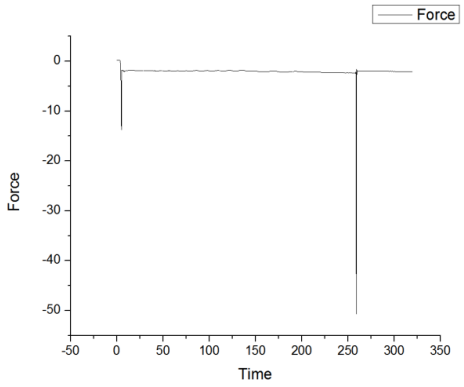
Force
Force
Time

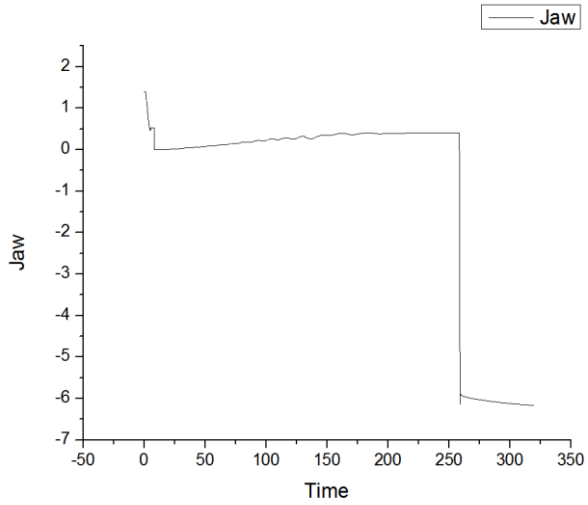
Jaw
Jaw
Time

APPENDIX B PSC SAMPLES GEOMETRY

1. AA3003 sample
2. AA4045 Sample
3. PSC Modified anvils
4. PSC Modified sample holder

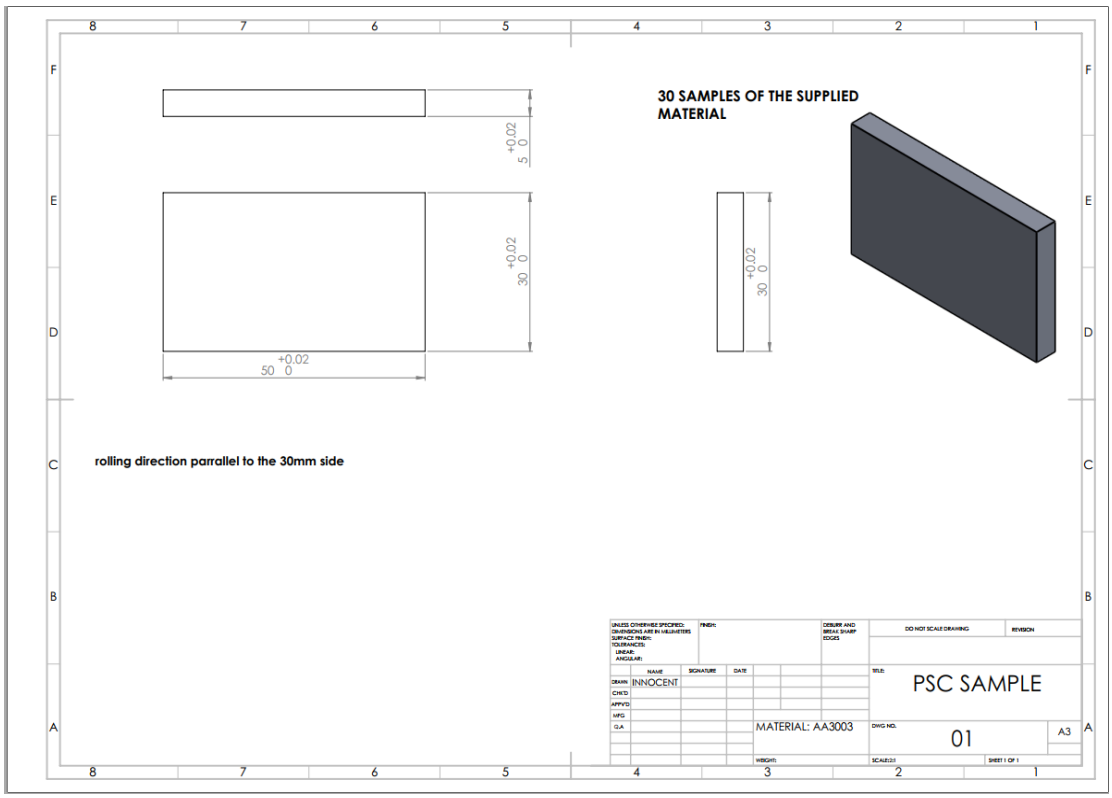

ASTM D3165 SPECIMEN GEOMETRY

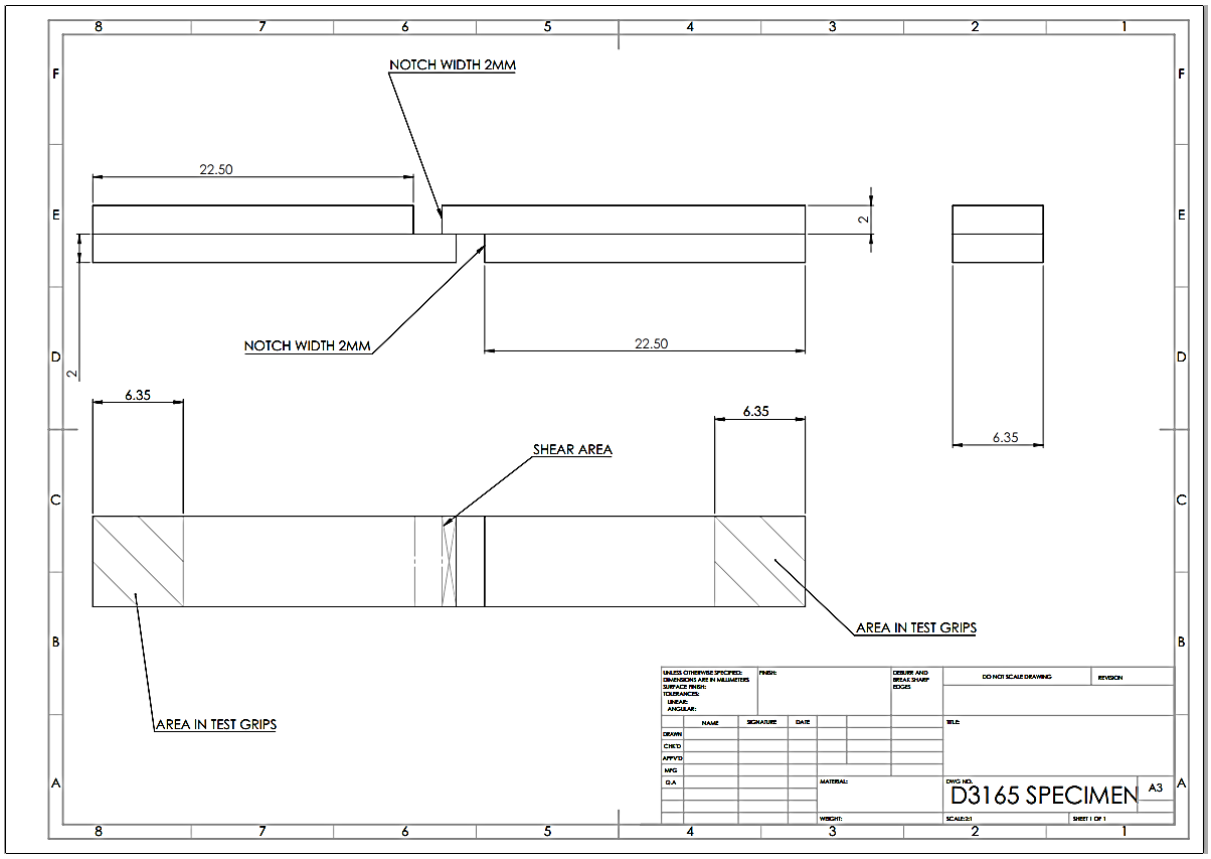

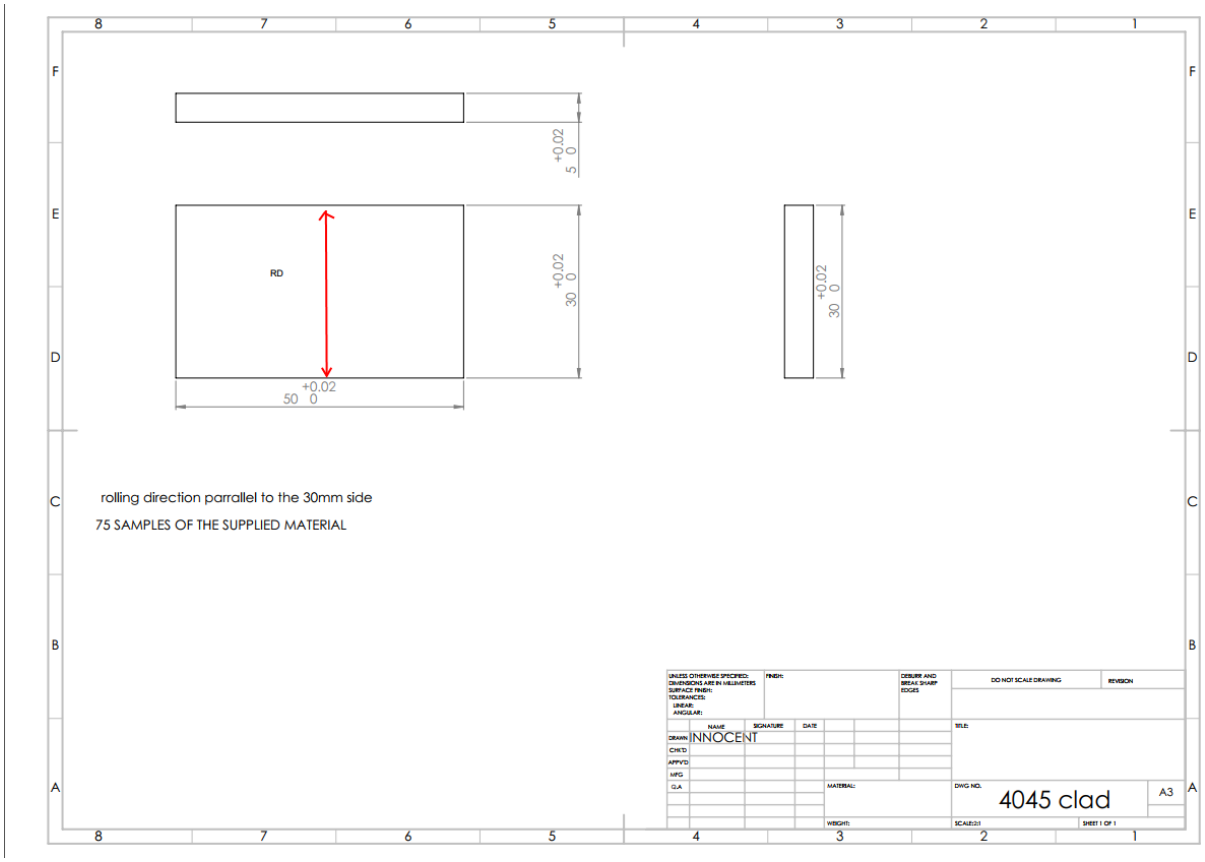

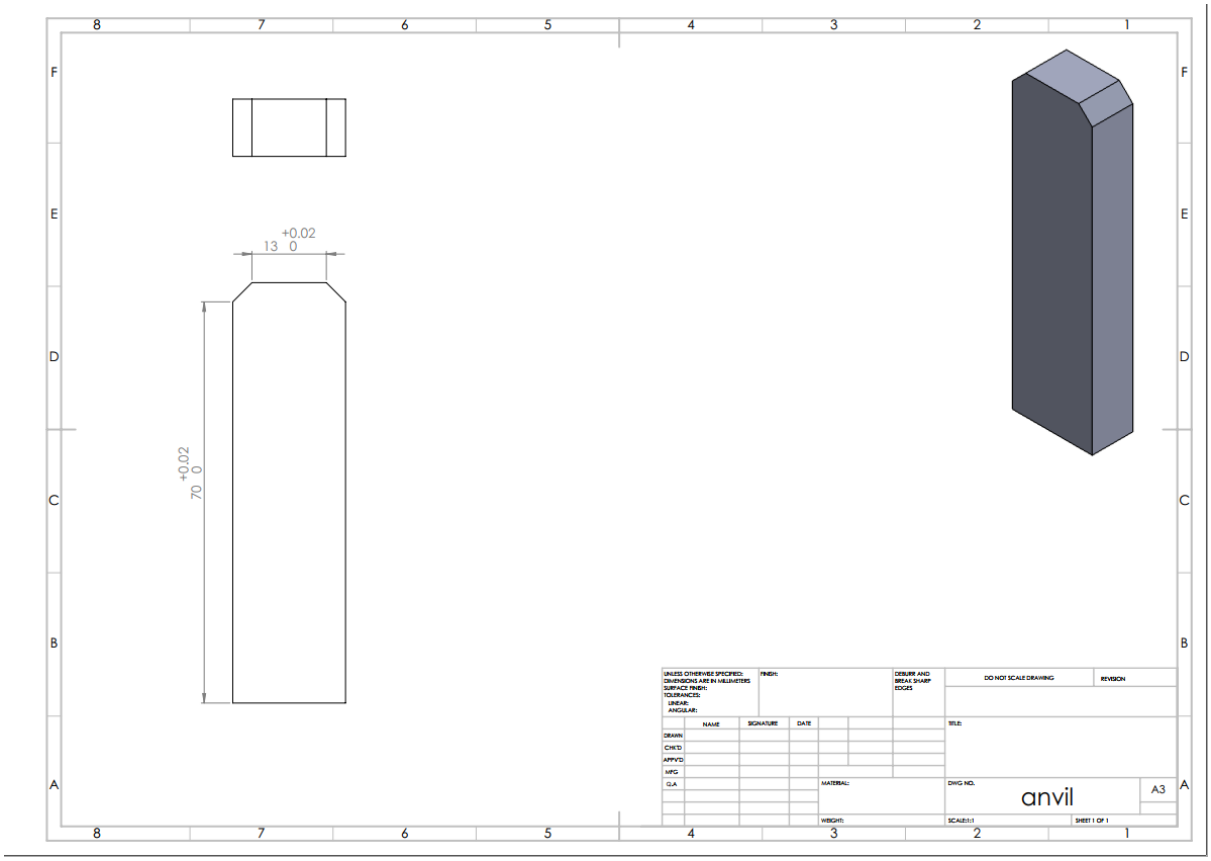
+0.02
13 0
+0.02
70 0
anvil
A3

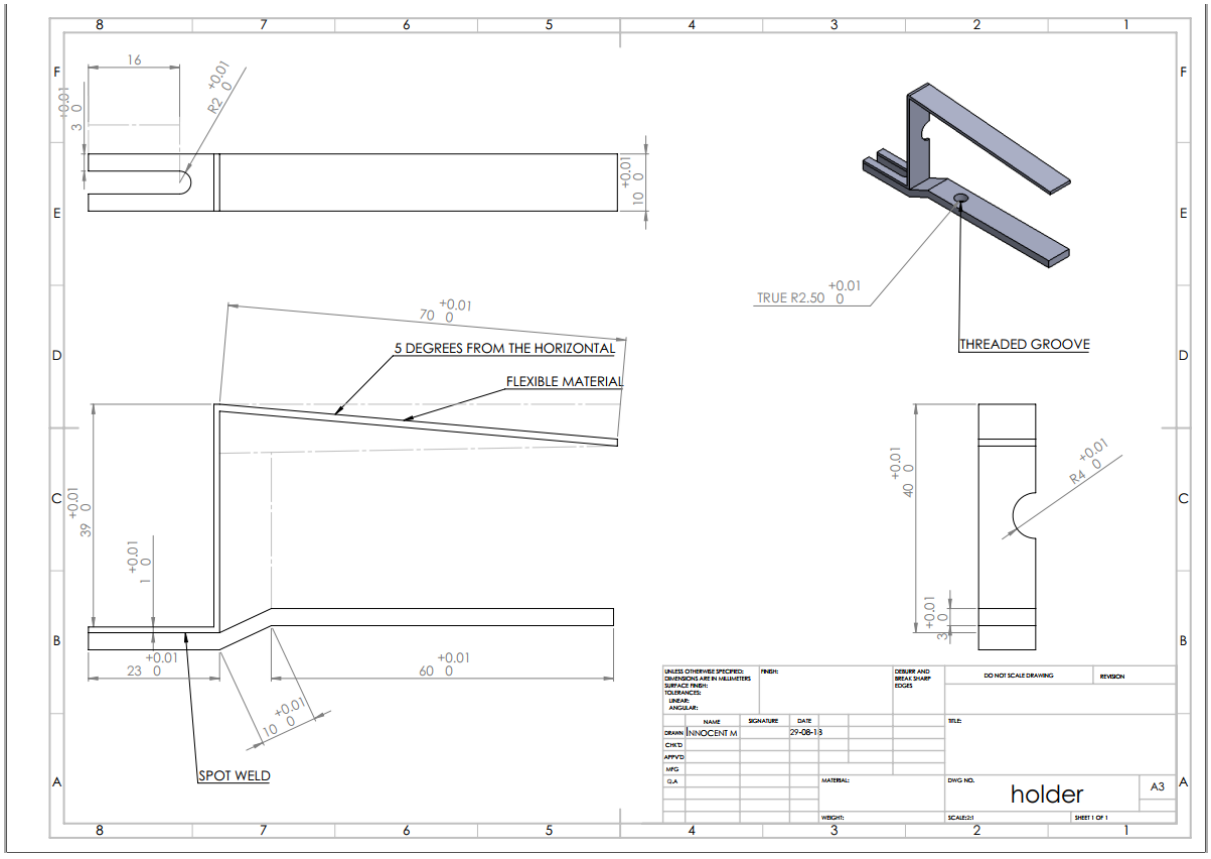
16
+0.01
R2 0
+0.01
3 0
+0.01
10 0
+0.01
70 0
5 DEGREES FROM THE HORIZONTAL
FLEXIBLE MATERIAL
+0.01
39 0
+0.01
1 0
+0.01
23 0
+0.01
60 0
+0.01
10 0
SPOT WELD
TRUE R2.50 +0.01 0
THREADED GROOVE
+0.01
40 0
+0.01
R4 0
+0.01
3 0
INNOCENT M
29-08-13
holder
A3